8-2019

Intermittent Turbulent Exchanges and Their Role in Vineyard Evapotranspiration

Sebastian Alexander Los
Utah State University

INTERMITTENT TURBULENT EXCHANGES AND THEIR ROLE IN VINEYARD EVAPOTRANSPIRATION

by

Sebastian Alexander Los

A thesis submitted in partial fulfillment
of the requirements for the degree

of

MASTER OF SCIENCE

in

Climate Science

Approved:

_____	_____
Lawrence E. Hipps, Ph.D.	S.-Y. Simon Wang, Ph.D.
Major Professor	Committee Member
_____	_____
Bruce G. Bugbee, Ph.D.	William P. Kustas, Ph.D.
Committee Member	Committee Member

_____
Richard S. Inouye, Ph.D.
Vice Provost for Graduate Studies

UTAH STATE UNIVERSITY
Logan, Utah

2019

ABSTRACT

Intermittent Turbulent Exchanges and Their Role in
Vineyard Evapotranspiration

by

Sebastian A. Los

Utah State University, 2019

Major Professor: Dr. Lawrence Hipps
Department: Plants, Soils and Climate

Vitus vinifera sees extensive production in semi-arid areas that have limitations on water resources and drought risk. High value of the crop, beneficial relationships between controlled plant stress and fruit quality, and large evaporative demand by the atmosphere, all drive a growing need for daily, sub-field scale estimates of vineyard evapotranspiration (ET). Yet, monitoring crop ET remains difficult because of the complex atmosphere-biophysical interactions, particularly for such heterogeneous surfaces. The USDA-ARS created the Grape Remote sensing Atmospheric Profile & Evapotranspiration eXperiment (GRAPEX) to validate an ET modeling system at several sites in California's Central Valley. This system utilizes a two-source energy balance (TSEB) model which computes water and energy exchange using radiometric land surface temperature measurements. However, both measurement and modeling methods for estimating water vapor transport rely on assumptions that exchanges are temporally consistent over a given averaging period. Vineyards in semi-arid climates present factors that can complicate turbulence behavior and resulting fluxes. First, vineyard structure creates a complex canopy pattern of that can complicate turbulent flow. Second, typical strong synoptic high pressure often yields daytime periods of light winds and unstable conditions, that promotes episodic convective motions that could cause vertical transport to be dominated by low frequency, intermittent events.

The objectives of this thesis research were to document conditions related to intermittent turbulence in vineyards, quantify the effects of this behavior on water vapor fluxes, and test the TSEB model's ability to estimate vineyard ET for intermittent conditions vs. more steady transport. Eddy covariance data from above the canopy and within the canopy sublayer of two vineyards during portions of several growing seasons were analyzed. Intermittent turbulence was linked to periods of light winds and highly unstable/convective conditions, and dominant lower frequency events. Time series of instantaneous fluxes and temperature gradients revealed that the vineyard canopy environment became more variable and had reduced coherency with the air above during intermittent behavior. The TSEB model exhibited reduced agreement with measurements during intermittency, with the best performance during steadier periods. Results presented here have important implications for the monitoring of ET from vegetation with complex canopies.

(132 pages)

PUBLIC ABSTRACT

Intermittent Turbulent Exchanges and Their Role in

Vineyard Evapotranspiration

Sebastian A. Los

Vineyards are often grown in semi-arid climates, such as California's central valley, where water resources can be limited. Summer weather conditions result in high water use by these plants. For wine grapes, a high-value commodity, there are known benefits to fruit quality in irrigating grapevines with slightly below optimum for the plant. Growers would like to be able to precisely irrigate without overusing water or overstressing the vines. This calls for improving ways to monitor vineyard water use by estimating the combined soil evaporation and plant transpiration known as evapotranspiration (ET). A computer model developed by the USDA called the Two-Source Energy Balance model (TSEB) can estimate ET through satellite or aircraft measurements of land surface temperature. The model has been successful for simple, uniform vegetation such as maize, soybeans, and grasslands. The ability of TSEB to estimate vineyard ET has been tested through a field experiment called the Grape Remote sensing, Atmospheric Profile, & Evapotranspiration eXperiment or GRAPEX.

Water is primarily transported away from the ground and plants by turbulent swirls in the wind. Models such as TSEB assume these swirls occur in a consistent manner over a few minutes to hours. Yet, interactions between the wind, the complex vineyard canopy, and heating near the ground can cause them to be episodic or intermittent. There are questions of if and how intermittent water vapor transport might happen in vineyards, and whether the TSEB model will still estimate ET well in such cases. In this study wind, humidity, air temperature, and surface temperatures are used to examine when intermittent behavior occurs, how it affects ET from the vineyard canopy, and how TSEB performs for intermittent versus more steady conditions. Results show that intermittent turbulence significantly alters the microclimate in the vineyard canopy compared to more ideal, steady behavior. The TSEB model was successful but showed reduced ability to estimate ET

during times of intermittent behavior. The knowledge gained is an important step toward using TSEB as a powerful tool for sustainable water management, not only in vineyards, but other cash crops with complicated canopies such as orchards, as well as natural ecosystems.

DEDICATION

This work is dedicated to my father, who alongside my mother, is the source of all my curiosity. He was a father who when a young me apologized for asking so many questions would answer back, *no, ask more*! My measure of success in life will always be to try to match his kindness, his work ethic, and the quality he placed in any craft. I sorely miss our conversations about gravity, engine designs, radio waves, thunderstorms, trees, and the precise number of Christmas lights that can be safely used on a given extension cord. I hope you would have found the following interesting.

Sebastian A. Los

ACKNOWLEDGMENTS

Funding for this research was provided by NASA Grant #NNX17AF51G and Utah Agriculture Experiment Station Project Grant UTAO 1186. Funding provided by E.&J. Gallo Winery made possible the collection of much of the data during the GRAPEX field campaign. In addition, the staff of the Viticulture, Chemistry and Enology Division of E.&J. Gallo Winery and the staff of the Borden Vineyard should be acknowledged for their excellent logistical support as part of the GRAPEX project.

I send out many thanks to the scores of great people I was lucky to work with on the GRAPEX project from the USDA-ARS, E&J Gallo, IRTA, and NASA, among other institutions. Anyone on the team would agree that the GRAPEX group is a special gathering of folks. I was able to learn so much just by chatting with you or working beside you. I especially thank my publication co-authors Drs. Joseph Alfieri, John Prueger, Hector Nieto, and Bill Kustas for their insight and help.

I would like to greatly thank each of my committee members, Drs. Shih-Yu (Simon) Wang, Bruce Bugbee, and Bill Kustas for their exceptional mentorship and assistance during my study, research, and degree completion. Calling them helpful is an understatement. I will be ever thankful for the great deal I learned from each of you.

Finally, I extend my utmost gratitude to my advisor Dr. Larry Hipps. I had not imagined when entering graduate school that I would have the chance to work with an advisor who was so deeply interested in the knowledge I gained and my growth as a young scientist. From day one it was clear that my learning was paramount and a well-rounded background was key. Thank you for all of the effort you put into me. It is hard

to think of a better mentor. I am especially thankful for the trove of great conversations. Few were not profound.

Sebastian A. Los

CONTENTS

LIST OF TABLES

LIST OF FIGURES

CHAPTER I
GENERAL INTRODUCTION

An increasingly large portion of global grape production, a high value commodity (Ashenfelter et al. 2018), occurs in arid and semi-arid regions where there is increased uncertainty and limitation on water resources, while the evaporative demand on the crop is high (Kool et al. 2016). In addition to these factors, it is recognized that slight water stress during certain points in the growing season improves grape quality (Robinson 2006). A noteworthy example of this situation are the vineyards in the Central Valley of California which have constraints on water resources, risk of drought impacts, and high evaporative demand during the growing season. Given all of these factors, there is a need for daily, field-scale estimates of evapotranspiration (ET) in order to precisely manage vineyard irrigation.

While there exist several methods for estimating the ET of vegetated surfaces, a number of factors prevent their practical, widespread use in estimating field-scale vineyard ET. Traditional methods such as lysimeter and sapflow measurements, represent point values that are difficult to both implement and to scale up to the field (Hillel 2004). The eddy covariance method, the current gold standard, does measure mass and energy exchange over larger surface areas. However, it requires a great deal of data analyses, and represents a variable footprint dependent on conditions (Foken et al. 2012). These direct approaches to determine ET also involve expensive equipment and

require expertise to interpret findings. In order to practically address ET across more extensive spatial scales another approach must be utilized. Considerable success has been made estimating ET through radiometric temperature measurements of vegetated surfaces through remote sensing (Quattrochi and Luvall 2004). The USDA Agricultural Research Service (ARS) has developed a satellite-based ET modeling system, known as ALEXI/DisALEXI, and has successfully validated its performance over a number of natural and agricultural landscapes (Anderson et al. 2011). This modeling system shows significant promise in providing field-scale estimates of ET for vineyard surfaces. Unknowns remain, however, regarding the complexities in vineyard ET processes, and how well these complexities are handled by the ET modeling system.

In order to test the ALEXI/DisALEXI modeling approach over vineyard surfaces, the Grape Remote sensing Atmospheric Profile and Evapotranspiration eXperiment (GRAPEX) was begun in 2013 as a collaboration between the USDA-ARS, NASA, E&J Gallo Winery, Utah State University, and number of other institutions (Kustas et al. 2018). During the 2013 – 2016 growing seasons the experiment focused on two Pinot Noir vineyard blocks near the town of Lodi in the Central Valley. Both vineyard blocks were heavily instrumented including measurements of standard meteorological data, plant-biophysical properties, soil variables, net radiation, infrared surface temperatures, and fast-response gas concentrations and 3-D anemometry. Using this rich dataset, GRAPEX had three primary objectives. First was to validate the USDA-ARS modeling system's performance for vineyard surfaces, second to develop ET products for the grape and wine industries, and third to generate new knowledge of water and energy balance and transport processes in vineyards.

1.1 ALEXI/DISALEXI and the TSEB Model

The ALEXI/DisALEXI ET modeling system begins by gathering information such as surface temperature, leaf area index (LAI), and other surface properties from multiple satellites (Semmens et al. 2016). To achieve high spatial resolution, Landsat 7 and 8 data are used for their 30 m resolution available every 8 – 16 days, while data from the MODIS and GOES satellites, at 4 km and 1 km resolution respectively available daily, are used between Landsat overpasses to achieve high temporal resolution. These data are then processed through the ALEXI model. Within ALEXI, surface temperature and vegetative fraction are ultimately related to a sensible heat flux. This is achieved through a Two-Source Energy Balance (TSEB) model, which models near surface turbulent exchange, in conjunction with a separate atmospheric boundary layer model. The TSEB model simulates net radiation, soil heat flux, and exchange of sensible heat. ET is then calculated as the residual latent heat flux of energy balance. The TSEB model then iterates solutions in conjunction with the atmospheric boundary layer model until they agree on all fluxes. Then, modeled results from multiple satellite platforms are combined through a data fusion algorithm known as DisALEXI and downscaled to the spatial resolution of the most recent Landsat imagery. The final result is a daily, 30 m resolution spatial estimate of ET (Semmens et al. 2016).

The novelty of the TSEB model approach is that it decomposes a surface into separate vegetation and soil sources using information about vegetative fraction, LAI, and radiometric surface temperature (Norman et al. 1995). This allows the TSEB model to more realistically simulate fluxes from sparse canopies than previous remotely sensed

ET estimation methods. The TSEB model relates a surface temperature from each source to a sensible heat flux (H) through a set of gradient and resistance pathways (Fig. 1.1). One gradient, between the canopy temperature (T_c) and the canopy sublayer air temperature (T_{ac}), controlled by resistance R_x, is sourced from the vegetation. Another gradient, between the soil temperature (T_s) and T_{ac}, controlled by resistance R_s, is sourced from the bare soil surface. An aggregate gradient between the T_{ac} and the temperature of air above the canopy (T_a) is controlled by resistance R_a. By estimating net radiation and soil heat flux, H is determined along these pathways and a latent heat flux is estimated as a residual yielding an estimated ET (Kustas et al. 2016). Most of the information regarding turbulent exchanges on the vineyard scale is parameterized within the computation of R_a between the canopy and air above. The TSEB model has been shown to effectively estimate H and in turn ET for many sparse, heterogeneous vegetated surfaces. However, because of the particular characteristics of vineyard systems, such as row structure, elevated canopy, and below-canopy surface variability, it is unknown how well the TSEB model will be able to parameterize turbulent exchanges under various wind directions, stabilities, and turbulence characteristics.

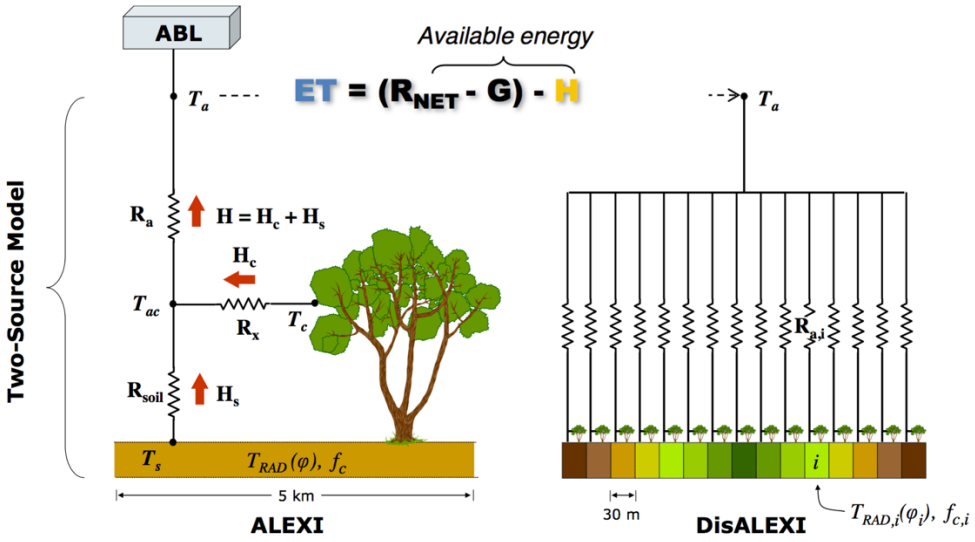

Fig. 1.1 Representations of ALEXI, including the TSEB model, and DISALEXI.

1.2 Vineyard Structural Complexity

A number of characteristics inherent to the structure of vineyards complicate the transport processes that govern their ET. These characteristics were typified by the vine cropping methods at the GRAPEX sites (Kustas et al. 2018). There vines were grown on a fixed row trellis system with an elevated canopy. The rows were spaced at 3.3 m with individual vines spaced along the row at 1.5 m increments. Maximum canopy height during the growing season was typically ~ 2 – 2.5 m. Later into the growing season vines extend the canopy laterally into the row interspace. This growth is partially governed by the vineyard management, but is generally rather complex in space. The inter-row surface within vineyards may consist of bare soil or, as in at the GRAPEX vineyard sites, a cover crop. This cover crop typically was green in the spring and then senesced during the dry summer. Directly below the canopy within the row was an above surface drip

irrigation system. This overall structure creates a 3-D pattern of vegetation where complex shading complicates energy balance and water vapor sources are heterogeneous between differing parts of the canopy and surfaces below. This provides a complex surface to examine from both remote sensing and turbulence exchange perspectives. Moreover, vineyard structural characteristics generally changes across the growing season as the canopy extent varies due to vine growth.

Aside from these structural effects, an additional confounding factor to turbulent transport processes emerges as a result of typical atmospheric conditions within semi-arid climates. Daytime conditions during growing seasons within these climates typically consist of clear skies, high maximum temperatures (30 – 40+°C), and frequent light winds (<1.5 ms^{-1}) (Peixoto and Oort 1992). This is exemplified in the Central Valley of California where frequent light winds and high solar radiation result in high sensible heat fluxes. This often supports a highly unstable, near free-convective environment near the surface where dominant buoyancy forces can cause turbulence to become intermittent and dominated by low frequency events.

Despite the motivations mentioned previously, the quantity of research concerning vineyard ET, and particularly turbulence transport of water vapor in vineyards, has been limited. This is likely due in large part to the difficulty presented by vineyard structure heterogeneity. Research done in this area has included basic energy and water mass balance measurements, more complex radiation balance and modeling approaches, investigations of turbulent exchanges, and more recently, numerical simulation and remote sensing. Within the broader field of turbulence research, the problem of intermittency in turbulence flows has received continued interest for many

decades. Intermittent turbulence, where turbulent behavior becomes episodic and irregular, has been shown to significantly influence fluxes (Lee 2009). The following is an overview of previous research concerning vineyard exchange processes and broader issues of turbulence intermittency in plant canopies.

1.3 Vineyard Evapotranspiration

Study of grapevine water balance occurred as early as the 1960s using chamber methods (Kato et al. 1965) and using simple micrometeorological measurements during the 1970s (Weiss and Allen 1976). Hicks (1973) was one of the first to use eddy covariance over vineyards showing the importance of wind direction, row orientation, and drag coefficients to fluxes; showing increased latent heat flux with cross-row flow. Work in the 1980s and early 1990s began to utilize the Bowen Ratio method (Kernich 1985; Heilman et al. 1994) and lysimeters in irrigated vineyards (Evans et al. 1991) to make estimates of ET. Oliver et al. (1992) measured radiation balance in a vineyard, attempted to partition evaporation and transpiration, and determined a set of crop coefficients for vineyard surfaces. They reported difficulty, however, that was attributed to unknowns regarding energy and water balance relationships between vines and inter-row bare soil. Trambouze et al. (1998) using mini-lysimeters and sap-flow measurement techniques, found that separate measurement of soil and vegetation water exchange was much more precise at estimating ET than simple energy balance and soil water balance methods.

The mid 1990s to the present have seen some attention to studying turbulent transport of heat and water vapor within vineyards through the application of fast-response measurements. De Bruin et al. (1995) applied scintillometry and eddy covariance methods to measure sensible heat flux aggregated across a vineyard plot and reported that discrepancies between the two methods were significant and varied across stabilities and wind speeds. McInnes et al. (1996) investigated the effects of wind speed and direction on aerodynamic conductances of heat and water vapor near the soil surface, finding a dependence on wind direction in relation to row orientation. Kordova et al. (2000) measured spatial variability of fluxes with a horizontal transect of three closely spaced eddy covariance systems just above a vineyard canopy. They observed significant differences horizontally between sensible and latent heat fluxes for along-row flow, more horizontally homogenous fluxes for cross-row flow, and greater turbulence intensity for cross-row flow. Recent studies have expanded the scope of vineyard research using numerical simulation. Chahine et al. (2014) conducted large eddy simulations (LES) of vineyards and compared them to 3-D anemometry measurements. They found that cross-row flow behaved similarly to that of a more uniform canopy, while along-row flow showed increased spatial variability, increased intermittency of turbulence, and larger fluxes of momentum.

Studies have applied energy balance models to address vineyard heterogeneity, including using multi-source models developed for sparse vegetation. Work by van den Hurk et al. (1995) compared three published soil-vegetation-atmosphere transfer models and found that predicted fluxes, particularly from the multiple source methods, agreed with measurements but varied widely between modeling schemes during high sensible

heat flux. Other studies have confirmed the superiority of more complex multi-source models as compared to simpler homogeneous "Big Leaf" models in estimating vineyard ET (Greenspan and Matthews, 1996; Ortega-Farias et al., 2007; Poblete-Echeverria et al., 2009). Extensive research has been published applying the TSEB approach using radiometric surface temperatures to other types of sparsely vegetated surfaces (Kustas and Norman 1999; Anderson et al. 1997; Colaizzi et al. 2014). Recently this research has extended to vineyard systems (Cammalleri et al. 2010).

1.4 Turbulence Intermittency

Intermittent behavior has been observed for decades in many dynamical systems, yet a complete definition of intermittency remains elusive (Vassilicos 2010). The term intermittency can describe a range of chaotic behaviors that occupy the spectrum between continuous, steady-state behavior and behavior that is truly random. Intermittency can manifest as quasi-periodic shifts in system behavior to variations in system variables that approach pure disorder (Vassilicos 2010). Intermittency can appear as deviations from a Gaussian distribution in higher statistical moments of momentum or scalars, or both (Ditlevsen 2004). Given these broad, ambiguous definitions, quantifying this behavior has proven difficult.

Intermittency in turbulence near the surface may arise from external or 'global' processes such as features in the planetary boundary layer flow, or from internal, small-scale processes such as non-linear interactions between locally driven turbulence and surface heterogeneity (Mahrt 1989). Much of the study concerning intermittent

turbulence has been focused on nocturnal stable stratification where intermittency is often very defined forming as distinct, bursts, or break-ins of activity separated by relatively longer quiescent periods with little activity (Mahrt 1998; Poulos et al. 2002; Ansorge et al. 2014).

For daytime conditions with neutral or unstable stability, study has focused on the fact that intermittent behavior in turbulence can often be related to the presence of coherent turbulent motions. Seminal work in the 1960s revealed intermittent boundary layer behavior to be linked to coherent structures in the flow consisting of a long 'sweeps' toward the wall (surface) followed by shorter ejections of fluid away from the wall forming a 'sweep-ejection cycle' (Kline et al. 1967). Since then the relative importance of ejections and sweeps in momentum and heat transport over various environmental surfaces has seen extensive study (Shaw et al.1983; Gao et al. 1989; Katul et al. 1997a; Finnigan 2000). Intermittent turbulent events can cause exchanges of energy and mass between a plant canopy sublayer and the air above to become constrained to sporadic "bursts". This appears as ramp-like signatures in scalar time series where the slow accumulation of a scalar is followed by a sudden drop as the canopy is vented. It has become clear that fluxes in heterogeneous canopies are often significantly influenced by coherent low frequency turbulent events. (Paw U et al. 1992).

Indeed a few studies have investigated the efficiency of ejection/sweep structures in vineyards, confirming a dominant role in flux processes (Francone et al. 2012). Leveraging this fact, the largest portion of this work has been efforts to apply the surface renewal method to vineyards (Shapland et al. 2012), where turbulent sensible heat flux from a crop can be estimated by quantifying ramp-like signatures in temperature time

series for some conditions yielding an ET estimate (Spano et al. 2000). Despite these studies, considerably little attention has been given to studying the effects on exchanges from plant canopies of more general turbulence intermittency that includes behavior beyond just that associated with coherent structures (Lee 2009). Given the limited research on how intermittent turbulence behavior affects scalar fluxes from vineyard surfaces, many unknowns remain concerning the role of intermittency in vineyard ET.

1.5 Objectives

Given the promise of the TSEB model and ALEXI/DISALEXI to estimate vineyard ET at the field scale and significant unknowns concerning intermittency and vineyard ET, the research of this thesis seeks to develop a more thorough understanding of how turbulence characteristics, vineyard structure, and atmospheric conditions relate to vineyard ET, and how ET models interpret these relationships. Ramp-like signatures are evident in preliminary analysis of time series data from the GRAPEX study sites similar to those found by others (Paw U et al. 1992). Fig. 1.2 shows an example of this with time series of water vapor density within the canopy and vertical velocity above the canopy over a 2.5-hour period. Evident throughout the series are ramps in water vapor density series that coincide with quiescent turbulent periods. These are followed by sharp falls in water vapor density during bursts of turbulent activity in the above canopy air. The suggested relationship between bursts of turbulent activity and venting of the canopy is congruent with previous research in elevated plant canopies, but the dynamics that cause it to arise in vineyard systems are not fully known. Nor is it yet apparent how such

intermittent behavior is captured by the flux-gradient relationships within the TSEB model.

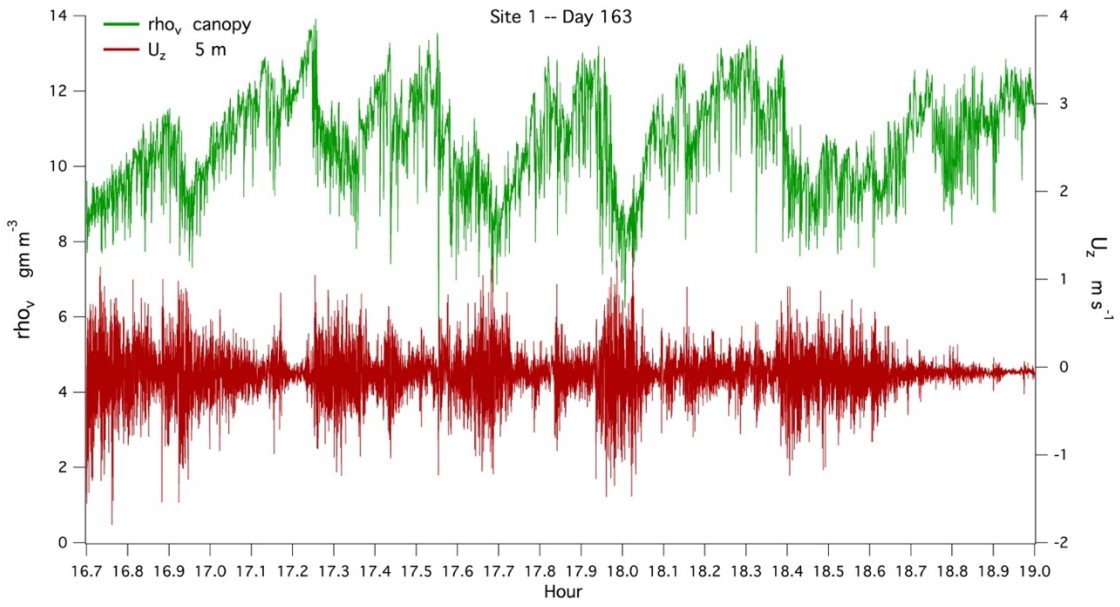

Fig. 1.2 Time series from vineyard site #1 of water vapor density (green) below the canopy top at 1.6 m and the vertical component of wind, U_z, (red) above the canopy at 5 m. The time period consists of 2.3 hours during the late afternoon on a warm, light wind day in June. Intermittent bursts of activity in U_z can be seen collocated in the time series with episodic water vapor exchanges, manifested as ramps followed by abrupt drops, from the canopy.

The two primary objectives of this research are to

1) investigate the relationships between vineyard structure and atmospheric conditions for periods when turbulence driven exchanges of heat and water vapor do and do not become intermittent, particularly light wind, convective conditions,

2) evaluate how well the TSEB performs across the range of conditions and stabilities that occur at the vineyard sites, with particular focus on periods displaying intermittency.

The research presented exploits the rather unique opportunity in the GRAPEX data to compare synchronized fast-response data from both above and within the canopy, along with fast-response IRT surface temperatures of the soil and canopy. Because the direct output of TSEB is a modeled *H*, evaluation of TSEB focuses on comparing modeled and eddy covariance measured *H* above the canopy. Particular emphasis is placed on the model's validation during periods of light winds and high sensible heat flux associated with turbulence intermittency.

1.6 References

Alfieri JG, Kustas WP, Nieto H, Prueger JH, Hipps LE, McKee LG, Gao F, Los SA (2018) Influence of wind direction on the surface roughness of vineyards. Irrigation Sci. https://doi.org/10.1007/s00271-018-0610-z

Anderson MC, Kustas WP, Norman JM, Hain CR, Mecikalski JR, Shultz L, Gonzales-Dugo MP, Cammalleri C, d'Urso G, Pimstein A, Gao F (2011) Mapping daily evapotranspiration at field to continental scales using geostationary and polar orbiting satellite imagery. Hydrol Earth Syst Sci 15:223-239

Anderson MC, Norman JM, Diak GR, Kustas WP, Mecikalski JR (1997) A two-source time-integrated model for estimating surface fluxes using thermal infrared remote sensing. Remote Sens Environ 60(2):195-216

Ansorge C and Mellado JP (2014) Global intermittency and collapsing turbulence in the stratified planetary boundary layer. Bound-Layer Meteorol 153:98-116

Ashenfelter O, Gergaud O, Storchmann K,Ziemba W (2018) Handbook of the Economics of Wine:Volume 1: Prices, Finance, and Expert, World Scientific Publishing Co. Pte. Ltd.

de Bruin HAR, van den Hurk BJJM, Kohsiek W (1995) The scintillation method tested over a dry vineyard area. Bound-Layer Meteorol 76: 25-40

Cammalleri C, Anderson MC, Ciraolo G, Durso G, Kustas WP, La Loggia G, Minacapilli M (2010) The impact of in-canopy wind profile formulations on heat flux estimation in

an open orchard using the remote sensing-based two-source model. Hydrol Earth Syst Sci 14: 2643-2659

Chahine A, Dupont S, Sinfort C, Brunet Y (2014) Wind-flow dynamics over a vineyard. Bound-Layer Meteorol 151:557-577

Colaizzi PD, Agam N, Tolk JA, Evett SR, Howell TA, Gowda PH, O'Shaughnessy SA, Kustas WP, Anderson MC (2014) Two-source energy balance model to calculate E, T, and ET: comparison of Priestly-Taylor and Penman-Montieth formulations and two time scaling methods. Trans of the ASABE 57(2):479-498

Ditlevsen PD (2004). Introduction to turbulence. Turbulence and Climate Dynamics. J & R Frydenburg A/S, Copenhagen

Evans RG, Kroeger MW, Mahan MO (1991) Installation and operation of large drainage lysimeters on grapes. Proceedings of the International Symposium on Lysimeters for Evapotranspiration and Environmental Measurements; Honolulu, HI, USA; 23 July 1991 through 25 July 1991

Finnigan J (2000) Turbulence in plant canopies. Ann Rev of Fluid Mech 32:519-557

Foken T, Aubinet M, Leuning R (2012) The Eddy Covariance Method. In: M Aubinet et al. (eds) Eddy covariance: a practical guide to measurement and data analysis. Springer Atmospheric Sciences. pp 1-19

Francone C, Katul GG, Cassardo C, Richiardone R (2012) Turbulent transport efficiency and the ejection-sweep motion for momentum and heat on sloping terrain covered with vineyards. Agric For Meteorol 162-163: 98-107

Gao W, Shaw RH, Paw U KT (1989) Observation of organized structure in turbulent flow within and above a forest canopy. Bound-Layer Meteorol 47:349-377

Greenspan MD and Matthews MA (1996) On-site vineyard water status from simple and complex canopy models. In, International Conference on Evapotranspiration and Irrigation Scheduling, C. R. Camp (Ed.), American Society of Agricultural Engineers 650-655

Heilman JL, McInnes KJ, Savage MJ, Gesch RW, Lascano RJ (1994) Soil and canopy energy balances in a west Texas vineyard. Agric For Meteorol 71:99-114

Hicks BB (1973) Eddy fluxes over a vineyard. Agric For Meteorol 12:203-215

Hillel, D (2004) Introduction to environmental soil physics. Elsevier Academic Press, Amsterdam.

van den Hurk BJJM, Verhoef A, van den Berg AR, de Bruin HAR (1995) An intercomparison of three vegetation/soil models for a sparse vineyard canopy. Q J R Meteorol Soc 121:1867-1889

Kato I, Naito Y, Taniguchi R (1965) Studies of evapotranspiration 4. the amounts of transpiration and evapotranspiration in a vineyard. Bulletin Tokai-Kinki National Agricultural Experimental Station 13:54-69

Katul GG, Kuhn G, Schieldge J, Hsieh CI (1997) The ejection-sweep character of scalar fluxes in the unstable boundary layer. Bound-Layer Meteorol 83(1):1-26

Kernich AM (1985) Measurements of seasonal evapotranspiration from non-homogeneous vegetation using EPER. Hydro and Water Res Symp 85(2):187-19

Kline SJ, Reynolds WC, Schraub FA, Runstadler PW (1967) The structure of turbulent boundary layers. J Fluid Mech 30:741-773

Kool D, Kustas WP, Ben-Gal A, Lazarovitch N, Heitman JL, Sauer TJ, Agam N (2016) Energy and evapotranspiration partitioning in a desert vineyard. Agric For Meteorol 218-219:277-287

Kordova L, Mahrer I, Schwartz C (2000) Estimation of actual evapotranspiration from vineyard by utilizing eddy correlation method. Proc. 3rd IS on Irrigation Hort. Crops. Acta Hortic 537:167-175

Kustas WP, Norman JM (1999) Evaluation of soil and vegetation heat flux predictions using a simple two-source model with radiometric temperatures for partial canopy cover. Agric For Meteorol 94:13-29

Kustas WP, Nieto H, Morillas L, Anderson MC, Alfieri JG, Hipps LE, Villagarcia L, Domingo F, Garcia M (2016) Revisiting the paper "Using radiometric surface temperature for surface energy flux estimation in Mediterranean drylands from a two-source perspective". Remote Sens Environ 184:645-653

Kustas WP, Anderson MC, Alfieri JG, Knipper K, Torres-Rua A, Parry CK, Nieto H, Agam N, White WA, Gao F, McKee L, Prueger JH, Hipps LE, Los S, Alsina MM, Sanchez L, Sams B, Dokoozlian N, McKee M, Jones S, McElrone A, Heitman JL, Howard AM, Post K, Melton F, Hain C. (2018) The grape remote sensing atmospheric profile and evapotranspiration experiment. Bull Amer Meteor Soc 99:1791-1812

Lee Y-H (2009) The influence of local stability on heat and momentum transfer within open canopies. Bound-Layer Meteorol 132:383-399

Mahrt L (1989) Intermittency of atmospheric-turbulence. J Atmos Sci 46:79–95

Mahrt L (1998) Stratified boundary layers. Bound-Layer Meteorol 90: 375-396

McInnes KJ, Heilman JL, Lascano RJ (1996) Aerodynamic conductances at the soil surface in a vineyard. Agric For Meteorol 79:29-37

Norman JM, Kustas WP, Humes KS (1995) Source approach for estimating soil and vegetation energy fluxes in observations of directional radiometric surface temperature. Agric For Meteorol 77:263-293

Oliver HR and Sene KJ (1992) Energy and water balances of developing vines. Agric For Meteorol 61:167-185

Ortega-Farias S, Carrasco M, Olioso A, Acevedo C, Poblete-Echeverria C (2007) Latent heat flux over cabernet sauvignon vineyard using the Shuttleworth and Wallace model. Irrigation Sci 25:161-170

Paw U KT, Brunet Y, Collineau S, Shaw RH, Maitani T, Qiu J, Hipps L (1992) On coherent structures in turbulence within and above agricultural plant canopies. Agric For Meteorol 61:55-68

Peixoto JP and Oort AH (1992) Physics of climate. American Institute of Physics

Poblete-Echeverria C, Ortega-Farias S (2009) Estimation of actual evapotranspiration for a drip-irrigated merlot vineyard using a three-source model. Irrigation Sci 29:65-78

Poulos GS, Blumen W, Fritts DC, Lundquist JK, Sun J, Burns SP, Nappo C, Banta R, Newsom R Cuxart J, Terradellas E, Balsley B, Jensen M (2002) CASES-99: A comprehensive investigation of the stable nocturnal boundary layer. Bull Amer Meteor Soc 83:555-581

Quattrochi D (Ed.) and Luvall J (Ed.) (2004) Thermal Remote Sensing in Land Surface Processing. Boca Raton: CRC Press

Raupach MR (1981) Conditional statistics of Reynolds stress in rough-wall and smooth-wall turbulent boundary layers. J Fluid Mech 108:363-382

Raupach MR, Finnigan JJ, Brunet Y (1996) Coherent eddies and turbulence in vegetation canopies: The mixing-layer analogy. Bound-Layer Meteorol 78:351-382

Robinson J (Ed.) (2006) The oxford companion to wine (3rd ed.) Oxford University Press

Robinson SK (1991) Coherent motions in the turbulent boundary layer. Ann Rev Fluid Mech 23:601-639

Shapland TM, Snyder RL, Smart DR, Williams LE (2012) Estimation of actual evapotranspiration in winegrape vineyards located on hillside terrain using surface renewal analysis. Irrigation Sci 30(6):471-484

Semmens KA, Anderson MC, Kustas WP, Gao F, Alfieri JG, McKee LG, Prueger JH, Hain CR, Cammalleri C, Yang Y, Xia T, Sanchez L, Alsina M, Velez M (2016) Monitoring daily evapotranspiration over two California vineyards using Landsat 8 in a multi-sensor data fusion approach. Remote Sens Environ 185: 155-170

Shaw RH, Tavangar J, Ward DP (1983) Structure of Reynolds stress in a canopy layer. J Climate Appl Meteorol 22:1922-1931

Spano D, Snyder RL, Duce P, Paw U KT (2000) Estimating sensible and latent heat flux densities from grapevine canopies using surface renewal. Agric For Meteorol 104:171-183

Trambouze W, Bertuzzi P, Voltz M (1998) Comparison of methods for estimating actual evapotranspiration in a row-cropped vineyard. Agric For Meteorol 91(3-4):193-208

Vassilicos JC (2010) Intermittency in turbulent flows. Cambridge: Cambridge University Press

Weiss A and Allen LH (1976) Air-flow patterns in vineyard rows. Agric For Meteorol 16:329-342

CHAPTER II
INTERMITTENCY OF WATER VAPOR FLUXES FROM VINEYARDS DURING LIGHT WIND AND CONVECTIVE CONDITIONS[1]

2.1 Introduction

A large portion of global vineyard cultivation occurs in semi-arid regions where water is limited, and uncertainty of water resources is growing, while water use by the crop is high (Kool et al. 2016). In addition, it is recognized that modest water stress during certain points in the growing season can improve grape and wine quality (Robinson 2006). Given these factors, there is a need for daily, field-scale estimates of evapotranspiration (ET) in order to more precisely manage vineyard irrigation and water use. Transport of water vapor away from plant canopies occurs chiefly through turbulence and in turn turbulent water vapor transport can be measured. The most commonly deployed micrometeorological method to quantify ET is eddy covariance. However, the method typically represent values for a small area, involves expensive equipment, and requires expertise to interpret findings. Though there exist several well-developed eddy covariance flux networks globally, these networks are unable to retrieve continuous, spatial estimates of ET over large heterogeneous landscapes.

---

[1] Portions of this chapter were published in the journal Irrigation Science of Springer Nature as Los, S.A., Hipps, L.E., Alfieri, J.G., Kustas, W.P., Prueger, J.H. (2019). Intermittency of water vapor fluxes from vineyards during light wind and convective conditions. Irrigation Sci. 37:281-295, DOI 10.1007/s00271-018-0617-5.

Increasing success has been made estimating ET from vegetated surfaces through combining remote sensing information with soil-vegetation-atmosphere transfer models that are able simulate turbulent exchange. The USDA Agricultural Research Service (ARS) has developed an ET modeling system known as ALEXI/DisALEXI (Atmospheric Land EXchange Inverse/Disaggregation ALEXI) utilizing the Two-Source Energy Balance model (TSEB) land surface scheme (Norman et al. 1995) to estimate turbulent fluxes using satellite measured land surface temperature (Semmens et al. 2016). The TSEB approach computes energy exchanges by partitioning a surface between soil and vegetation components and then solving for energy balance along a set of temperature gradients between these components, a canopy air temperature, and the air temperature of the surface layer above (Anderson et al. 2005). This modeling system has successfully been validated over a number of homogeneous natural and agricultural landscapes, and shows significant promise in providing field-scale estimates of ET for more heterogeneous surfaces such as vineyards. However, unknowns remain on the particular complexities involved in vineyard ET processes and how well these complexities are handled by the TSEB approach. The Grape Remote Sensing Atmospheric Profile and Evapotranspiration eXperiment (GRAPEX) seeks to validate ALEXI/DisALEXI performance for vineyard surfaces and to generate new knowledge of energy balance and transport processes in vineyards. The study reported here emerges from these general goals of the GRAPEX investigations.

Measurement and modeling methods to estimate evapotranspiration through turbulent exchange, such as TSEB, rely on assumptions of how transport by turbulence is behaving over specific lengths of time. In the eddy covariance method, flux-averaging

periods of 30 to 60-minute increments are typically used near the surface (Foken et al. 2012) in order to capture a sufficient sample of all fluctuations contributing to the flux. Remotely-sensed ET/energy balance models connect vertical transport to time-averaged vertical gradients with the assumption that the remotely-sensed land surface temperature, collected instantaneously, can represent a suitable time-averaged value in flux-gradient formulations (Kustas et al. 2002). Thus, there is an implicit assumption that turbulence fluxes will have a reasonably steady behavior over the averaging period, in order for the averaged vertical gradients to be directly proportional to the fluxes. This includes a premise that a sufficient number of transport events occur during the averaging period whose separations in time are small enough relative to the averaging period to be considered pseudo-homogeneous. In other words, here *steady* behavior refers to the case where the distribution of scalar transport in time is fairly consistent, and variations occur at a high enough frequency as compared to the averaging period length. However, it is known that a number of factors can cause turbulence in plant canopies to deviate from this ideal (Finnigan 2000), and indeed some degree of non-steady, intermittent behavior, at various time and space scales, can often be expected.

Intermittent behavior in boundary turbulence may arise from global processes external to the surface layer, such as large-scale eddies that are irregularly distributed in time and space (Mahrt 1989) or from large convective thermal plume structures in the planetary boundary layer (Li and Bou-Zeid 2011). But, it may also originate as local, small-scale intermittency caused by shear-gradient effects related to complexities in foliage and canopy structure of the local surface (Lee 2011). Much of the previous work on intermittent boundary layer turbulence has been concentrated on nocturnal stable

stratification where global intermittency appears as distinct episodes of activity separated by relatively longer quiescent periods with little activity (Mahrt 1998; Poulos et al. 2001; Ansorge and Mellado 2014). For daytime conditions with neutral or unstable stability, studies have focused on the presence of coherent motions such as *ejections* and *sweeps* within the wind field. This behavior often manifests as ramp-like signatures in scalar time series where the slow accumulation of a scalar near the surface is followed by a sudden drop as near surface air is vented. The relative importance of ejections and sweeps on momentum and heat transport from plant canopies has been extensively studied (Shaw et al. 1983; Katul et al. 1997; Finnigan 2000) and it has become clear that fluxes from heterogeneous canopies can be significantly influenced by coherent turbulent events (Gao et al. 1989; Paw U et al. 1992).

Despite the importance of episodic behavior, defining intermittency quantitatively has remained difficult (Vassilicos 2010), since it is describing properties more profound than simple measures of variability, or even harmonics. It is associated with high amplitude variability and the uneven *clustering* of events, and methods such as telegraphic approximation have been applied to relate individual properties such as clustering to sources of intermittent variability such as foliage and atmospheric stability (Cava and Katul 2009). However, these individual properties are unable to completely capture the range of behaviors that can be considered intermittent, since intermittency arises from the interplay between coherent spatial structures in the wind field, heterogeneity in the surface, and thermal stratification (Lee 2011). For example, as the boundary layer becomes increasingly convective, ejection-sweep features become altered by the large influence of buoyancy effects, and transition from eddy structures toward

primarily large, low-frequency thermal plume structures (Li and Bou-Zeid 2011). Given this complex interplay, intermittency may manifest in momentum and scalar time series in a variety of ways beyond simple ramp-like features.

In the case of vineyards in semi-arid climates, both the physical vineyard structure and the local atmospheric conditions serve as confounding factors that could complicate turbulence and the resulting transport processes that govern vineyard ET. The canopy is organized in the sense that there are rows, but the spatial variability of the foliage extensions into the interspace presents a complicated pattern to the wind field, while depending on vineyard management, the foliage of the canopy crown can be quite heterogeneous as well. Shear across the overall surface is therefore relatively non-uniform as portions of eddies dissipate energy unevenly across the canopy row spacing and individual roughness elements in the crown. The partially open canopy, where substantial radiation reaches the soil surface, suggests that local buoyancy will be important in altering eddy morphology (Lee 2009). Chahine et al. (2014) conducted large eddy simulations of vineyards and compared them to 3-D anemometry measurements to examine wind direction/row structure interactions on local scale transport. They found that cross-row flow behaved similarly to that of a more uniform canopy, while along-row flow showed increased spatial variability, increased intermittency of turbulence, and resulted in larger fluxes of momentum. Further, the growing season of warm, semi-arid climates often features strong, persistent synoptic high pressure and resulting subsidence (Peixoto and Oort 1992). This can result in small horizontal winds, even during the day, and the large radiation often induces unstable, convective conditions near the surface, leading to infrequent, large convective structures.

If intermittent, episodic exchange events were pronounced in conditions frequent to semi-arid vineyard settings, this could have important implications for measurement and modeling methods by lengthening the necessary flux averaging period and calling into question flux-gradient assumptions in model formulations. Because light wind, unstable conditions that may favor intermittent behavior are somewhat common in many winegrowing regions, there is a need to address these concerns in light of their possible impact on efforts to monitor vineyard ET.

Two general questions emerge. First, how large is the intermittent behavior of water vapor flux or ET from vineyards during light wind and strongly convective conditions? Second, how are moisture transport processes altered during intermittency in ways that have implications for eddy covariance methodology, and for ET models? In this study we examine the intermittent behavior of water vapor exchanges in vineyards. The specific objectives are: (1) to document the relative importance of lower frequency and episodic exchange events during periods of light wind and large convection and (2) to quantify how intermittency in the water vapor exchanges affects key properties of turbulent water vapor transport and the required averaging period for eddy covariance fluxes.

2.2 Materials and methods

Site Description

The sites for this study were part of the USDA-ARS Grape Remote sensing Atmospheric Profile and Evapotranspiration eXperiment (GRAPEX), consisting of two drip-irrigated vineyards closely located in California's Central Valley near Lodi, CA (38.29 N, 121.12 W, 38.4 m elev.). The two sites were each relatively flat blocks of *V. vinifera* (Pinot Noir), with one being 7 years old (north block, site #1) and one 4 years old (south block, site #2) at the beginning of the 2014 growing season. Fig. 2.1 depicts the study area location and layout of the two study vineyard blocks. The area experiences a semi-arid Mediterranean climate, typical of many areas in California, with precipitation almost entirely confined to the cool season and very little if any during the growing season. Daytime conditions during the growing season typically consisted of high maximum air temperatures (35 – 40+ °C) and mostly clear skies with high net radiation (>500 – 600 W m^2). Winds were often light before noon (< 1 – 2 m s^{-1}), strengthening gradually during the day, and often peaking in the mid to late afternoon (~ 2 – 4 m s^{-1}), though periods of light winds could be observed throughout the day.

Vines at both sites were grown on identical quadrilateral cordon fixed trellis systems with rows oriented East-West. The rows were spaced at ~3.35 m with individual vines spaced along the row at ~1.52 m increments and maximum canopy height during the growing season typically reaching ~2.5 m. Late into the growing season vine growth extended the canopy laterally into the row interspace. This growth was partially

governed by the vineyard management, but resulted in a complex spatial pattern of foliage. The inter-row surface within the vineyards consisted of a grass cover crop that typically senesced early in the growing season as spring precipitation ended. Directly below the vine canopy in each row was a strip of bare soil that was moistened routinely by the above ground drip irrigation. The elevated canopy/trellis structure included a significant open space between the bottom of the canopy crown and the soil surface below of ~0.7 m in height occupied nearly exclusively by the narrow trellis posts and drip irrigation line.

Instrumentation

Data presented here were collected during intensive observation periods (IOPs) of several days each conducted 3-4 times throughout the 2014, 2015, and 2016 growing seasons resulting in a total of 39 days of measurements from each of the two sites. Surface fluxes and environmental conditions were measured at two towers, one at each site, placed near the eastern edge of the respective vineyard block so to enjoy maximum footprint from the dominantly westerly winds (Fig 2.1), achieving a typical fetch of ~400 m. Fluctuations of 3-D wind velocities and water vapor above the canopy were measured on each tower using an IRGASON, combining a 3-D sonic anemometer (CSAT-A, Campbell Scientific Inc., Logan, UT[2]) and open path infrared gas analyzer (EC-150,

[2] The mention of trade names of commercial products in this article is solely for the purpose of providing specific information and does not imply recommendation or endorsement by the US Department of Agriculture.

Campbell Scientific Inc., Logan, UT). These instruments were mounted facing due West at a height of 5 m agl. Net radiation was measured from the tower at 6.5 m agl using a four-component net-radiometer (CNR-1, Kipp & Zonen, Delft, The Netherlands). Soil heat flux was calculated using a diagonal transect of five equidistant (0.92 m) soil heat flux plates immediately south of each tower that extended from beneath one canopy row and across the row-space to beneath the next canopy row. The plates were placed at 0.08 m depths (HFT-3, Radiation Energy Balance Systems, Bellevue, WA) with two thermocouples near each plate at 0.02 and 0.06 m depths and soil moisture probes (HydraProbe, Stevens Water Monitoring Systems, Portland, OR) at 5 cm depth. An additional open-path IRGA (LI-7500A, LI-COR Biosciences, Inc., Lincoln, NE) was placed in the row space between canopies immediately north of each tower at a height of 1.5 m agl (Fig. 2.1). The term *within canopy* here describes these IRGA measurements from the inter-row space below the canopy top, but outside the true canopy crown. The within canopy IRGAs were sampled by each tower's datalogger such that they were synchronized with the other tower instrumentation. Data were sampled by a CR3000 datalogger (Campbell Scientific Inc., Logan, UT) at a sampling rate of 20 Hz except for two IOPs during 2016 where the sampling rate was lowered 10 Hz due to technical constraints. A more detailed description of site and instrumentation details is presented by Kustas et al. (2018).

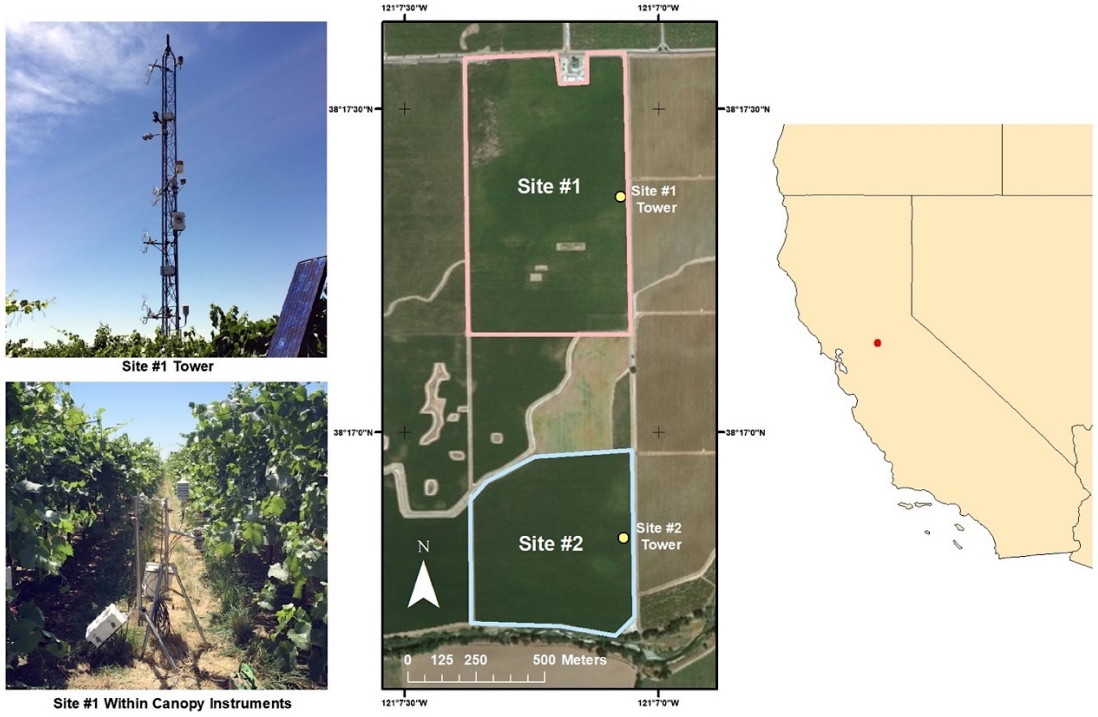

Fig. 2.1 Locations of the two GRAPEX sites. The northern vineyard block (site #1) is outlined in red, while the southern block (site #2) is outlined in blue. Tower locations, and collocated within canopy instruments, are marked with yellow dots. Photographs of the tower and within canopy instrumentation from site #1 are also shown.

Analyses

Fast response measurements of velocity and water vapor were quality-controlled, including removing periods of bad or missing data, spike detection, and replacement when possible. Periods of interest were selected from the daytime hours (7:00 – 19:00 LST) of the 39 IOP days at both sites for further analysis. Time series of the vertical wind component (U_z, m s^{-1}), water vapor density (ρ_v, g m^{-3}), and instantaneous vertical water vapor transport ($U_z{}' * \rho_v'$, g m^{-2} s^{-1}) were plotted and visually surveyed to initially

qualitatively isolate periods of high amplitude fluctuations that appeared episodic and unequally spaced in time. Likewise, periods of relatively frequent and more evenly spaced fluctuations were also identified. A quantitative procedure for this discrimination was also employed, as discussed later. Selected periods were restricted to predominately along row flow, i.e. from the West, to eliminate complicating effects on turbulence of changes in wind direction with row orientation (Alfieri et al. 2018). The result was two sets of periods, one of 100 individual hours classified as intermittent and one of 100 individual hours classified as steady. These data sets were used to statistically compare the differences between the two behaviors in terms of fluxes and atmospheric conditions including mean winds, stability, and vapor pressure deficit.

Custom computer scripts were used to calculate hourly turbulent fluxes of sensible heat (H) and latent heat (λE) from the 5 m fast response data for all selected periods. Corrections applied during flux computations included a simple 2-D coordinate rotation, detrending, frequency corrections (Massman 2000), density corrections (Webb et al. 1980), as well as other corrections and computations to the raw covariances. Soil heat flux (G) was calculated as the sum of the heat flow across the heat flux plates (G_p) and the term for storage in the soil layer above the heat flux plates (G_s) as $G = G_p + G_s$ (Campbell and Norman 1998). In addition to these fluxes, the friction velocity u_* and the stability parameter z/L were calculated at z = 5 m for each hour, where L is the Monin-Obukhov length scale (Stull 1988).

Time series of U_z and ρ_v for the 100 periods within each set were compared to time series of mean hourly horizontal wind (U_{horiz}) and z/L. Through this approach the concurrent timing of changes in mean wind and stability with the onset and duration of

intermittent behavior was examined. To quantify the time scales of fluctuations in humidity and the vertical flux of moisture, particularly in the low frequencies, a further subset was isolated from each of the 100-hour sets consisting of 10 representative two-hour periods for each, where the classified behavior, either intermittent or steady, persisted through two consecutive hours. These two subsets were used in order to capture the influence of potential low frequency behavior during spectral analysis and analysis of flux averaging periods explained below.

In-house code written to perform discrete Fourier transforms was used to detrend the data, apply a Hann window, assemble power spectra and cross-spectra for the sub-selected periods, and apply a smoothing routine to the raw spectra. Cross-spectra for vertical velocity and water vapor density (U_z, ρ_v) were computed from the 5 m eddy covariance instruments and averaged for each set, producing an average water vapor flux cross-spectra for each behavior. Further, to quantify the relationships of humidity fluctuations between the surface layer above the canopy and the canopy sub-layer, power spectra and cross-spectra were created for the two 10-period subsets from water vapor density measurements both above and within the canopy. In this way the time scales of humidity changes of the individual layers, via ρ_v power spectra at each height, as well as the coherent humidity changes between the layers, via the $\rho_{v\ above}, \rho_{v\ within}$ cross-spectra, could be addressed.

Keeping in mind the interest in flux measurement and modeling, the impact of intermittent versus steady behavior on flux averaging was investigated. For eddy covariance measurements, the flux-averaging time period must be long enough to account for all eddy length and time scales that significantly contribute to the fluxes (Finnigan et

al. 2003). Near the surface, for many atmospheric conditions, 30 to 60-minute averaging periods are sufficient to capture all of the contributing eddy sizes to the turbulent fluxes. However, given that intermittency may cause turbulence to become dominated by low frequency events, longer averaging period length may be necessary to account for all processes contributing to the flux during intermittency. Cross-spectra of vertical velocity and scalars can be used to quantify the importance of low frequency fluctuations and determine if all significant scales are being captured by determining the lowest spectral peaks that are distinctly separate from the red noise at the lowest end of the spectrum associated with non-stationary effects.

Additionally, energy balance requires that the turbulent fluxes must balance with the sources and sinks of energy in the system:

$$\lambda E + H = R_{net} - G - P - S \quad (2.1$$

where R_{net} is the net radiation, S is the storage of energy by vegetation above the surface, and P is the energy used for photosynthesis (Campbell and Norman 1998). S and P are considered negligible in this case, and are neglected. Energy balance closure is therefore:

$$\frac{\lambda E + H}{R_{net} - G} \quad (2.2$$

where a value of unity would be a perfect accounting for all energy. Since errors degrade covariances, actual values for (2) are generally less than 1. Twine et al. (2000) present an approach to forcing the values to one, by first assuming the H /λE or Bowen Ration is been measured correctly. Energy is then added to H and λE in proportion to the Bowen ratio, forcing conservation of energy. Here we are concerned with the appropriate

length of the flux-averaging period, which can be determined by calculating flux values for increasingly larger time lengths until the original energy balance closure ratio approaches a maximum value. As with cross-spectra, caution must be taken to ensure a longer averaging period is not associated with significant non-stationary effects. The turbulent fluxes were calculated for the 10 two-hour periods from the intermittent and steadier period subsets using averaging periods of 15, 30, 60, 90, and 120 minutes. Energy balance closure was then computed for each averaging period length.

The discrimination between steady versus intermittent periods was initially qualitative. A simple quantitative approach to make the separation more objective is clearly desirable. Hence, we decided to quantify the intermittency of water vapor exchanges through the construction of simple metrics. Doing so is problematic, however, as intermittency not only exhibits low frequency turbulence events, which can be addressed via spectral methods, but also events that are both irregular and also possibly coherent. This represents not only a difference in the time scales responsible for the flux compared to more steady behavior, but also a variability in the time distribution of events at each time scale.

A first way to quantify the differing exchange behavior of the intermittent and steadier periods was to examine time series of instantaneous vertical water vapor transport ($U_z{}' * \rho_v{}'$) and document the temporal distribution of water vapor exchanges. Time series of the multiplied squared perturbations ($U_z{}'^2 * \rho_v{}'^2$) were created as well (not shown) to better assess the distribution of absolute exchange *activity* in time and these were examined for coherent and intermittent patterns. The distribution of $U_z{}' * \rho_v{}'$ values during and between distinctly coherent events was used to determine positive and

negative thresholds to isolate events that appeared to be significant from the quiescent periods between them (Fig. 2.2). The more *active* instantaneous fluxes that occurred outside the thresholds could then be summed and divided by the sum of all instantaneous flux values for the period, yielding a ratio of *active* to total flux.

$$Flux\ Ratio = \frac{\Sigma\ U_z{}'\rho_v{}'\ (points\ exceeding\ threshold)}{\Sigma\ U_z{}'\rho_v{}'\ (entire\ period)} \quad (2.3$$

Likewise, the sum of *active* time length over the total period length was calculated to yield the ratio of time of active flux divided by total time.

$$Time\ Ratio = \frac{\Sigma\ s\ (points\ exceeding\ threshold)}{\Sigma\ s\ (entire\ period)} \quad (2.4$$

Then the ratio of (3) over (4), a unitless flux/time ratio, is a metric of the degree of intermittency in the flux, where larger values of flux ratio divided by smaller values of time ratio denote more intermittency.

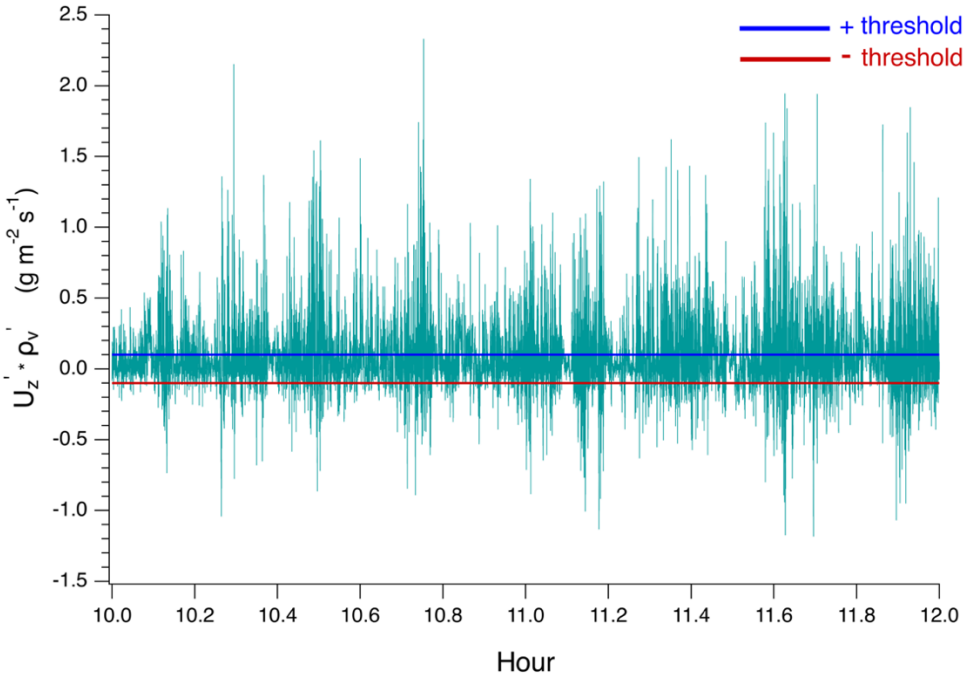

Fig. 2.2 Time series of instantaneous vertical water vapor transport at z = 5 m during period 8:00 – 10:00 LST on DOY 152 of 2015 at site #1. Positive and negative thresholds for the period are shown.

A second approach was constructed as follows (Hipps, personal communication). Since turbulence kinetic energy (TKE) is such a fundamental property of the intensity of turbulence, we first computed the time series of TKE values. Then the standard deviation of TKE was determined using several windows of different lengths (20, 600, 1200, 2400, 3600 and 4800 consecutive points). At the 20 Hz sampling rate, these translated to 1, 30, 60, 120, 180 and 240 s). For each window, the standard deviation of TKE was determined for each window location, then averaged with the window's passage over the entire time series. For a purely random time series, the value of the standard deviation would be identical for all window sizes. As expected, the standard deviation value grew

larger as the window was expanded, reaching a maximum no later than the 4800 value. The ratio of the maximum value of standard deviation to the minimum value (always at the shortest window), defines the strength of episodic behavior. Fig. 2.3 shows the results of the ratio for a number of the cases previously identified as steady or intermittent. The results clearly show a rather clean differentiation at a ratio value of about 2.6. The results of this quantitative approach did reverse several of the earlier classifications of steady versus intermittent based on the qualitative criteria. This approach then quantitatively defines steady versus intermittent in this study.

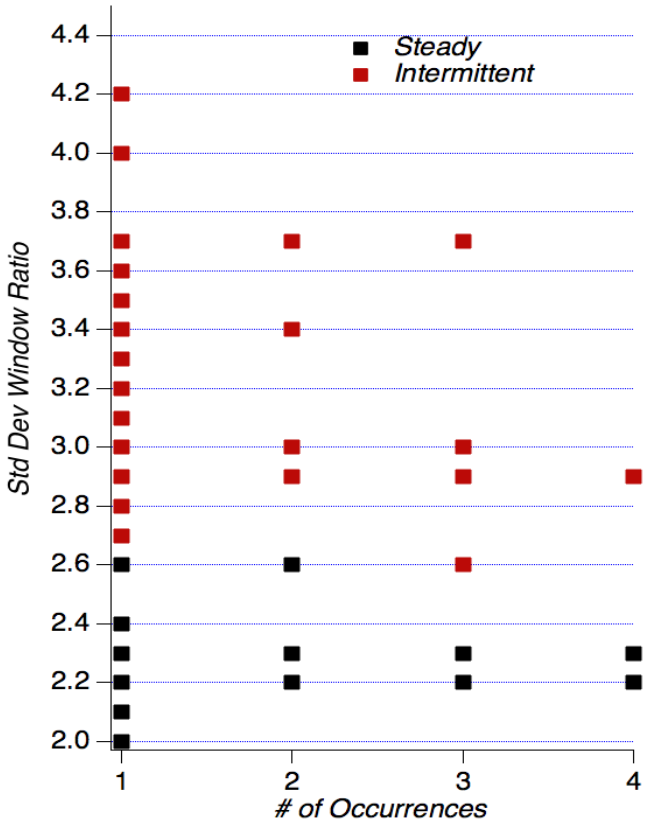

Fig. 2.3 Ratio of max/min standard deviation of TKE in set of windows for various cases identified as steady or intermittent. A demarcation is apparent at the value 2.6.

2.3 Results

Here we report results from comparative analyses between periods demonstrating episodic, intermittent behavior and those displaying relatively steadier behavior. We focus first on connecting time series of velocity & humidity to time-variations in atmospheric conditions and present summary statistics for observed conditions during the two time-period types. Next, we discuss power and cross-spectra results in order to examine the dominant time scales of exchanges and humidity fluctuations above and within the canopy, with particular emphasis on the influence of low frequency variability. Then we describe efforts to quantify differences between the two behaviors that arise from the temporal distributions of flux events, including the impact on flux averaging periods.

Time Series and Atmospheric Conditions

Across the three growing seasons the vast majority of IOP days had dry conditions and dominant west winds ideal for the purposes of this study. Surveying time series of U_z and ρ_v at both sites, and from both above and within the canopy, presented a range of behaviors between what could be qualitatively classified has intermittent or steady. However, distinctly intermittent periods and distinctly steadier periods of one to four hours in length were frequently observed for nearly all IOP days. Examples of these distinct periods are illustrated in Fig. 2.4 for two periods during the afternoon of DOY 191 of 2015 from site #1. Fig. 2.4a demonstrates a 40-minute section of behavior identified as intermittent, where time series for humidity and vertical velocity show a

patchy distribution of relatively high amplitude fluctuations separated by durations of quiescent activity. Fig. 2.4b is a 40-minute example of steady behavior; occurring about an hour after the example in Fig. 2.4a. Here, fluctuations are considerably more consistent in both amplitude and distribution in time. Fig. 2.4c and Fig. 2.4d present $U_z{}' * \rho_v{}'$ time series during the same two periods. Here the contrast between the two periods is even more evident with the first period exhibiting strong, low-frequency clustering in time not apparent in the second period. By surveying periods in this manner, the 100 representative hours of each behavior type were initially isolated into two sets for comparison in the subsequent analyses.

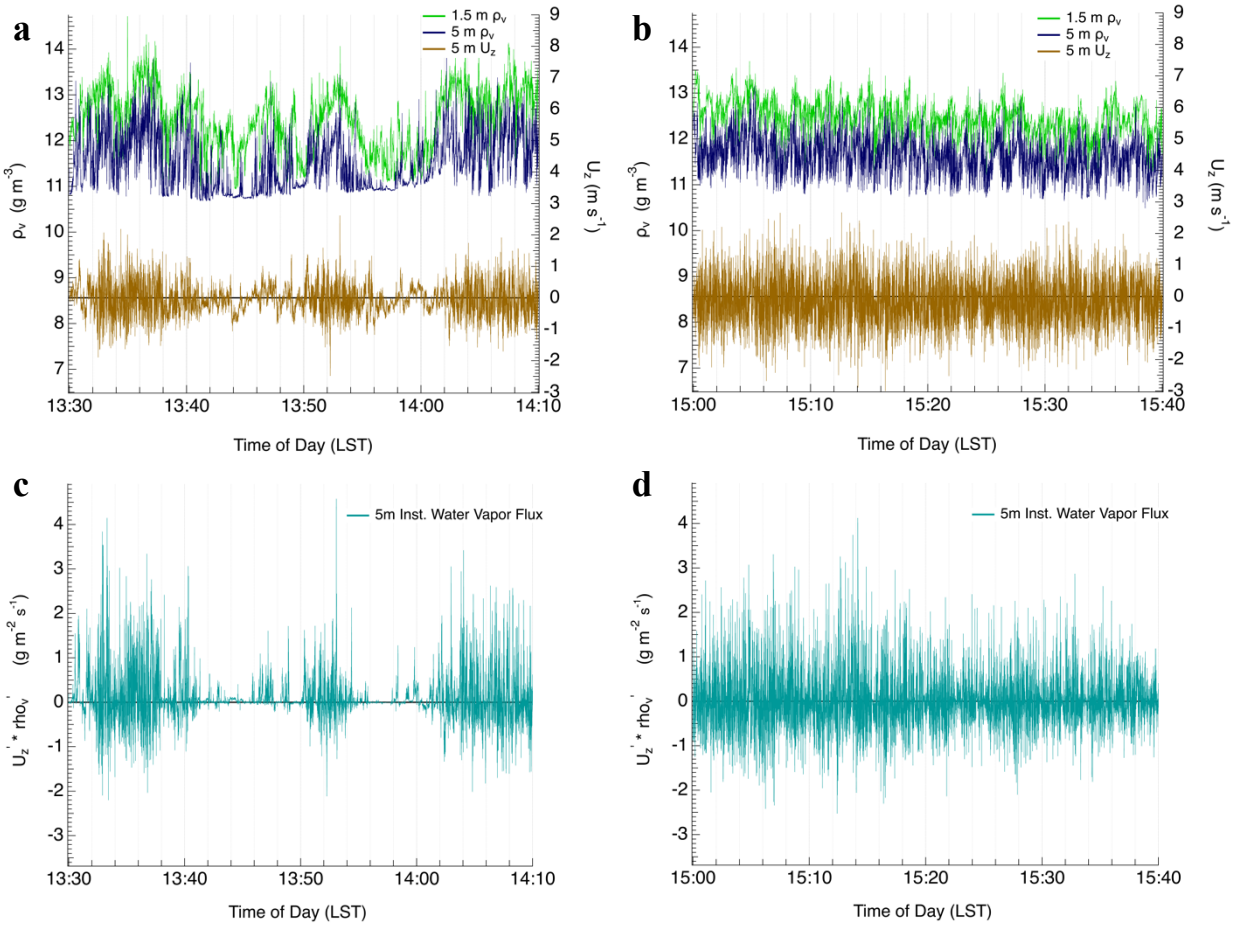

Fig. 2.4 Time series of the z=5 m (blue) and z=1.5 m (green) water vapor density (ρ_v), and 5 m vertical wind (U_z) for two 40-minute periods on DOY 191 of 2015. (**a**) intermittent fluctuations; (**b**) more steady fluctuations. Also, time series of the instantaneous water vapor transport, for intermittent case (**c**); steady case (**d**).

A first effort was to establish general relationships between the occurrence of the contrasting behaviors and atmospheric conditions. Fig. 2.5a presents humidity, above and within the canopy, and the above canopy vertical wind component again for DOY 191 of 2015 from site #1, but for a longer period from 09:30 LST to 18:30 LST. During the late morning hours, time series become increasingly transient, displaying a patchy

distribution of large variations interspersed with smaller, more consistent values. Around 15:00 LST there was a relatively rapid transition to a period of steadier activity where U_z and ρ_v fluctuations occurred more uniformly at higher frequencies. This type of distinct transition between periods of intermittent and more steady behavior was found to occur frequently and served as a convenient cutoff between the two behaviors for period selection.

Fig. 2.5b depicts U_{horiz} and z/L for the same daytime period. Here mean U_{horiz} decreased from higher morning values to values below 1.5 m s^{-1} during the 11:00 – 14:00 LST time period, before increasing to ~2.9 m s^{-1} by 16:00 LST. Values of z/L became increasingly negative during this light wind period before becoming less negative while winds increased into the afternoon. This example expresses a pattern common to nearly all of the intermittent periods where they initiated at the onset of light winds and more unstable conditions. Conversely, periods classified as steady were most often associated with transitions to higher mean winds and lower instability.

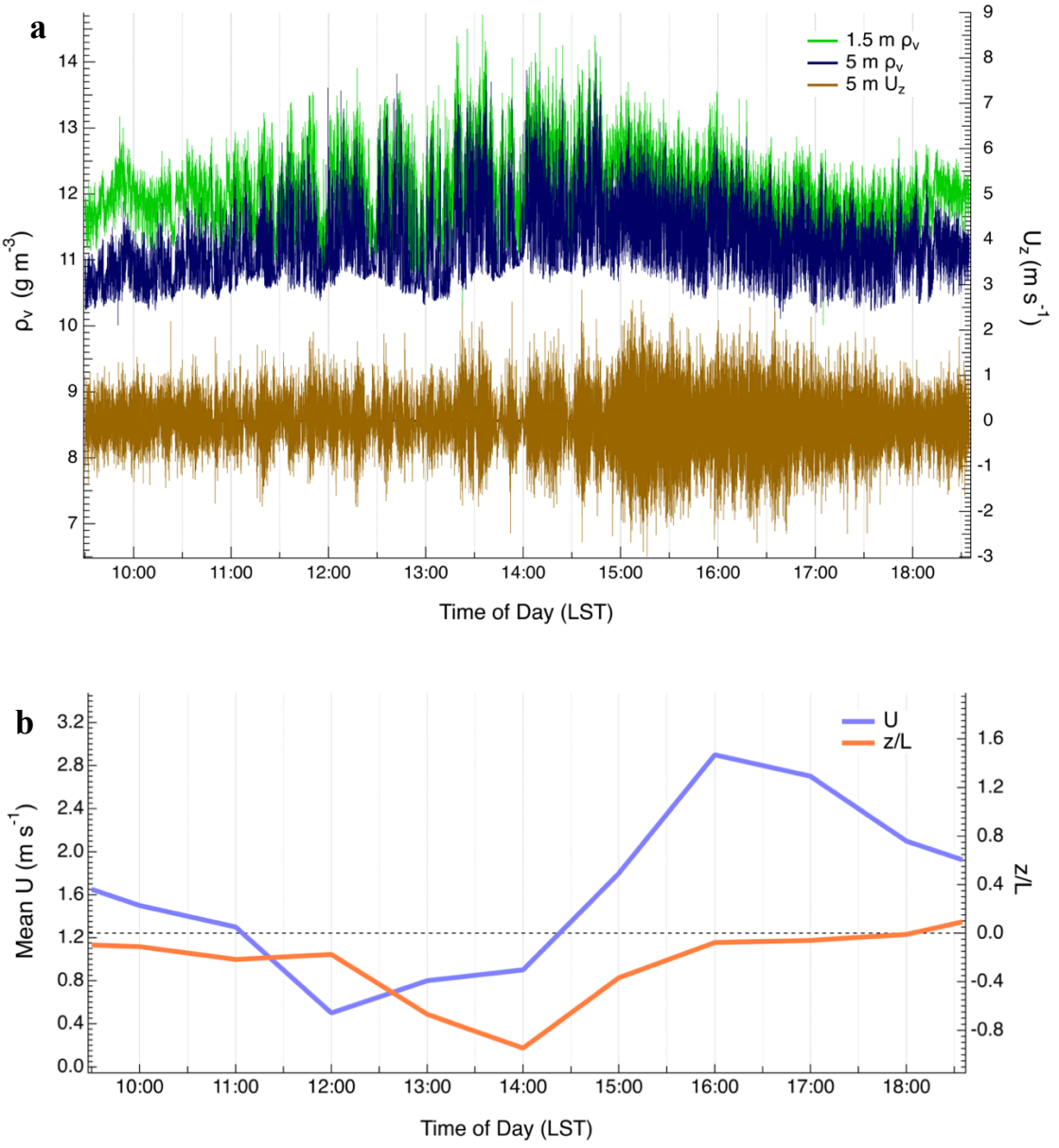

Fig. 2.5 (**a**) Time series of the 5 m (above canopy, in blue) and 1.5 m (within canopy, in green) water vapor density, and 5 m vertical wind component for 9-hour period on DOY 191 of 2015 at site #1. (**b**) Hourly mean horizontal wind and stability parameter (z/L) for the same period.

These associations between wind velocity, stability, and behavior are quantitatively summarized through comparative statistics for key variables from the 100 intermittent and 100 steady hour sets (Table 2.1). Fluxes of net radiation, sensible heat, and latent heat are consistently higher for the intermittent periods than for the more steady periods. This can largely be explained by the fact that hours classified as intermittent occurred most often during the midday, with greater than 68% of the periods having fallen between the hours of 10:00 and 14:00 LST. Most of the steady periods, however, took place later in the afternoon (after 13:00 LST), with a smaller portion associated with the hours before mid-morning (before 10:00 LST), and few during midday. Energy balance closure was higher for steady hours (0.89), compared to intermittent hours (0.85). Intermittent hours also had larger variability in closure values as denoted by the difference in standard deviations. As expected, mean horizontal wind and friction velocity were notably lower for the intermittent cases, which were also associated with higher instability as indicated by their lower mean z/L. This mean value of z/L for the intermittent periods is not especially large (-0.33), though it was variable with a standard deviation near the magnitude of the mean. Of the intermittent periods, 16 had z\L values of -1.00 or below, while the lowest value for a steady period was -0.41. In tandem with light winds, behavior of time series seemed to be quite sensitive to small changes in instability. Vapor pressure deficit was more or less consistent between the period sets, a notable consistency in the mean humidity and evaporative demand despite the increased amplitude of fluctuations present during intermittency compared to steady behavior.

Table 2.1 Means, standard deviations, T-statistics, and p-values of key variables for intermittent and steady periods. The critical T-statistic for a p = 0.001 is |3.39|, for significance of differences between means of each period.

		R_{net} W m^{-2}	H W m^{-2}	λE W m^{-2}	Closure	VPD kPa	U_{horiz} m s^{-1}	$u*$ m s^{-1}	z/L
Intermittent Periods	*Mean*	562	192	311	0.85	2.041	2.13	0.33	-0.327
	σ	110	90	85	0.09	0.794	0.40	0.07	0.325
Steady Periods	*Mean*	324	82	222	0.89	2.216	2.72	0.40	-0.071
	σ	188	91	101	0.06	0.823	0.70	0.11	0.115
	T-statistic	8.79	6.54	6.30	-4.22	0.28	-9.12	-7.55	-8.55
	p-value	2.64E-15	5.41E-10	1.96E-09	4.03E-05	0.78	3.43E-16	3.84E-12	5.03E-14

Spectra

Given the differences noted above in the characteristics of the two behavior classifications, spectra were calculated in order to estimate the structure of turbulence and time scales of transport for the two sets of conditions. Cross-spectra of vertical motion and water vapor density (U_z, ρ_v) consistently exhibited differing time scales of exchange between intermittent and more steady periods. In Fig. 2.6 cross-spectra have been averaged for the 10 representative intermittent and 10 representative steadier two-hour subset periods. The two composites are similar in the high frequencies as expected. The values grew larger as frequencies became lower for the intermittent cases, indicating more flux contribution from low frequency events. Note the log scales here, so that the differences at the lower frequency are larger than they appear. The peak value for the intermittent composite translates to time scales of an hour or more, suggesting longer

averaging periods than typically used would be necessary to recover accurate flux values. The energy balance closure analysis described later further addressed this issue.

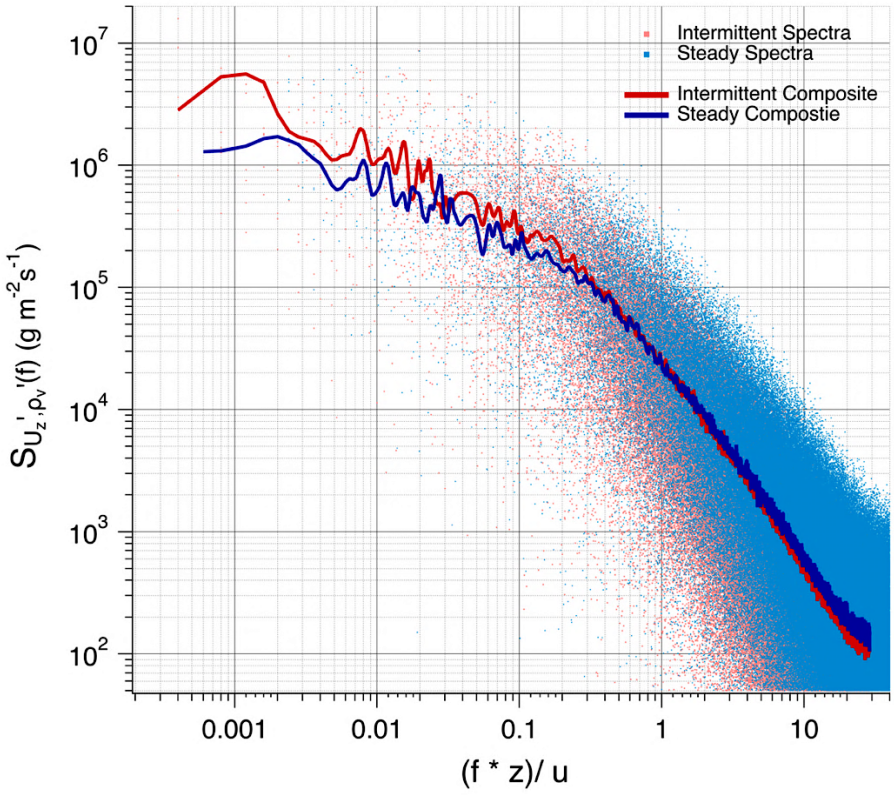

Fig. 2.6 Log-log plot of cross-spectra of vertical wind (U_z) and water vapor density (ρ_v) above the canopy (z=5 m). Spectra are depicted as points for 10 individual two-hour intervals (red) and 10 steady two-hour periods (blue). Composite average spectra for both sets of 10 intervals are shown with solid lines.

Noting both the increased variability in the amplitude and clustering of humidity fluctuations and the dominance of low frequency exchanges during intermittent periods, it becomes of interest to examine how this might be affecting the time scales of humidity variations within the canopy as compared to the air above canopy. Utilizing the

synchronized IRGAs at 5 m and 1.5 m, ρ_v power spectra were calculated separately for above canopy and within canopy subsets of 10 intermittent and 10 steady two-hour periods. Fig. 2.7 illustrates selected examples of these, comparing ρ_v power spectra for two periods on DOY 163 of 2016 from site #1. These spectra correspond to consecutive periods, one with more steady behavior from 15:00 – 17:00 LST and mean winds ~2.6 m s^{-1} (Fig. 2.7a), which was followed by a drop in mean winds to ~1.3 m s^{-1} and a quick transition to an intermittent period that extended from 17:00 – 19:00 LST (Fig. 2.7b). Spectra from the steadier period correlate strongly between the two heights, showing shared peaks across a range of frequencies, suggesting that the exchanges at the two heights are well coupled. For the intermittent period in Fig. 2.7b, the above canopy spectrum displays a relatively smooth curve in this same range of frequencies. Yet the spectrum within the canopy is somewhat reduced at the higher frequencies and some of the lower frequencies, and more variable at the lowest frequencies, suggesting the canopy is acting as a filter to various scales of transport. Similar findings were observed for the 9 other periods in each subset.

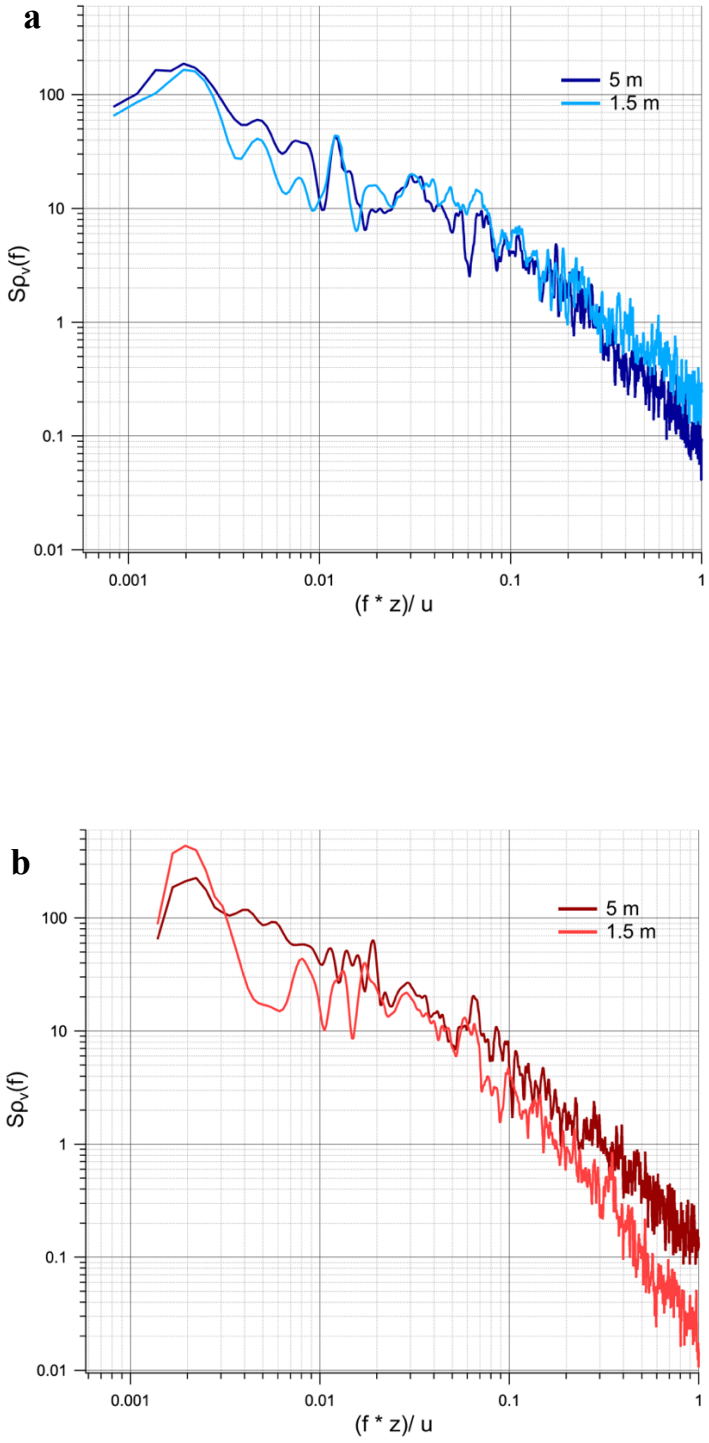

Fig. 2.7 Power spectra of water vapor density (ρ_v) above canopy (5 m) and within canopy (1.5 m) for two consecutive 2-hour periods on DOY 163 of 2016. (**a**) steady case from 15:00 – 17:00 LST and (**b**) intermittent case from 17:00 – 19:00 LST.

To further examine differences in the relationship between the above and within canopy layers, cross-spectra of water vapor density measurements from above and within the canopy ($\rho_{v\ above}$, $\rho_{v\ within}$) were also computed for the two 10-period subsets. Fig. 2.8 depicts selected examples of these corresponding to an intermittent period and more steady period both from DOY 152 of 2015 from site #2; depicted in semi-log form to emphasize the differences in the low frequencies. The results further exhibit a strong enhancement of low frequency signal during periods of intermittency. These contrasting patterns in covariance between the two behaviors were apparent in comparing all 10 periods in the two subsets.

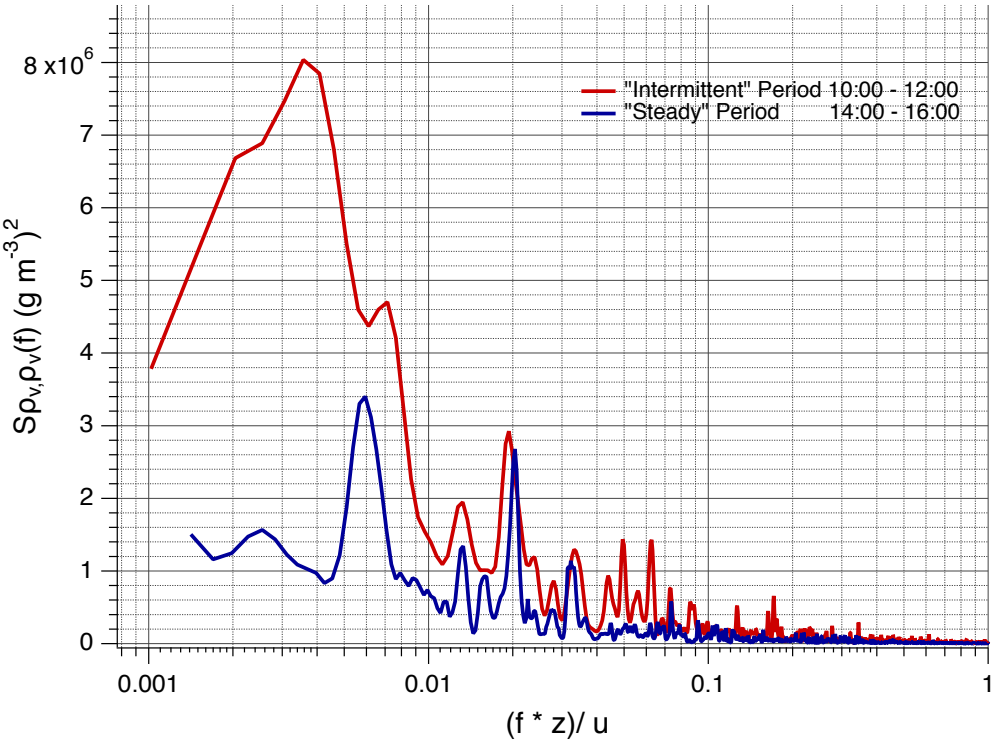

Fig. 2.8 Semi-log plot of cross-spectra of water vapor density (ρ_v) above canopy (5 m) and within canopy (1.5 m) for an intermittent and steady period at site #2.

Fluxes

Considering the impact of enhanced low frequency variability in water vapor exchange during intermittency, a next step was to address how intermittency affects the temporal distribution of transport and in turn the characteristics of the overall water vapor flux. As previously noted in Fig. 2.4c and Fig. 2.4d, distinct differences in the temporal distribution of the water vapor transport can be identified by examining the time series of U_z', ρ_v'. Intermittent periods were marked by patchy distributions of larger, infrequent exchanges, separated by less active sections of the time series, indicating that the flux is being confined to relatively short amounts of time. Steady periods, however, were characterized by smaller, more numerous events that were more consistently spaced at higher frequencies.

To better quantify these temporal distributions, $U_z' * \rho_v'$ and ${U_z'}^2 * {\rho_v'}^2$ time series, were used to isolate the dominant exchanges in the $U_z' * \rho_v'$ series, using the threshold approach depicted in Fig. 2.2, for both sets of periods of interest. The proportion of the water vapor transport that occurred above or below the thresholds, and the time over which this proportion occurred, were summed for the periods from the intermittent and more steady period subsets. Table 2.2 lists the results for a portion of the periods analyzed from both sites. Striking differences were observed between the two types of condition. On average during steadier periods 97 – 99 % of the water vapor flux occurred in 75 – 85% of the total time length for each two-hour period. During intermittent periods, however, 85 – 95% of the water vapor flux occurred in only 28 – 39% of the total time. Resulting ratios of flux per time for intermittent periods

consistently yielded much higher values than those of steadier periods, often more than double, forming two distinct groups of values between the sets. As shown previously, hours from the intermittent set were nearly always associated with lower values of mean U_{horiz} and larger negative values of z/L, and in turn we see this relationship with flux time ratio.

Table 2.2 Proportion of the water vapor flux outside the thresholds, proportion of time this flux occurred for each period, and resulting flux/time ratios for five intermittent and five periods. Also, the 5 m hourly mean horizontal wind, stability parameter z/L, and latent heat flux values from eddy covariance measurements.

Intermittent Periods

Year	DOY	Time	Site	Proportion Flux	Proportion Time	Ratio Flux/Time	z/L	U_{horiz}	λE
								m s^{-1}	*W m^{-2}*
2014	181	1200 - 1400	1	0. 91	0. 33	2. 78	-0. 399	1. 70	319. 5
2015	152	0800 - 1000	1	0. 88	0. 29	3. 02	-0. 709	1. 05	153. 7
2015	152	1000 - 1200	1	0. 94	0. 39	2. 38	-0. 542	1. 40	200. 3
2016	123	1100 - 1300	2	0. 91	0. 34	2. 67	-0. 891	1. 00	234. 4
2016	162	0900 - 1100	2	0. 90	0. 31	2. 90	-0. 174	1. 85	255. 2

Steady Periods

Year	DOY	Time	Site	Proportion Flux	Proportion Time	Ratio Flux/Time	z/L	U_{horiz}	λE
								m s^{-1}	*W m^{-2}*
2014	216	0800 - 1000	1	0. 97	0. 81	1. 24	-0.090	2.27	116.3
2015	152	1500 - 1700	1	0. 99	0. 82	1. 21	-0. 086	2. 75	185. 3
2015	152	1700 - 1900	1	0. 97	0. 75	1. 30	0. 006	3. 20	87. 1
2015	191	1500 - 1700	1	0. 99	0. 84	1. 18	-0. 068	2. 80	210. 5
2016	123	1600 - 1800	2	0. 99	0. 80	1. 23	0. 012	2. 10	180. 4

Calculations of energy balance closure for various flux-averaging period lengths revealed marked differences between intermittent and steady periods. Fig. 2.9 shows a

comparison of these calculations between the two subsets of 10 two-hour periods. For the steadier periods, energy balance closure increases with increasing averaging period through 30 minutes, peaking at 60 minutes and then decreasing for periods of 90-minutes or more. This indicates that a 30 to 60-minute period would be ideal for averaging the fluxes. However, for the intermittent periods, the closure value failed to converge to a maximum value near unity until at least 120 minutes. Of course, there is always an issue of possible non-stationarity in longer averaging periods. However, in such a case, the flux estimates would be expected to become more variable rather than converge upon a higher value. Sun et al. (2006) and others have also reported a need for similar longer averaging periods for fluxes under conditions with enhanced low frequency convection. They highlight one location where the averaging period should be 60 – 120 minutes, very similar to the case we denote here. Given the low-frequency peaks in intermittent spectra and cross-spectra that correspond to time scales of 40 minutes to greater than hour, it seems reasonable that an averaging period of 90 minutes or more would indeed be necessary under this degree of intermittency to capture all of the processes contributing to the overall flux. Of note is the clear difference in the variability of closure values for the intermittent periods versus the more steady periods.

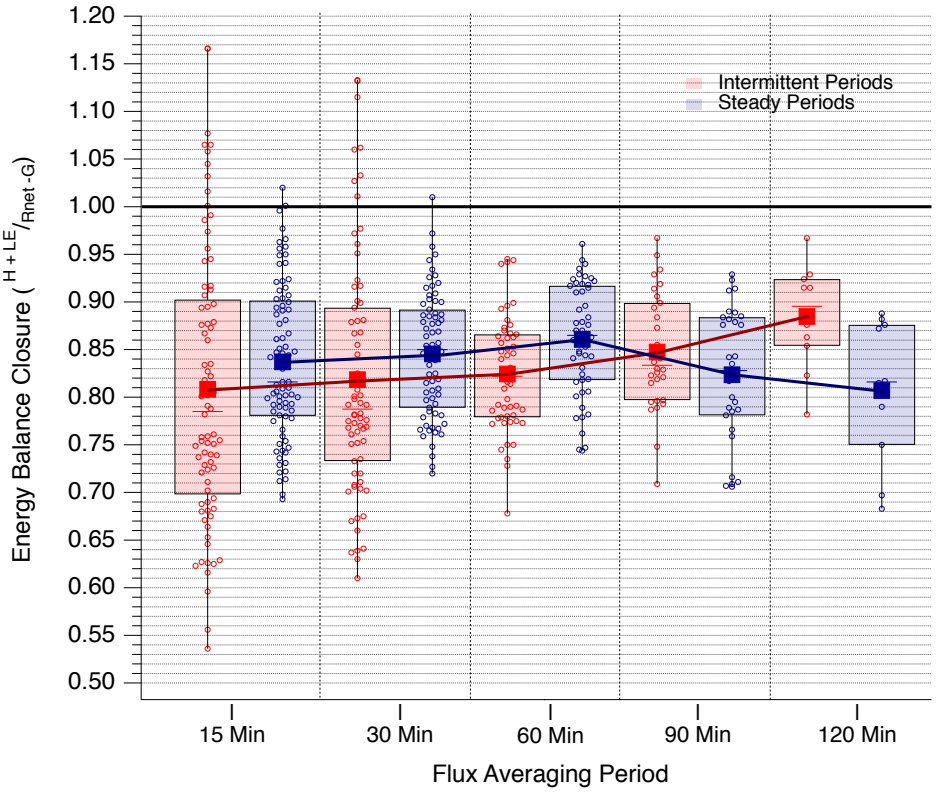

Fig. 2.9 Comparison of energy balance closure for 10 intermittent (red) and 10 steady (blue) two-hour periods. Fluxes were calculated for five averaging periods of increasing length. Boxes outline the middle 50% of the distribution, and lines depict trends for the mean closure values for intermittent and steady periods respectively.

2.4 Discussion and Conclusions

Through the comparisons of both time series and the summary statistics of key variables between intermittent and steady period sets, this study was able to delineate a strong connection between periods of light winds and unstable, convective stratification and the presence of intermittent turbulence transport. Intermittent behavior was most common during periods with mean winds of 1.5 – 2.5 m s^{-1} or less, while steady behavior

was nearly always associated with larger mean horizontal winds of >2 m s^{-1}. Further, intermittent periods were associated with buoyancy dominated periods indicated by larger negative values of z/L and high sensible heat flux. Neither the occurrence of light winds nor highly unstable stratification alone guaranteed the appearance of intermittent behavior, but overall, a clear association was quantified between light wind, convective periods and exchange behavior that is dominated by episodic, transient events.

Spectral analyses demonstrated that variations in water vapor density were often dominated by lower frequencies during light winds and highly unstable stratification. This suggests the importance of large, infrequent eddies or thermal structures in transporting water vapor under these conditions. This is not completely unexpected due to the nature of the initial classification of steady versus intermittent periods which focused on selecting periods with large amplitude variability with irregular distributions in time. However, this importance of low frequency events was most pronounced within the canopy, suggesting the physical presence of the vineyard canopy acted as a low pass filter to transport processes. The large peak in the lowest frequencies for the within canopy spectra, such as Fig. 2.7b, suggests that only eddies or convective structures with large enough spatial scales and kinetic energy are able penetrate the canopy and properly vent the canopy airspace during these periods. The broadness of the large, low frequency peaks in cross-spectra from intermittent periods, such as in Fig. 2.8, points to the importance of the irregular intervals between events during intermittency. Once fluctuations become more steady, the dominance of low frequencies diminishes and spectral curves are marked by a more regular distribution across a range of frequencies.

The sharper low frequency peaks in the canopy likely reflect distinct eddy sizes controlled by mechanical turbulence associated with canopy structure.

The analysis of flux-averaging period lengths demonstrates that substantially longer averaging periods may be necessary to calculate fluxes from eddy covariance during intermittent conditions. Assessing ET of vineyards in semi-arid regions may require reconsideration of appropriate time scales when conditions favorable for low frequency, episodic transport, i.e. lighter winds and large instability, are present. Unlike more steady conditions, episodic transport resulted in a large proportion of the flux happening in a relatively short proportion of the time. As suggested by flux/time ratios, the large majority of water vapor flux could occur in under one-third or less of a given time period. In such cases, a small number of large transport events can drastically affect average fluxes and this effect must be considered when modeling or making measurements. This also suggests that loading and venting of the canopy is less regular during intermittency, and may well affect the moment to moment microclimate within the canopy. We could expect that this more dynamic environment within the canopy sub layer would have possible implications for stomatal response on short time scales, and could potentially produce unexpected behavior in vertical gradients.

Given the proximity of the two sites and similar environmental conditions, considerable differences were not observed in the behavior of exchanges between the two sites. Due to the vine age difference between the two sites the canopy extent into the row-space of the older northern block (site #1) was generally somewhat larger than the southern block (site #2). Future work to more thoroughly compare turbulence

characteristics and exchange behavior between the two sites for given periods may prove beneficial in further determining any influence of vineyard structure.

Despite the importance of intermittent behavior in turbulence transport, unequivocal, objective identification remains problematic. Initial selection of periods for analysis was qualitative. However, it is clear throughout the analyses presented that periods classified as intermittent behave considerably differently than those of more steady transport. The flux/time ratios proved useful as both a quantitative metric for verifying intermittency and a method to compute differences in the amount of time fluxes occur over for a given period. The standard window technique provided an even clearer definition, with a distinct cutoff value of 2.6, for discriminating transient and non-transient activity. This allowed quantitative determination of the intermittent and steady period sets.

It is apparent that the behavior of turbulence transport of water vapor or ET in vineyards, is often fundamentally altered during light wind, convective conditions; conditions that are not unusual in many semi-arid regions. In addition, the large transport in short periods associated with intermittent conditions, suggests that they may not conform very well to assumptions required to connect fluxes to average gradients typically used in models. Of particular note is the favored timing of intermittency at these sites during the late morning to midday; times when most satellite retrievals used in remote-sensing based modeling approaches occur. Measurements made through the near instantaneous snapshot of these retrievals could prove vulnerable to effects from large-scale, low-frequency variability in fluxes. The effects of these transient conditions on the ability of schemes in models to simulate transport deserves more attention. Future work

is planned to document the performance of the TSEB model ET estimates during conditions of transient versus more idealized transport to investigate how the differing behavior effects a gradient driven model.

The temporal details of how turbulence transport occurs in vineyards appears to be important, and so how ET is occurring in time does matter. Hence, a better understanding of transient exchanges of ET under these conditions is worthy of further investigation.

2.5 Acknowledgements

Funding provided by Utah Agriculture Experiment Station Project UTAO 1186 and NASA Grant #NNX17AF51G. Much of the data collection during GRAPEX IOPs was made possible through funding provided by E.&J. Gallo Winery and the USDA-ARS. In addition, we would like to thank the staff of the Viticulture, Chemistry and Enology Division of E.&J. Gallo Winery for their logistical support as part of the GRAPEX project. Finally, this effort would not have been possible without the cooperation of Mr. Ernie Dosio of Pacific Agri Lands Management, along with the Borden vineyard staff, for logistical support of GRAPEX field and research activities. USDA is an equal opportunity provider and employer.

2.6 Conflicts of Interest

On behalf of all authors, there is no conflict of interest.

2.7 References

Alfieri JG, Kustas WP, Nieto H, Prueger JH, Hipps LE, McKee LG, Gao F, Los SA (2018) Influence of wind direction on the surface roughness of vineyards. Irrigation Sci. https://doi.org/10.1007/s00271-018-0610-z

Anderson MC, Norman JM, Li F, Kustas WP, Prueger JH, Mecikalski JR (2005) Effects of vegetation clumping on two-source model estimates of surface energy fluxes from an agricultural landscape during SMACEX. J Hydrometeorol 6:892–909

Ansorge C and Mellado JP (2014) Global intermittency and collapsing turbulence in the stratified planetary boundary layer. Bound-Layer Meteorol 153:98-116

Campbell GS and Norman JM (1998) Heat flow in the soil. In: An introduction to environmental physics. Springer, New York

Cava D and Katul GG (2009) The effects of thermal stratification on clustering properties of canopy turbulence. Bound-Layer Meteorol 130:307-325

Chahine A, Dupont S, Sinfort C, Brunet Y (2014) Wind-flow dynamics over a vineyard. Bound-Layer Meteorol 151:557-577

Finnigan J (2000) Turbulence in plant canopies. Annu Rev of Fluid Mech 32:519-557

Finnigan JJ, Clement R, Malhi Y, Leuning R, Cleugh HA (2003) A re-evaluation of long-term flux measurement techniques, part I: averaging and coordinate rotation. Bound-Layer Meteorol 107:1-48

Foken T, Leuning R, Oncley SR, Mauder M, Aubinet M (2012) Corrections and data quality control. In: M Aubinet et al. (eds) Eddy covariance: a practical guide to measurement and data analysis. Springer Atmospheric Sciences. pp 85-131

Gao W, Shaw RH, Paw U KT (1989) Observation of organized structure in turbulent flow within and above a forest canopy. Bound-Layer Meteorol 47:349-377

Katul GG, Kuhn G, Schieldge J, Hsieh CI (1997) The ejection-sweep character of scalar fluxes in the unstable boundary layer. Bound-Layer Meteorol 83. 1:1-26

Kool D, Kustas WP, Ben-Gal A, Lazarovitch N, Heitman JL, Sauer TJ, Agam N (2016) Energy and evapotranspiration partitioning in a desert vineyard. Agric For Meteorol 218-219:277-287

Kustas WP, Prueger JH and Hipps LE (2002) Impact of using different time-averaged inputs for estimating sensible heat flux of riparian vegetation using radiometric surface temperature. J Appl Meteorol 41:319-332

Kustas WP, Anderson MC, Alfieri JG, Knipper K, Torres-Rua A, Parry CK, Nieto H, Agam N, White WA, Gao F, McKee L, Prueger JH, Hipps LE, Los S, Alsina MM, Sanchez L, Sams B, Dokoozlian N, McKee M, Jones S, McElrone A, Heitman JL, Howard AM, Post K, Melton F, Hain C (2018) The grape remote sensing atmospheric profile and evapotranspiration experiment. Bull Amer Meteor Soc 99:1791-1812

Lee Y-H (2009) The influence of local stability on heat and momentum transfer within open canopies. Bound-Layer Meteorol 132:383-399

Lee Y-H (2011) Intermittency of turbulence within open canopies. J Atmos Sci 47 2:137-149

Li D and Bou-Zeid E (2011) Coherent structures and the dissimilarity of turbulent transport of momentum and scalars in the unstable atmospheric surface layer. Bound-Layer Meteorol 10:243-262

Mahrt L (1989) Intermittency of atmospheric-turbulence. J Atmos Sci 46:79–95

Mahrt L (1998) Stratified boundary layers. Bound-Layer Meteorol 90: 375-396

Massman WJ (2000) A simple method for estimating frequency response corrections for eddy covariance systems. Agric For Meteorol 104:185-198

Norman JM, Kustas WP, Humes KS (1995) Source approach for estimating soil and vegetation energy fluxes in observations of directional radiometric surface temperature. Agric For Meteorol 77:263-293

Paw U KT, Brunet Y, Collineau S, Shaw RH, Maitani T, Qiu J, Hipps L (1992) On coherent structures in turbulence within and above agricultural plant canopies. Agric For Meteorol 61:55-68

Peixoto JP and Oort AH (1992) Physics of climate. American Institute of Physics

Poulos GS, Blumen W, Fritts DC, Lundquist JK, Sun J, Burns SP, Nappo C, Banta R, Newsom R Cuxart J, Terradellas E, Balsley B, Jensen M (2002) CASES-99: A comprehensive investigation of the stable nocturnal boundary layer. Bull Amer Meteor Soc 83:555-581

Robinson J (Ed.) (2006) The oxford companion to wine (3rd ed.) Oxford University Press

Semmens KA, Anderson MC, Kustas WP, Gao F, Alfieri JG, McKee LG, Prueger JH, Hain CR, Cammalleri C, Yang Y, Xia T, Sanchez L, Alsina M, Velez M (2016) Monitoring daily evapotranspiration over two California vineyards using Landsat 8 in a multi-sensor data fusion approach. Remote Sens Environ 185: 155-170

Shaw RH, Tavangar J, Ward DP (1983) Structure of Reynolds stress in a canopy layer. J Climate Appl Meteorol 22:1922-1931

Stull R (1988) Introduction to boundary layer meteorology. Kluwer Academic Publishers, Dordrecht

Sun MX, Zhu ZL, Wen XF, Yuan GF, Yu GR (2006) The impact of averaging period on eddy fluxes observed at China FLUX sites. Agric For Meteorol 137:188-193

Twine TE, Kustas WP, Norman, JM, Cook DR, Houser PR, Meyers TP, Prueger JH, Starks PJ, Wesely ML (2000) Correcting eddy covariance flux measurements over a grassland. Agric For Meteorol 103:279-300

Vassilicos JC (2010) Intermittency in turbulent flows. Cambridge: Cambridge University Press

Webb EK, Pearman GI, and Leuning R (1980) Correction of flux measurements for density effects due to heat and water vapour transfer. Q J R Meteorol Soc 106:85-100

CHAPTER III
EFFECTS OF INTERMITTENT TURBULENCE ON TWO-SOURCE ENERGY BALANCE MODELED FLUXES FROM VINEYARDS

3.1. Introduction

An increasingly large amount of global wine grape production, a high-value crop (Ashenfelter et al., 2018), occur in semi-arid and arid regions where water is limited, the evaporative demand on the crop is high, and uncertainty in water resources is growing (Li et al., 2009; Kool et al., 2016). Additionally, modest water stress during certain times in the growing season has been shown to improve grape and wine quality (van Leeuwen et al., 2009). To more precisely manage both grapevine growth and water resources, there is a need for daily, field-scale estimates of evapotranspiration (ET) in vineyards. Since the transport of water vapor away from plant canopies occurs chiefly through turbulence, the gold standard micrometeorological method to measure ET is eddy covariance. However, it is difficult to implement eddy covariance for monitoring moisture fluxes on a large-scale as measurements typically represent values for a small area, involve expensive equipment, and require expertise to interpret findings. Several well-developed eddy covariance flux networks exist globally, but these are unable to retrieve spatially variable patterns of ET across heterogeneous landscapes (Foken et al., 2012).

Remote sensing-based soil-vegetation-atmosphere transfer models that are able estimate turbulent exchange offer the ability to monitor ET at the field to sub-field scale

(Semmens et al., 2016). The USDA Agricultural Research Service (ARS) has developed an ET modeling system known as ALEXI/DisALEXI (Atmospheric Land EXchange Inverse/Disaggregation ALEXI) that utilizes the Two-Source Energy Balance (TSEB) land surface scheme (Norman et al., 1995) to estimate turbulent fluxes using satellite measured land surface temperature. By applying a data fusion approach that combines information from multiple satellite platforms of various temporal and spatial resolution, ALEXI/DisALEXI is able to make daily ET estimates at a 30 m resolution (Cammellari et al., 2014). This modeling system has successfully been validated over a number of homogeneous natural and agricultural landscapes, and shows significant promise in providing field-scale estimates of ET for more heterogeneous surfaces such as vineyards. However, unknowns remain on the particular complexities involved in vineyard ET processes and how well these complexities are handled by the TSEB approach. The Grape Remote Sensing Atmospheric Profile and Evapotranspiration eXperiment (GRAPEX) seeks to validate ALEXI/DisALEXI performance for vineyard surfaces and to generate new knowledge of energy balance and transport processes in vineyards. The study reported here emerges from these general goals of the GRAPEX investigations.

3.1.1. The Two-Source Energy Balance Model Description

The TSEB model, based on the formulation of Norman et al. (1995), uses a composite radiometric surface temperature (T_{RAD}) to solve a set of equations describing the energy fluxes from the soil and canopy components (Fig. 3.1). Other inputs include a radiometer viewing angle (θ), fractional vegetation cover (f_c) that can be derived from

estimates of leaf area index (LAI), and common meteorological variables such as mean air temperature and wind speed. Modeled values of net radiation (R_n), soil heat flux (G), and sensible heat flux (H) are partitioned between soil and canopy through a system of gradients between four temperatures, a soil temperature (T_S), canopy temperature (T_C), canopy-air temperature (T_{AC}), and surface layer air temperature (T_A), controlled by three resistances, a soil/substrate aerodynamic resistance (R_S), canopy aerodynamic resistance (R_c), and surface layer aerodynamic resistance (R_A). The fluxes of sensible heat from the soil (H_S), canopy (H_C), and combined surface (H) are found following Norman et al. (1995) as:

$$H_S = \rho C_P \frac{T_S - T_{AC}}{R_S} \tag{3.1}$$

$$H_C = \rho C_P \frac{T_C - T_{AC}}{R_C} \tag{3.2}$$

$$H = \rho C_P \frac{T_{AC} - T_A}{R_A} \tag{3.3}$$

where $\rho\ C_P$ is the volumetric heat capacity of the air. With an estimate of the canopy latent heat flux (LE_C) via Priestley-Taylor (PT), Penman-Monteith (PM) or Light Use efficiency (LUE) formulations, solutions can iteratively be found for all fluxes (Kustas et al., 2018). A detailed description of the model can be found in Kustas et al. (2002) and Kustas et al. (2012).

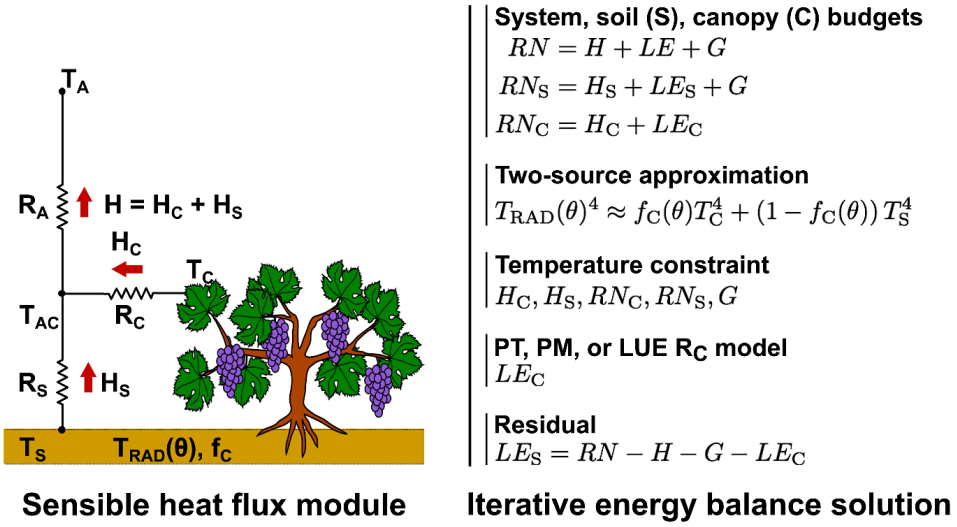

Fig. 3.1. A depiction of the gradient and resistance framework of the Two-Source Energy Balance (TSEB) model's sensible heat flux module as well as the system of equations for an iterative solution (Kustas et al., 2018).

3.1.2. Theoretical Considerations

Modeling methods to estimate evapotranspiration through turbulent exchange, such as TSEB, rely on assumptions that vertical transport by turbulence is connected to time-averaged vertical gradients and that the remotely sensed land surface temperature collected instantaneously can be used within time-averaged flux-gradient formulations (Kustas et al., 2002). Thus, there is an implicit assumption that turbulence fluxes will have a reasonably steady behavior over a defined period. This implies that a sufficient number of transport events occur during a given averaging period, and that these are separated by small enough amounts of time relative to the averaging period to be considered pseudo-homogeneous.

In other words, *steady* behavior refers to an idealized case where the rate of scalar transport is fairly consistent, and variations occur at a high enough frequency compared to the averaging period length. However, turbulence in plant canopies often deviates from this ideal (Paw U et al., 1992; Finnigan, 2000), and indeed some degree of non-steady, intermittent behavior, can typically be expected at various time and space scales.

Intermittent behavior in boundary layer turbulence may be due to global effects forced by processes external to the surface layer, such as large-scale eddies that are irregularly distributed in time and space (Mahrt, 1998), or by small scale shear-gradient interactions between the flow and complexities in the local surface (Lee, 2011). In the atmospheric boundary layer, much of the previous work on intermittent turbulence has been concentrated on nocturnal stable stratification where global intermittency appears as distinct bursts of activity separated by relatively longer quiescent periods with little activity (Mahrt, 1998; Poulos et al., 2001; Ansorge and Mellado, 2014). For daytime conditions with neutral or unstable stability studies have often linked transient behavior in turbulence to the presence of coherent motions such as *ejections* and *sweeps* (Shaw et al., 1983; Katul et al., 1997; Finnigan, 2000). Coherent motions often appear in scalar time series as ramp-like signatures where the slow accumulation of a scalar near the surface is followed by a sudden drop as near surface air is vented. The relative importance of ejections and sweeps on momentum and heat transport from plant canopies has been extensively examined, and it is clear that fluxes from heterogeneous canopies can be significantly influenced by coherent turbulent events (Gao et al., 1989; Li and Bou-Zeid, 2011). Francone et al. (2012) suggested that the influence of ejections and sweeps can be significant in vineyard canopies as well. Overall, however, studies

investigating intermittent behavior and their effect on transport processes in vineyards have been rather limited.

Vineyards in semi-arid climates present several confounding factors that serve to complicate turbulence and the resulting transport processes that govern vineyard ET. A first issue is the heterogeneity presented by overall vineyard structure. The partially open, spatially variable canopy/row-space pattern complicates wind flow by mechanical and thermal interactions of the plants and soil with the wind field at similar length scales to much of the turbulent eddies (Lee, 2009). Chahine et al. (2014) conducted large eddy simulations of vineyards and compared them to 3-D anemometry measurements to examine wind direction/row structure interactions on local scale transport. This work suggested that cross-row flow behaved similarly to that of a more uniform canopy, while along-row flow showed increased spatial variability, increased intermittency of turbulence, and resulted in larger fluxes of momentum. Given these effects, vineyards themselves can potentially induce transient, non-steady turbulent behavior that may cause intermittency in transport processes at local space and time scales. Another issue arises considering that the growing season of warm, semi-arid regions often features strong, persistent synoptic high pressure and resulting subsidence (Peixoto and Oort, 1992). The resulting combination of particularly low horizontal pressure gradient and mean horizontal winds, even during the day, and high net radiation can yield highly unstable, convective conditions near the surface that are conducive for the presence of infrequent, large convective structures. This would suggest that intermittent, episodic exchange events could become more pronounced during conditions that are common to the growing season.

This study examines the impacts of intermittent heat and water vapor fluxes on the vineyard canopy environment, and the ability of the TSEB model to estimate ET. Given the complexities of vineyard biophysics and possible consequences of intermittent turbulence for flux-gradient assumptions, this study's objectives were twofold. The first objective was to document intermittent behavior of key variables both above and within the canopy related to turbulent exchange such as temperature, humidity, and velocity. The second objective was to test TSEB against measured fluxes on multiple timescales, for both intermittent and steady conditions, to determine if intermittent transport adversely affects TSEB performance.

3.2. Materials and methods

3.2.1. Sites

The GRAPEX sites used in this study consisted of two closely located drip-irrigated *Vitis vinifera* (Pinot Noir) vineyard blocks (Fig. 3.2), one 4 years (south block, site #2) and one 7 years old (north block, site #1) at the beginning of the 2014 growing season. These were located in California's Central Valley near Lodi, CA (38.29 N, 121.12 W, 38.4 m elev.). The area experiences a semi-arid Mediterranean climate, typical of many areas in California, with precipitation almost entirely confined to the cool season and nearly no precipitation during the growing season. Daytime conditions during the growing season typically consisted of high maximum air temperatures (35 – 40+ °C)

and clear skies with high net radiation (>500 – 600 W m^2). Winds were often light before noon (~1 m s^{-1}), then strengthening gradually during the day, and often peaking in the mid to late afternoon (~2 – 4 m s^{-1}), though periods of light winds could be observed throughout the day.

Vines were grown in rows East-West rows spaced ~3.35 m apart on a fixed trellis system with individual vines spaced along the row at ~1.52 m. Maximum canopy height during the growing season was typically ~2.5 m. As the growing season progressed, canopy growth extended laterally into the row interspace, though this was partially governed by the vineyard management. The result was a complex spatial pattern of foliage. Directly beneath the vine canopy in each row was a strip of bare soil that was routinely watered by an above ground drip irrigation. Between the rows the surface consisted of a grass cover crop that typically senesced early in the growing season as spring precipitation ended and the dry summer period began. The canopy/trellis structure allowed for a significant open space in each direction between the soil surface and the bottom of the canopy crown of ~0.7 m.

3.2.2. Instrumentation

A tower at each site was placed near the eastern edge of the vineyard block so to enjoy maximum footprint from the prevailing westerly winds; achieving a fetch that was typically ~400 m (Fig. 3.3). Fluctuations of 3-D wind velocities and water vapor above the canopy were measured on each tower using an IRGASON, combining a 3-D sonic

anemometer (CSAT-A, Campbell Scientific Inc., Logan, UT[3]) and open path infrared gas analyzer (EC-150, Campbell Scientific Inc., Logan, UT). These instruments were mounted facing due West at a height of 5 m agl and sampled at 20 Hz. Net radiation was measured from the towers at 6 m agl using a four-component net-radiometer (CNR-1, Kipp & Zonen, Delft, The Netherlands). Soil heat flux was calculated using a cross-row transect near the towers of five soil heat flux plates at 8 cm depths (HFT-3, Radiation Energy Balance Systems, Bellevue, WA) with two thermocouples near each plate at 2 and 6 cm depths and soil moisture probes (HydraProbe, Stevens Water Monitoring Systems, Portland, OR) at 5 cm depth. Each tower also included a shielded slow-response thermometer at a height of 4.9 m. Data collection included nearly continuous data gathered during the 2014, 2015, and 2016 growing seasons.

In addition to the measurements above, further instrumentation was deployed during intensive observation periods (IOPs) of several days each were conducted ~ 3 – 5 times through the growing season (Table 3.1). The 39 IOP days serve as focus for the analyses presented here to leverage these supplementary measurements. During these times an additional open-path IRGA (LI-7500A, LI-COR Biosciences, Inc., Lincoln, NE) and 3-D sonic anemometer (SATI/3Vx Applied Technologies, Inc) were placed immediately next to each tower in the row space between canopies at a height of 1.5 m agl (Fig. 3.3). The term *within canopy* here describes these measurements from the inter-row space below the canopy top, but outside the true canopy crown. A shielded slow-response thermometer was also placed within the canopy at 1.5 m. Data were sampled by

[3] The mention of trade names of commercial products in this article is solely for the purpose of providing specific information and does not imply recommendation or endorsement by the US Department of Agriculture.

a CR3000 datalogger (Campbell Scientific Inc., Logan, UT) at a sampling rate of 20 Hz for all IOPs except for two during 2016 where the sampling rate was 10 Hz. The within canopy instruments during IOPs were wired into the tower dataloggers such that they were synchronized, with the exception that the ATI sonic anemometers were placed on separate data loggers during 2014 and 2015 due to technical constraints.

An array of six infrared thermometers (IRTs) was also deployed at each site during the 2016 IOPs, consisting of two SI-111s that viewed the inter-row surface and four SI-1H1s that viewed the canopy from various angles (Apogee Instruments Logan, UT). These were located approximately 18 m due West of the respective flux tower in each block (Fig. 3.3). These were sampled at 1 Hz on a separate datalogger from that of the tower and within canopy measurements.

A further description of site and instrumentation details is presented by Kustas et al. (2018).

Table 3.1

Listed are the GRAPEX IOPs and corresponding days of year (DOY) from which periods for analysis and testing of TSEB were selected.

	2014	*2015*	*2016*
IOP 1		111 – 113	121 – 123
IOP 2	116 – 119	152 – 154	161 – 163
IOP 3	181 – 183	191 – 194	208 – 211
IOP 4	217 – 222	222 – 225	
IOP 5	269 – 270		

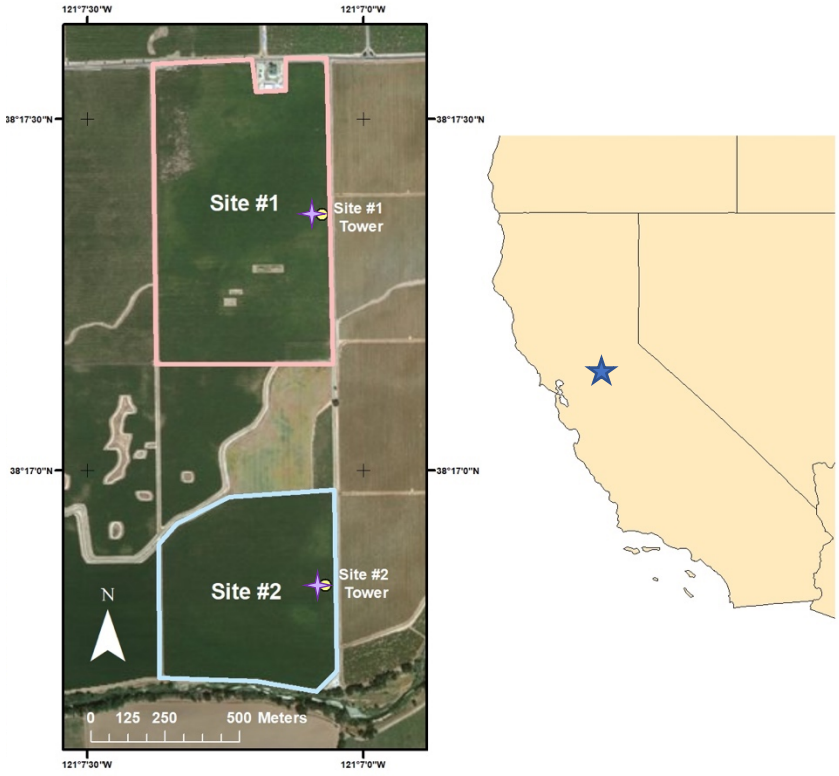

Fig. 3.2. Shown is a map of the two GRAPEX sites used in this study. The northern vineyard block (site #1) is outlined in red, while the southern vineyard block (site #2) is outlined in blue. The tower locations, with collocated within canopy instruments, are marked with yellow dots and the location of the infrared thermometer arrays immediately west of each tower are marked with purple stars. The blue star in the right panel shows the location in California's Central Valley.

Fig. 3.3. The three main sets instrumentation are pictured. The left panel shows the tower at site #1 with the 6 m net radiometer, 5 m 3-D sonic anemometer (among others) and infrared gas analyzer, and 4.9 m aspirated temperature shield. The top right panel shows a typical position of the within canopy 3-D sonic anemometer, infrared gas analyzer, and slow-response thermometer. The bottom right panel shows one of the IRT arrays.

3.2.3. Data Processing

Fast-response measurements of velocity and water vapor were quality-controlled, including removal periods with bad or missing data, identifying spikes, and replacing values using interpolation during sub-second periods where possible. After data sets

were cleaned, a sample population of hours was selected from the 2014, 2015, and 2016 IOPs at both sites (Table 3.1) that were during the daytime (7:00 – 19:00 LST), with relatively clear skies (where incoming solar radiation compared well with a clear sky model), energy balance closure was greater than 0.80, and the mean wind direction was predominantly along-row flow, i.e. between 225° – 315°, to eliminate complicating effects on turbulence of changes in wind direction with row orientation (Alfieri et al., 2018). This resulted in 417 selected hours representing a varied distribution of day of year (DOY) and vegetative growth from the two sites. From these 417 hours, two subsets were selected as periods of interest for further analysis; one group of hours classified as *intermittent* behavior, and one group classified as *steady* behavior. This was accomplished by a qualitative survey and then verified through a quantitative procedure. First, time series of the vertical wind component (u_z, m s^{-1}) and water vapor density (ρ_v, g m^{-3}) were examined for each hour. Intermittency was noted for periods of high amplitude fluctuations that appeared episodic or otherwise widely spaced in time distribution. Likewise, steady behavior was noted for periods of relatively small, frequent, and more evenly spaced fluctuations. Periods were chosen as those where the respective behavior was consistent across the hour. A quantitative discrimination method, described in Los et al. (2019), was then used to verify the selected periods in each subset. For a given hour, a time series of instantaneous turbulent kinetic energy (TKE) was generated from the respective 5 m 3-D sonic anemometer by:

$$TKE = \frac{1}{2}\sqrt{{u'_x}^2 + {u'_y}^2 + {u'_z}^2} \tag{3.4}$$

where u'_x, u'_y, u'_z are the perturbations (at 20 Hz) of the three directional wind components from the hourly average of each component (Stull, 1988). The method then computes the standard deviations of TKE produced by sliding windows of various widths over the time series. For each window size, the average of all the standard deviation values of each window position is determined. The window sizes ranged from 20 to 4800 points, or 1 to 240 seconds. A ratio is then made of the maximum standard deviation value (usually the longest window) over the minimum standard deviation (shortest window). The values of this ratio for intermittent and steady periods form two distinct groups allowing a clear, quantitative differentiation between the two behaviors. In this way, from the 417 original hours, 115 intermittent 1-hour periods and 102 steady 1-hour periods were parsed.

Having selected hours for analysis, custom Fortran scripts were used to calculate hourly turbulent fluxes of sensible heat (H) and latent heat (LE) from the 5 m fast-response data. Corrections applied during flux computations included among others: lag shifting to achieve maximum raw covariances to ensure synchronicity of measurements; a simple 2-D coordinate rotation; frequency and path length corrections (Massman, 2000); density corrections (Webb et al., 1980); and conversion of sonic temperatures and heat flux to actual temperatures and sensible heat flux. Soil heat flux (G) was calculated as an addition of the term for the heat flow across the heat flux plates (G_p) and the term for storage in the soil layer above the heat flux plates (S) as $G = G_p + S$ (Campbell and Norman, 1998). Measurements of net radiation (R_{Net}) from the 6 m net radiometer were used to complete energy balance:

$$R_{Net} = H + LE + G \tag{3.5}$$

Conservation of energy can be checked by using the above equation to form the energy balance closure (EBC) ratio, where $EBC = (H + LE)/(R_{Net} - G)$. Ideally this ratio would be equal to unity. Since any errors degrade covariances, fluxes are generally underestimated lowering EBC. For hours with non-unity closure the turbulent fluxes H and LE were adjusted to match the available energy by preserving their Bowen ratio, ($\beta = H/LE$), as per Twine et al. (2000), here referred to as Bowen ratio closure according to:

$$LE_{Closed} = \frac{R_{Net} - G}{\beta + 1} \tag{3.6}$$

$$H_{Closed} = \frac{R_{Net} - G}{1 + \frac{1}{\beta}} \tag{3.7}$$

There is some evidence from eddy covariance data collected in highly evaporative conditions to suggest that the error associated with measurements of LE may be significantly larger than that of H (Brotzge and Crawford, 2003). Therefore, an alternative form of EBC where $LE_{Closed} = R_{Net} - G - H$, has sometimes been proposed, here referred to as residual closure. Given that current understanding places similar measurement uncertainty on the methodologies of retrieving both LE and H, fluxes for this study have been closed via Bowen ratio closure. However, to provide an alternative comparison to modeled fluxes, residual closure was also applied to fluxes where noted for some of TSEB model evaluation.

In addition to these fluxes other turbulence parameters were calculated. The friction velocity (u_*) and the stability parameter z/L were calculated for each hour using the 5 m sonic anemometer at each tower, where L is the Obukhov length scale. The

aerodynamic resistance to heat (R_A) was calculated according to Brutsaert (2005) for each hour by:

$$R_A = \frac{ln\left(\frac{z_T - d_o}{z_{oH}}\right) - \psi_h\left(\frac{z_T - d_o}{L}\right) + \psi_h\left(\frac{z_{oH}}{L}\right)}{\kappa' u_*} \tag{3.8}$$

for stable conditions where $\zeta = (\frac{z_T - d_o}{L})$:

$$\psi_h(\zeta) = \psi_m(\zeta) = -a \ln\left[\zeta + \left(1 + \zeta^b\right)^{\frac{1}{b}}\right] \tag{3.9}$$

and for unstable conditions where $y = -\zeta$:

$$\psi_h(-\mathrm{y}) = [(1-d)/n] \ln[(c + \mathrm{y}^n)/c] \tag{3.10}$$

Here z_T is the temperature measurement height, z_{oH} is the roughness length for heat, d_o is the zero-plane displacement height, and a, b, c, d, n are constants. Also, to investigate both intermittent variability of turbulence and changes in coupling between the within and above canopy air above, time series of instantaneous turbulence kinetic energy (TKE) were calculated from both the 5 m and 1.5 m 3-D sonic anemometers using Eqn. 3.4.

This study sought to characterize how intermittent turbulent exchanges affect the vineyard canopy environment from the perspective of the TSEB framework. To document the high frequency behavior of air and surface temperatures of the vineyard structure, this study leveraged the instrumentation available during IOPs to create time series of the four TSEB model component temperatures: soil temperature (T_S), canopy temperature (T_C), canopy-air temperature (T_{AC}), and surface layer air temperature (T_A). The raw surface brightness temperatures from each of the array IRTs were corrected for emissivity and reflected longwave radiation by:

$$T_{Target} = \sqrt[4]{\frac{T_{sensor}^4 - (1-\epsilon)T_{background}^4}{\epsilon}} \quad (3.11)$$

(Blonquist et al., 2009), where ϵ was assumed as 0.97 for canopy temperatures and as 0.93 for soil temperatures. $T_{Background}$ for the canopy was set as the sky brightness temperature derived from the incoming longwave at the 6 m tower net radiometer using the Stephan-Boltzmann Law, and $T_{Background}$ for the soil was a weighted composite of the canopy brightness temperature and the sky brightness temperature by:

$$T_{Background} = f_c T_{Canopy} + (1 - f_c) T_{Sky} \quad (3.12)$$

Sonic temperatures from the 5 m and 1.5 m sonic anemometers were corrected for density effects from humidity into an air temperature by:

$$T_{air} = T_{sonic}/(1 + 0.51q) \quad (3.13)$$

where q is the specific humidity derived from the water vapor density measured by the collocated IRGA. To remove bias issues, in these sonic-derived temperatures were block averaged to 15 minutes and calibrated to the collocated slow-response sensors at their respective level and coefficients from a simple linear regression fit could be applied to the 20 Hz data. Once calibrated, 20 Hz sonic-derived temperature time series were block averaging to 1 Hz so to be on the same timescale as the IRT array data.

It is noted that because the IRT array was both somewhat displaced spatially from and not synchronized on the same datalogger as the tower and within canopy measurements, any direct high frequency relationships between their temperatures are not valid. However, for this study comparison between these temperatures was valid on minute to hour timescales and were useful for diagnosing gradient behavior from the perspective of the TSEB framework.

3.2.4. TSEB Model Evaluation

In order to investigate differences in performance of TSEB for intermittent and steadier behavior, the model was tested using two procedures: runs of the model on an hourly timescale versus hourly eddy covariance measurements for intermittent and steadier periods, and runs of the model on a 1 Hz timescale driven by a T_{RAD} derived from the 1 Hz IRT array data.

For the hourly runs a version of TSEB was used that utilizes a new canopy wind profile model proposed by Massman et al. (2017) that accounts for the non-uniform vertical distribution of leaf area and wind attenuation with depth throughout the canopy layer. The model determines dimensions of canopy height, height from the surface to the canopy bottom, and the horizontal row-space width from relationships based on LAI. A detailed description of the particular TSEB formulation used here can be found in Nieto et al. (2018). Inputs for TSEB included meteorological data consisting of hourly mean air temperature, wind speed, and vapor pressure at 5 m, and the mean incoming shortwave from the 6 m net radiometers. Input LAI was taken from a data set created during the GRAPEX project via a reference-based technique (Gao et al., 2012) that estimates daily LAI from Landsat using reference MODIS imagery. The procedure and resulting LAI product are provided in Sun et al. (2017). An hourly input T_{RAD} was calculated from the 6 m tower net radiometers by:

$$T_{RAD} = \left(\frac{L_{\uparrow} - \left(1 - \epsilon_{surf}\right) L_{\downarrow}}{\sigma \epsilon_{surf}} \right)^{1/4} \tag{3.14}$$

where $L_{\uparrow}$ is the hourly mean outgoing longwave radiation, $L_{\downarrow}$ is the hourly mean incoming longwave radiation, and σ is the Stephan Boltzmann constant. Here ϵ_{surf} is a function of an assumed soil emissivity of 0.93 and an assumed canopy emissivity of 0.97 by:

$$\epsilon_{surf} = 0.97 f_c + 0.93(1 - f_c) \tag{3.15}$$

and the fractional cover f_c is calculated as a function of view angle by:

$$f_c = 1 - exp\left(\frac{-0.5\Omega LAI}{cos\theta}\right) \tag{3.16}$$

where θ is the view angle (set as zero) and Ω is a dimensionless clumping index, which indicates the degree of heterogeneity in the spatial distribution of the leaf area (Anderson et al., 2005). To perform energy balance calculations TSEB has the ability to model G, typically as a fraction of modeled R_{Net}. However, because this approach may not always produce appropriate G values and to limit sources of error, in this study TSEB was run using measured values of G.

Once TSEB runs for the 417 hours were completed, the resulting modeled fluxes were compared to hourly eddy covariance fluxes for each hour closed by both Bowen ratio closure and residual closure (all "missing" energy added to the LE term). TSEB results for the 115 intermittent hours and 102 steady hours were then separated from the full 417 hours and these results were then each compared to the corresponding eddy covariance measured fluxes as well. Error statistics were calculated for the modeled versus measured fluxes for the 417 'all hour', intermittent hour, and steady hour sets. Statistics used were the coefficient of determination (r^2) and slope from a simple linear

regression fit as well as the root mean square error (RMSE), mean absolute error (MAE), and the bias as determined by:

$$RMSE = \sqrt{\frac{1}{n-1}\sum_{i=1}^{n}(y_i - \hat{y}_i)^2} \tag{3.17}$$

$$MAE = \frac{1}{n-1}\sum_{i=1}^{n}|y_i - \hat{y}_i| \tag{3.18}$$

$$Bias = \frac{1}{n-1}\sum_{i=1}^{n}(y_i - \hat{y}_i) \tag{3.19}$$

where y_i is the measured value and $\hat{y}_i$ is the modeled value.

The intent of the 1 Hz timescale TSEB tests was to address the fact that operationally the model receives a remotely sensed input T_{RAD} from a satellite overpass that is essentially an instantaneous retrieval. This input is therefore analogous to a snapshot, while the other inputs are typically derived from mean values averaged over minutes to hours. This difference in timescale can be considered trivial if steady state assumptions apply to a surface being monitored. However, high frequency variations of land surface temperature for a given period associated with intermittency could limit the validity of these assumptions. Runs of TSEB were conducted for various periods using an input T_{RAD} derived from the 1 Hz IRT array data. Time series of a composite input T_{RAD} were created by combining the corrected soil temperature (T_S, 2 sensors) and

canopy temperature (T_C, 4 sensors) components through a weighting by fractional cover as follows:

$$T_{RAD}^4(\theta) = f_c(\theta)T_C^4 + [1 - f_c(\theta)]T_S^4 \quad (3.20)$$

For these 1 Hz IRT tests the standard version of TSEB, that does not include specific vineyard structure wind attenuation, was used in order to provide a more general results of the performance of TSEB on this high frequency timescale. Ten 1-hour periods from between 9:00 LST and 14:00 LST, corresponding to typical satellite overpass times, were selected for analysis from 2016 IOP days, the season IRT array data was available. For these hours TSEB was run for each time step of a 1 Hz T_{RAD} time series while using hourly mean values held as constants for all other inputs (T_{air}, mean wind, etc.). This produced time series of modeled fluxes where each value (at 1 second intervals) represents a model outcome from a possible quasi-instantaneous, *snapshot* retrieval.

3.3. Results and Discussion

3.3.1. Fast-response Time Series

Time series of 5 m height fast-response vertical velocity (u_z), water vapor density (ρ_v), and sonic temperature measurements from both sites were surveyed across daytime hours of IOPs during 2014, 2015, and 2016, which found a wide range of variability in the frequency and amplitude of fluctuations. Distinctly intermittent and more steady behavior were both observed to occur frequently at the sites for 1 to 4-hour periods. Fig.

3.4 demonstrates these two distinct behaviors over a 3-hour afternoon period from site #1 on DOY 191 of 2015. The period before 15:00 LST (left of the yellow line) displays a patchy, episodic distribution of activity in u_z while the humidity above and within the canopy shows large amplitude variations that are unevenly spaced in time. This intermittent period occurred during lighter mean horizontal winds of ~1.5 m s^{-1}. The period following 15:00 LST (right of the yellow line) saw an increase of mean winds to ~2.9 m s^{-1} and exhibits a marked difference in behavior where turbulent activity appears much more consistent in time and humidity variations are smaller and more consistent. This rapid transition between an intermittent regime to a steadier regime, in association with a rapid change from an extended lighter wind period to one of higher mean winds, was found to occur often and served as a convenient delineation between intermittent and steady periods for analysis.

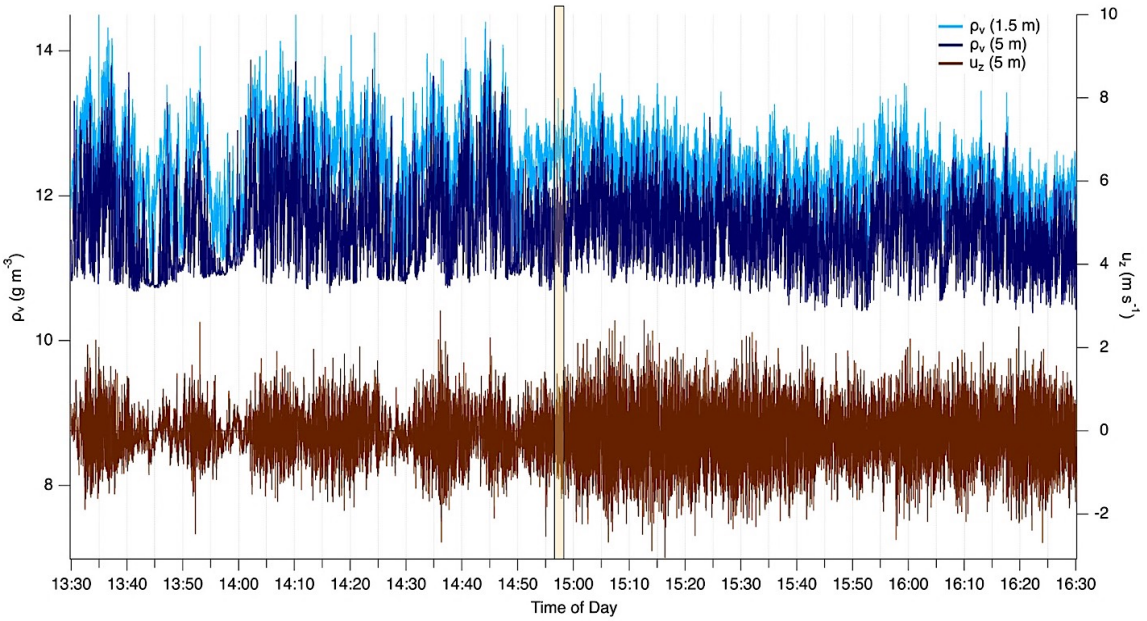

Fig. 3.4. Time series of water vapor density (ρ_v) at 1.5 m (light blue) and 5 m (dark blue), and the vertical wind component (u_z) at 5 m (brown) at site #1 (north vineyard block) on DOY 191 in 2015. The period from 13:30 ST to just before 15:00 LST (before the yellow rectangle) is characterized by patchy, intermittent events with large amplitude variations. The period thereafter is characterized by more consistent, steady variation.

Since it is a fundamental measure of turbulence, time series of instantaneous turbulence kinetic energy (TKE) were calculated for a range of intermittent and steady periods. Fig. 3.5a and 3.5b illustrate an example of two 20-minute periods on the same DOY as shown in Fig. 3.4. Fig. 3.5a, during steady conditions with hourly mean horizontal winds of 2.9 m s^{-1}, shows highly similar behavior between the 5 m and 1.5 m TKE. The variance at both heights is reasonably stationary in time and though the 1.5 m height's values are generally somewhat lower they correlate well with the pattern at the 5 m height. The intermittent period in Fig. 3.5b, with mean winds of 1.3 m s^{-1}, displays

discrete episodes of high TKE at the 5 m height interspersed between much lower values. The series of TKE at 1.5 m during this time shows increased values during only the largest bursts of activity at 5 m, and the variability is considerably damped. Compared to the steady case in Fig. 3.5a, TKE at 1.5 m in Fig. 3.5b shows much less correlation with that of the 5 m height. This suggests that the within canopy air is at times becoming decoupled from the activity above and this points to a loss of coherence between the canopy sub-layer and the above canopy surface layer.

In surveying the three years of IOPs, time series of TKE consistently showed these distinct differences in behavior where periods determined as steady showed a high correlation between the canopy airspace and the air above, while periods showing intermittency had displayed markedly less continuity between the behavior at the two heights. This would seem to challenge the validity of flux-gradient relationships during intermittent periods. The distinct differences in above and within canopy TKE for intermittent versus steady periods also served as another effective method to verify periods as being either intermittent or steadier for the latter analyses.

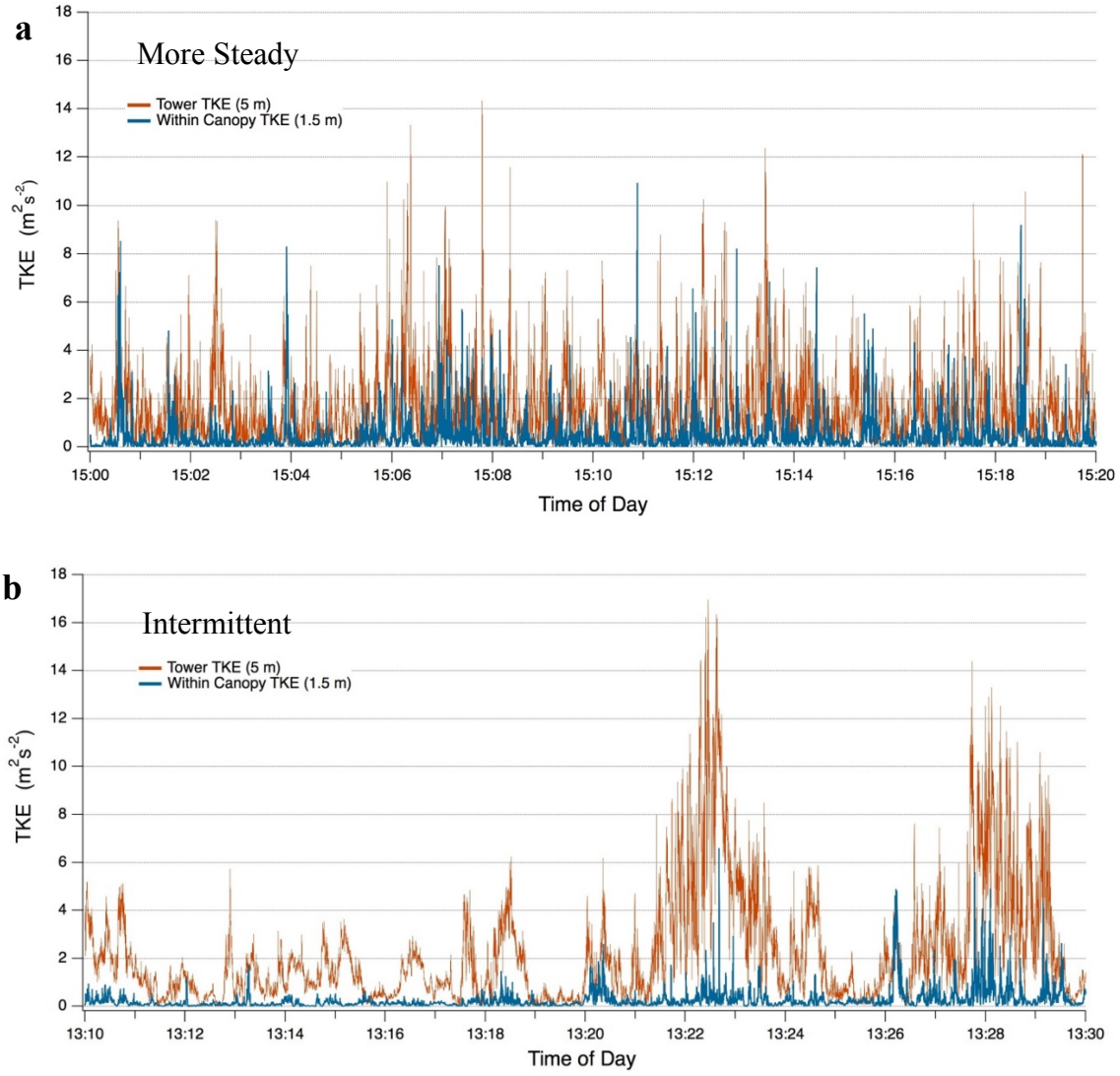

Fig. 3.5. 20-minute time series of instantaneous turbulent kinetic energy. The orange traces denote the height above the canopy at a height of 5 m, and the blue traces are from within canopy at 1.5 m.

3.3.2. Temperature Gradients

Using the 1 Hz IRT observations during the 2016 growing season along with above and within canopy fast-response measurements, high frequency time series of

temperatures and temperature gradients were created such that they mirrored the framework of TSEB's gradient/resistance pathways. Fig. 3.6 depicts these temperatures and gradients where colored circles correspond to measured values of T_A from the 5 m sonic anemometer (red), T_{AC} from the 1.5 m sonic anemometer (blue), and T_S (brown) and T_C (green) from the IRT array. The colored bars correspond to the gradients between these temperatures: T_{AC} - T_A (red), T_S - T_{AC} (tan), and T_C - T_{AC} (green). Time series of these temperatures and gradients were surveyed for the 417 hours with particular interest in hours displaying intermittent and steadier behavior.

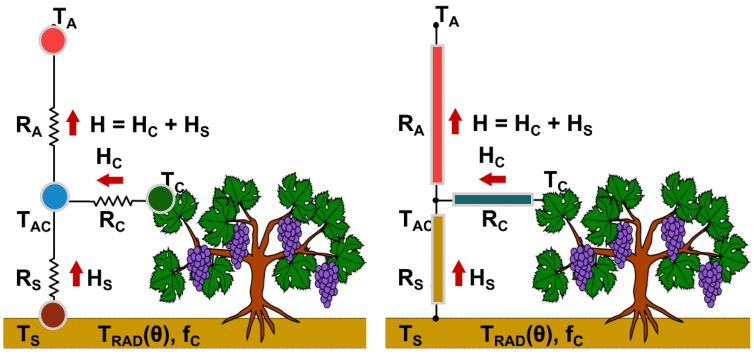

Fig. 3.6. Depictions of the individual temperatures and gradients of the TSEB model. Colored circles correspond to measured T_A from the 5 m sonic anemometer (red), T_{AC} from the 1.5 m sonic anemometer (blue), and T_S (brown) and T_C (green) from the IRT array. Colored bars correspond to the gradients between these: T_{AC} - T_A (red), T_S - T_{AC} (tan), and T_C - T_{AC} (green). Colors correspond to those of Fig. 3.8. and 3.9.

The following are two example periods chosen to perform analyses of temperature gradients described above. Fig 3.7a and Fig 3.7b show time series of 20 Hz u_z and ρ_v at 5 m on the tower at site #1 on DOY 162 of 2016. Fig 3.7a corresponds to a 30-minute morning period showing intermittent turbulence when mean winds were 1.4 m

s^{-1}, while Fig 3.7b corresponds to a 30-minute afternoon period with steadier behavior and mean horizontal winds of 2.7 m s^{-1}.

Fig. 3.8a and Fig. 3.8b present the time series of the temperatures T_A, T_{AC}, T_S, and T_C for the same two 30-minute periods as shown in Fig. 3.7a and Fig. 3.7b. The temperature scales on the y-axes of Fig. 3.8 have the same range from max to min to aid in comparison between the two periods. Air temperatures within the canopy (blue) remain a few degrees higher than the air above (red) for both periods which is consistent with a mean upward sensible heat flux for daytime hours. Air temperatures show limited variation in the steady period in Fig. 3.8b, while showing considerably larger variability in the intermittent case of Fig. 3.8a. These larger variations correspond to the intermittent behavior in the turbulence in Fig. 3.7a. The soil temperatures (brown) in both figures are higher than any other component, however the difference is larger during the afternoon which is consistent with larger surface soil heating. The canopy temperature during the intermittent period ranged from a few degrees higher to slightly cooler than the within canopy air.

Intermittent

More Steady

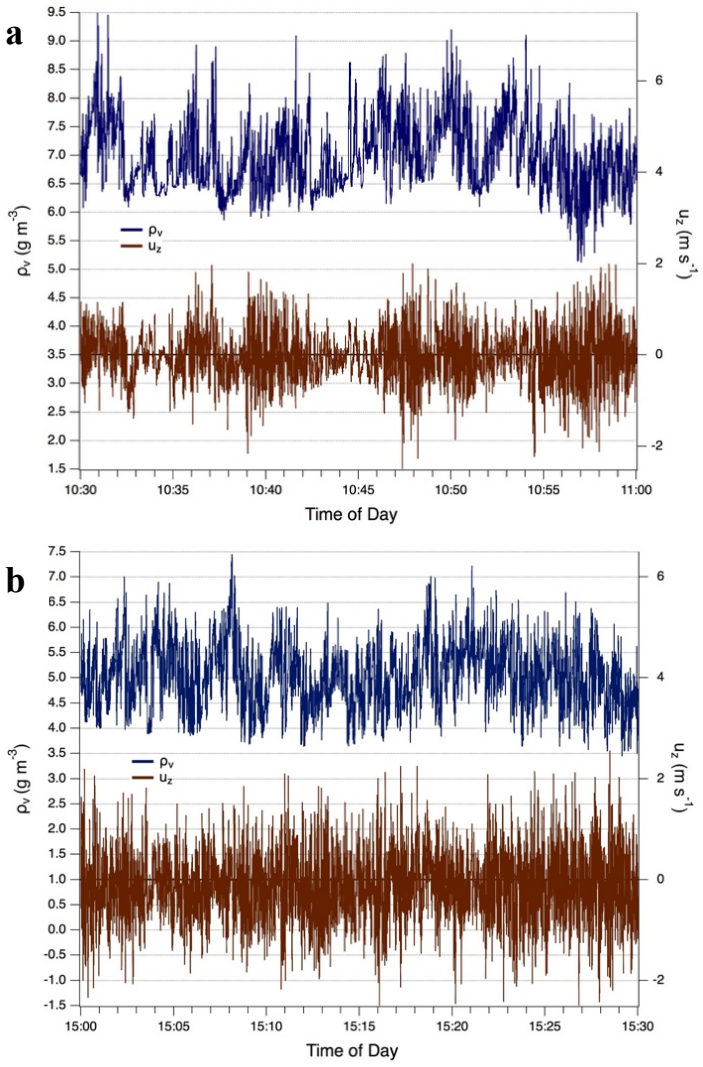

Fig. 3.7. Shown here are two 30-minute time series of water vapor density (ρ_v) and the vertical wind component (u_z) measured above the canopy (5 m) from at site #1 (north vineyard block) on DOY 162 of 2016. (**a**) corresponds to an intermittent period with mean winds of 1.7 m s^{-1}, while (**b**) shows a steadier case with hourly mean horizontal winds of 2.7 m s^{-1}.

Intermittent

More Steady

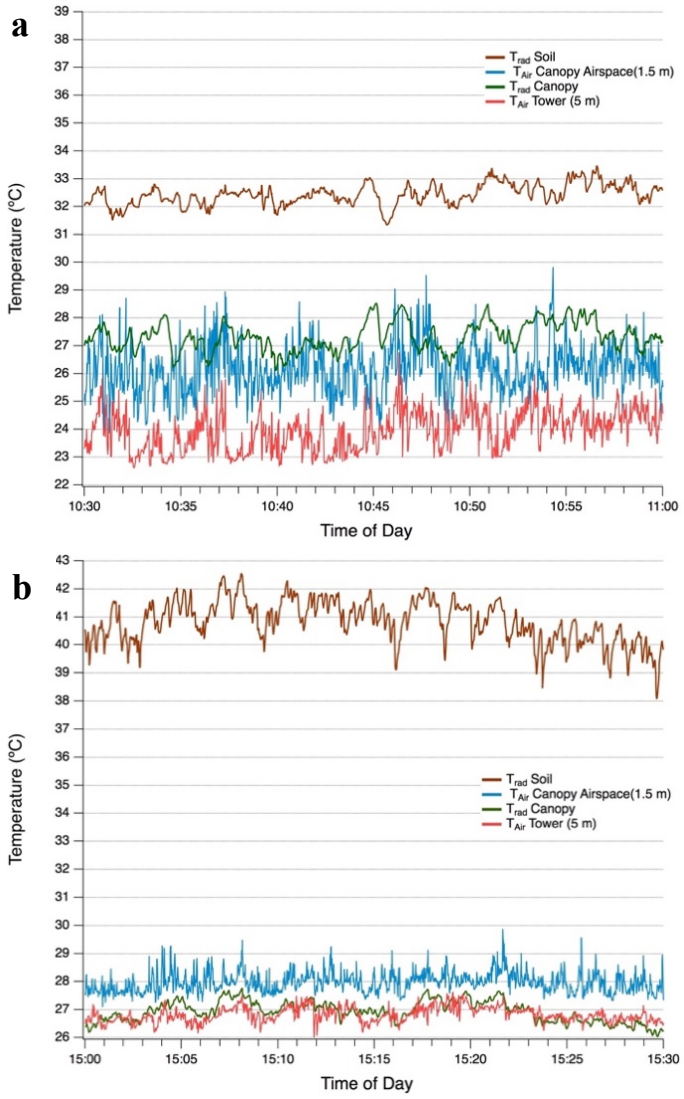

Fig. 3.8. Hz time series of T_A from the 5 m sonic anemometer (red), T_{AC} from the 1.5 m sonic anemometer (blue), and T_S (brown) and T_C (green) from the IRT array at site #1 on DOY 162 of 2016. (**a**) corresponds to an intermittent period, while (**b**) is a steadier case.

During the steady period the canopy temperature remains a degree or two below the within canopy air. Of note is the coherence between the variations of T_A, T_{AC}, and T_C during the steady period. There is, however, a distinct lack of coherence or consistency

in the intermittent periods where each of these temperatures appears to vary somewhat independently.

Fig. 3.9a and Fig. 3.9b show the resulting temperature gradients between T_{AC} - T_A (red), T_S - T_{AC} (tan), and T_C - T_{AC} (green) again for the same two 30-minute periods as in Fig. 3.7 and Fig. 3.8. Here the two panels show marked differences in both the magnitude and temporal behavior of the three temperature gradients. During the intermittent period all three of the gradients show large high frequency fluctuations, associated with the large variations in T_A and T_{AC}. The lower frequency variations in the three gradients match in time with intermittent patches of turbulence activity noted in the times series of u_z (Fig 3.7a). Of particular interest is the variation in the sign of the T_C - T_{AC} gradient showing that the canopy temperature is alternating between being lower and higher than that of the canopy air space. Clearly, the size and direction of the temperature gradients are transient under these conditions, with significant inconsistency. This contrasts with the steady period in Fig. 3.9b where all the three gradients demonstrate consistently smaller variations of constant sign.

The disparity in behaviors between the intermittent and steadier periods illustrated in Fig. 3.7, Fig. 3.8, and Fig. 3.9 was typical in the vineyards. This indicates that the differing behaviors in turbulence are associated with distinctly different temperature relationships within the vineyard structure. The large variability of temperature gradients during intermittent conditions presents implications for remote sensing models that by necessity use instantaneous temperature values. The low coherence between canopy temperatures and those of the within and above canopy air during intermittency suggests

that the canopy is not remaining in a consistent thermal equilibrium with the air over the typical flux averaging periods (Schymanski et al., 2013).

Intermittent

More Steady

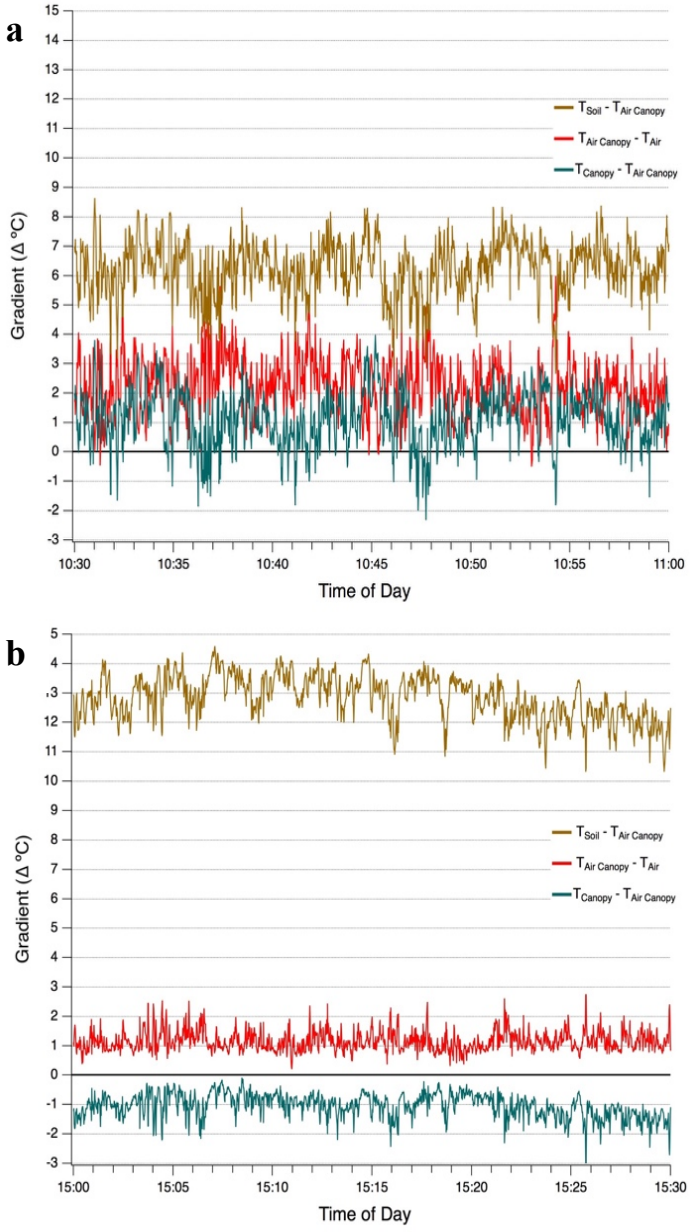

Fig. 3.9. Shown are two 30-minute time series of the gradients between these: T_{AC} - T_A (red), T_S - T_{AC} (tan), and T_C - T_{AC} (green) at site #1 (north vineyard block) on DOY 162 of 2016. (**a**) corresponds to an intermittent period, while (**b**) is a steadier case.

3.3.3. Hourly TSEB Model Evaluations

Fig. 3.10 is a scatter plot of hourly TSEB modeled fluxes versus those measured by eddy covariance for the full 417 hours set, including both intermittent and steady cases. Here measured fluxes are closed by Bowen ratio or assuming the original H/LE from the eddy covariance fluxes was valid. Table 3.2 lists statistics for the results in Fig. 3.10 in the 'All Hours' column. It should be emphasized that though modeled LE values are the end goal of TSEB to compute ET, LE is estimated as the residual of energy balance closure meaning it incorporates errors from modeled H, R_{Net}, and measurements of G. Therefore, because H is directly simulated by TSEB's resistance pathways, evaluation of modeled H values can be considered a more direct test of TSEB's performance. Modeled H values generally show agreement with measurements ($r^2 = 0.85$, $RMSE = 41.6$ W m^{-2}, $MAE = 34.6$ W m^{-2}), however, there is a systematic overestimation by the model at values, < ~140 W m^{-2}, and an underestimation at higher values. This is highlighted by the shallower slope (0.69) of the H regression fit as compared to the 1:1 line. LE values also demonstrate reasonable agreement ($r^2 = 0.85$, $RMSE = 43.3$ W m^{-2}, $MAE = 35.7$ W m^{-2}), but with noticeably less of a bias dependent on the magnitude of the flux, with a slope much closer to 1 (0.91). Diurnal curves of R_{Net}, G, H, and LE for various IOP days, not shown here, frequently indicated periods where H values became negative in the mid-afternoon (before 17:00 LST) suggesting heat advection from large fields of dry vegetation in the local region of the vineyard sites (within 5 – 10 km). Some of these hours are noted in Fig. 3.10 as the group of negative measured H values (those left of the y-axis). These values denote large

model underestimations of H and correspond to some of the largest overestimations of LE again due to the relationship of H and LE via energy balance closure. Modeled H values have a small overall bias for underestimation of 5.5 W m^{-2}, while modeled LE values have an overall bias for overestimation of -14.3 W m^{-2}.

Fig. 3.11 is a scatter plot of results for the same 417 hours, but for TSEB modeled fluxes versus eddy covariance measurements closed by residual energy balance closure. Here both modeled fluxes show noticeably improved agreement with measurements compared to Fig. 3.10. This is confirmed by improvements in the statistics for both fluxes (not listed in Table 3.2). Modeled H values have a similar r^2 to those of Fig 3.10 (0.85), but with an appreciably improved slope of the regression line (0.79 vs. 0.69) and d smaller errors ($RMSE = 35.2$ W m^{-2}, $MAE = 28.9$ W m^{-2}). Modeled LE also demonstrates improved agreement with of a larger r^2 (0.91 vs. 0.85) and considerably smaller errors ($RMSE = 32.4$ W m^{-2}, $MAE = 26.7$ W m^{-2}) as compared to measurements closed using Bowen ratio closure. However, the better agreement when all residual energy is put into LE as opposed to H, does not ensure that this approach is more correct than the Bowen ratio closure. It may be fortuitous, and the "best" method of energy balance closure remains to some extent unresolved.

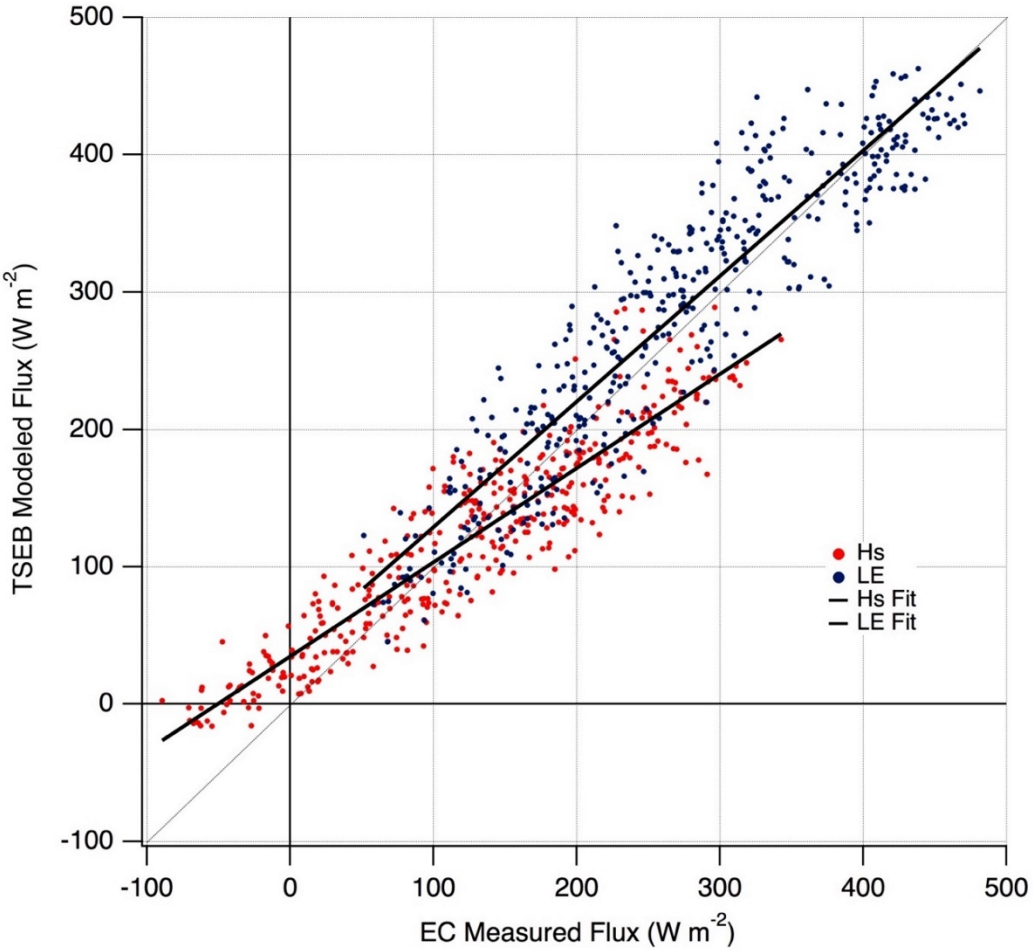

Fig. 3.10. Results for TSEB modeled sensible heat flux (H) (red) and latent heat flux (LE) (blue) versus eddy covariance fluxes closed by energy balance residual distributed by Bowen ratio. Also shown are linear regression fits for each, and a 1:1 ratio line.

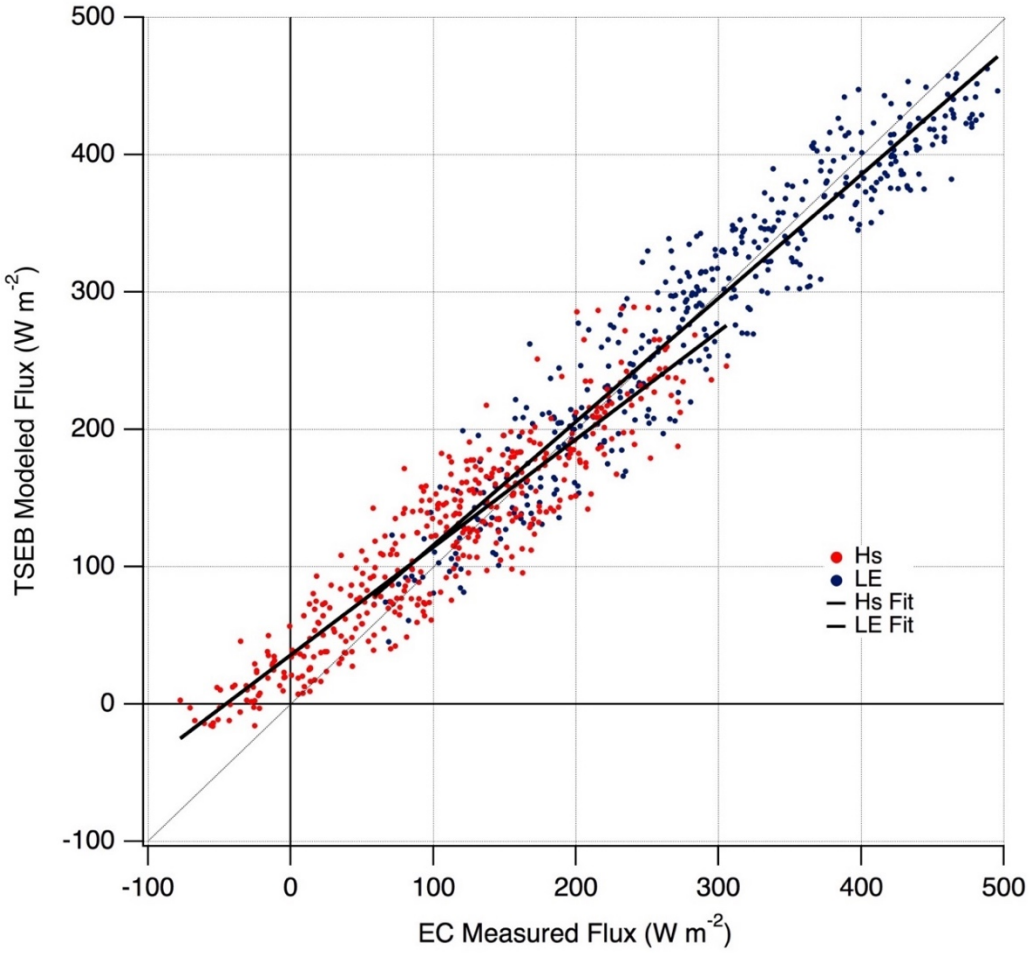

Fig. 3.11. Results for TSEB modeled sensible heat flux (H_s) (red) and latent heat flux (LE) (blue) versus eddy covariance fluxes that have been closed by assigning all residual energy to latent heat flux. Also shown are linear regression fits for each and a 1:1 ratio line.

With the model results for all 417 hours as a baseline, the intermittent and steady hour subsets were evaluated. Fig. 3.12 displays TSEB modeled H values versus eddy covariance measurements closed via their Bowen ratio for the 115 intermittent hours and 102 steady hours, while Fig. 3.13 displays the same for modeled LE values. Statistics for both fluxes from both subsets are listed in Table 3.2. H values for the intermittent hours

appear generally similar in distribution to those from steady hours, but with notable differences in their statistical metrics. The slope of the regression fit for intermittent hours (dashed line) is lower (0.61) than the steady hours (solid line) (0.72) highlighting a tendency for an underestimation of modeled fluxes at higher flux values during intermittency. The error metrics for intermittent periods are decidedly larger ($RMSE = 50.2$ W m^{-2}, $MAE = 44.6$ W m^{-2}) than compared to those of the steady hours ($RMSE = 37.0$ W m^{-2}, $MAE = 29.1$ W m^{-2}), and intermittent periods had much larger bias than steady periods (18 W m^{-2} vs. 1.7 W m^{-2}). LE values for the intermittent hours compared to those from steady hours (Fig. 3.13) demonstrate similar differences in statistics as seen in H. The slope of the regression fit for the LE during intermittent hours (dashed line) again has a lower value (0.77) than that of the steady hours (solid line) (0.99). This at first is counterintuitive considering LE is determined within TSEB by residual, suggesting that the shallow slope for the intermittent H regression line in Fig. 3.12 should be mirrored as a slope steeper than a 1:1 of the LE regression line in Fig. 3.13. However, through their relationship of the Bowen ratio, higher magnitude H values are associated with lower magnitude LE values, providing a compensating effect such that the modeled H and LE have similar trends in error with increasing flux. The error metrics for modeled LE during intermittent periods are notably larger ($RMSE = 54.7$ W m^{-2}, $MAE = 47.9$ W m^{-2}) than compared to those of the steady hours ($RMSE = 35.3$ W m^{-2}, $MAE = 28.1$ W m^{-2}) and intermittent periods show an increased bias over steady periods (-25.8 W m^{-2} vs. 9.2 W m^{-2}).

In examining the statistics between intermittent, steady, and all hours (Table 3.2), of particular significance is that during intermittent hours TSEB shows the least

agreement with measurements compared to both the all hours and steady sets for all metrics. Furthermore, the model shows the best agreement for the steady hours by all statistics compared to not only the intermittent hours, but also to the all hours set. This differentiation of model performance in the three sets of hours suggests the assumptions in the model are most valid during steady periods when gradient behavior is most consistent. It also indicates that the model assumptions seem to be less valid for intermittent hours where flux-gradient relationships may not completely explain how the flux of H is occurring in the vineyards under those conditions.

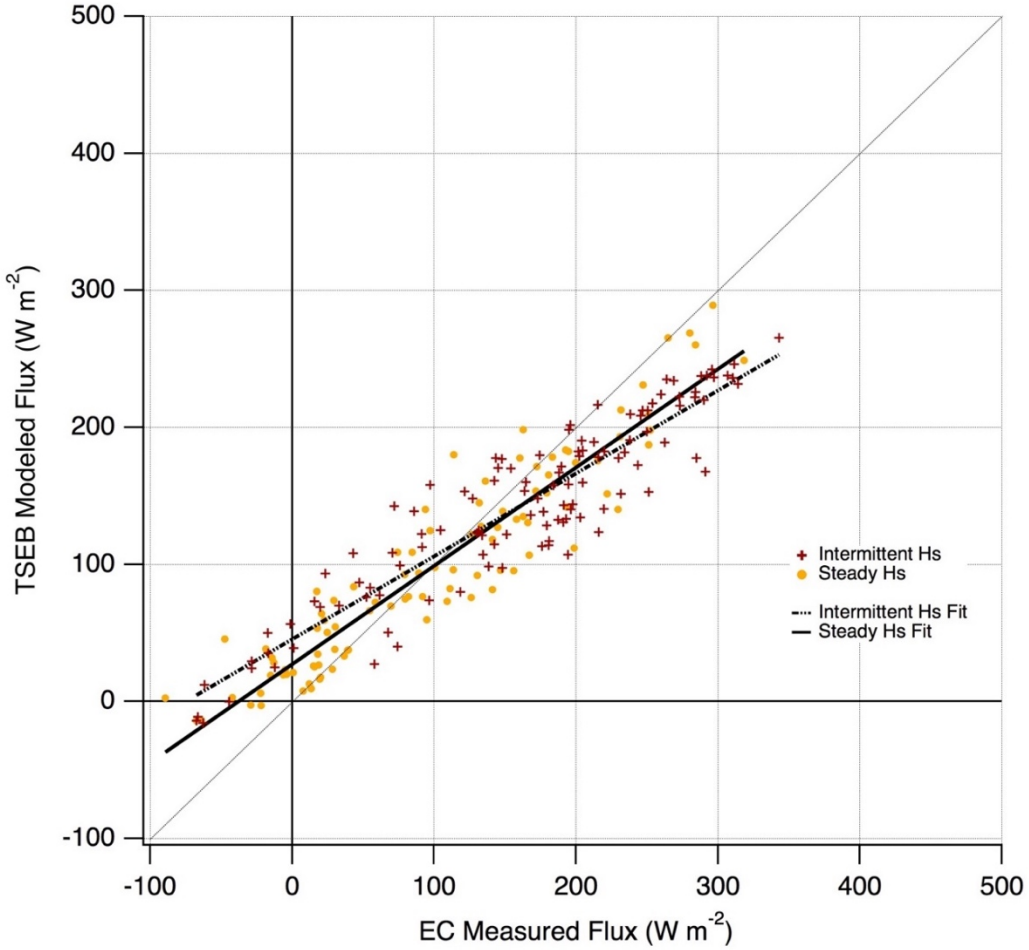

Fig. 3.12. Results for TSEB modeled sensible heat flux (H) for intermittent periods (red crosses) and steady periods (yellow points) versus eddy covariance fluxes closed by Bowen ratio. Also shown are linear regression fits for intermittent hours (dashed line), steady hours (thick solid line), and a 1:1 ratio line.

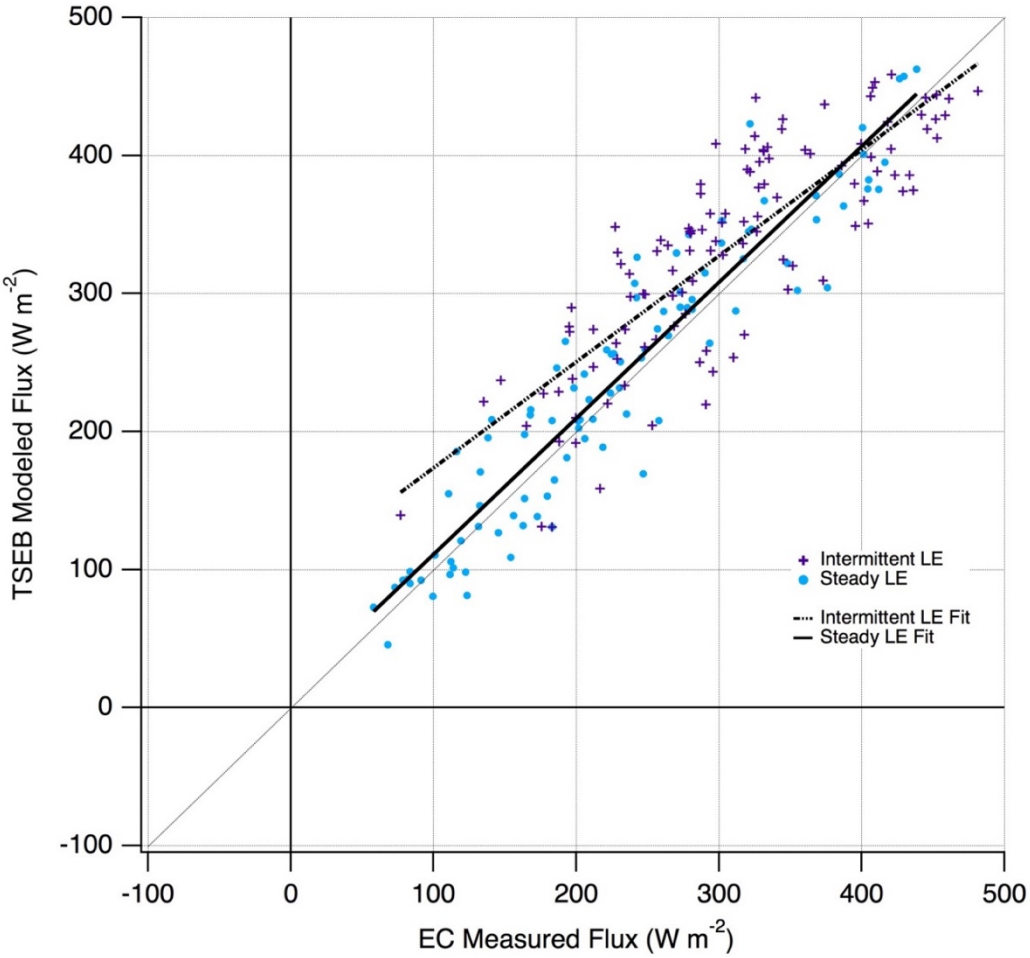

Fig. 3.13. Results for TSEB modeled latent heat flux (LE) for intermittent periods (purple crosses) and steady periods (blue points) versus eddy covariance fluxes closed by Bowen ratio. Also shown are linear regression fits for intermittent hours (dashed line), steady hours (thick solid line), and a 1:1 ratio line.

Table 3.2
Statistics for TSEB hourly modeled sensible heat flux (H) and latent heat flux (LE) versus eddy covariance measurements for all hours, intermittent hours, and steady hours. All eddy covariance data for these results were closed by Bowen ratio closure.

	H			LE		
	All Hours (Bowen)	Intermittent Hours	Steady Hours	All Hours (Bowen)	Intermittent Hours	Steady Hours
r^2	0.85	0.85	0.88	0.85	0.68	0.89
Fit Slope	0.69	0.61	0.72	0.91	0.77	0.99
RMSE ($W\ m^{-2}$)	41.6	50.2	37	43.3	54.7	35.3
MAE ($W\ m^{-2}$)	34.6	44.6	29.1	35.7	47.9	28.1
Bias ($W\ m^{-2}$)	5.5	18	1.7	-14.3	-25.8	-9.2

Fig. 3.14a and 3.14b depict the relationships of the difference in TSEB modeled H and eddy covariance H (closed by Bowen ratio) (3.14a) as a function of measured Obukhov length (L) (Fig. 3.14a) and the mean hourly horizontal wind speed (3.14b). Fig 3.14a indicates little relationship of the error with larger negative L values, i.e. when the influence of buoyancy is less, but shows a sharp tendency to underestimate H values, and therefore overestimate LE values, as L approaches zero from the negative (more unstable). This suggests that the model has increasing difficulty estimating H as buoyancy increasingly dominates and the stability becomes more unstable. Fig. 13.4b illustrates a moderate relationship between model error and mean wind speed where lower speeds see an underestimation of H and higher speeds see a shift to overestimation. This transition occurs at winds of ~ 2 – 2.5 m s^{-1} which corresponds well with the range of mean winds that often are associated with the transition between intermittent and

steadier behavior (Fig. 3.4). Together Fig. 3.14a and 3.14b suggest that the same light wind, unstable conditions associated with intermittent behavior (Los et al., 2019) are associated with systematic underestimation of H. This further agrees with the model error statistics for H during intermittent hours (Table 3.2).

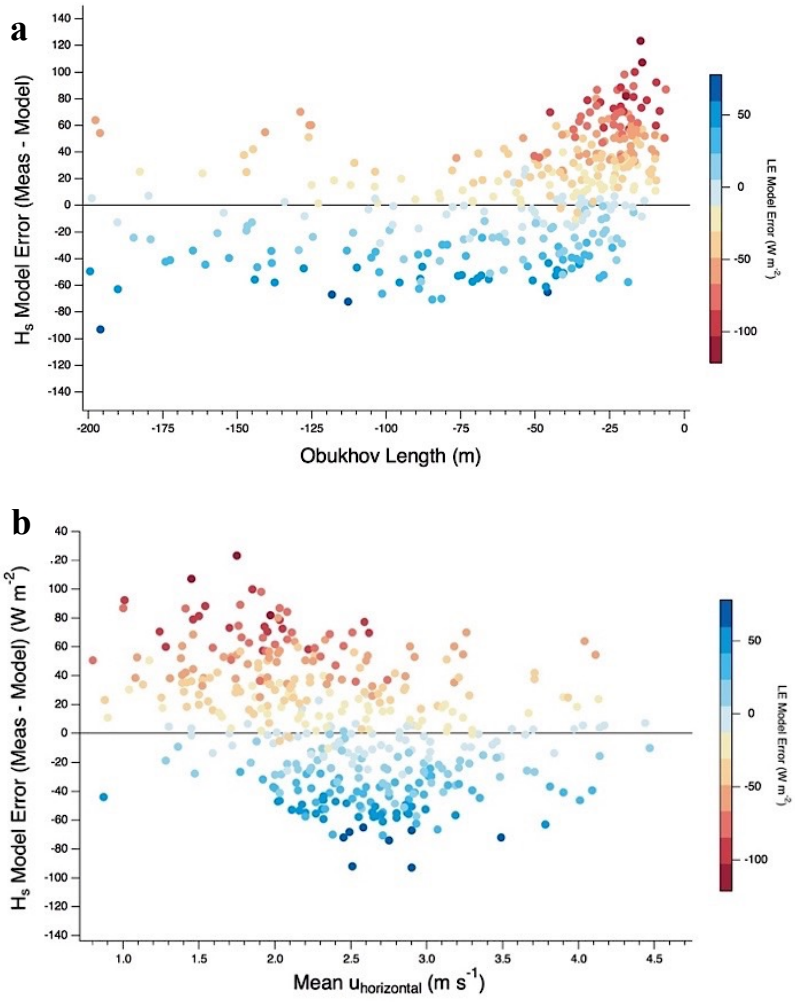

Fig. 3.14. TSEB model error in sensible heat flux (eddy covariance measured – TSEB modeled) vs. (**a**) Obukhov length, and (**b**) mean hourly horizontal wind. The color scale of the points corresponds to the error in latent heat flux (eddy-covariance measured – TSEB modeled) where warm colors represent overestimation and cool colors represent underestimation.

In order to further evaluate the performance of TSEB, Fig. 3.15 shows TSEB modeled versus eddy covariance derived aerodynamic resistance (R_A, 3.15a) and friction velocity (u_*, 3.15b) for the all hours and intermittent periods. Modeled R_A in Fig. 3.15a is underestimated compared to measurements for nearly all hours tested. Modeled u_* in Fig. 3.15b on the other hand, which is a term in the calculation of R_A, shows a consistent tendency to be somewhat overestimated by the model. Given that higher modeled values of u_* should cause a reduced R_a, all else being equal, this suggests that a systematic overestimation of u_* may be partially responsible for the underestimation R_A for these test hours. However, this is somewhat in conflict with the modeled error results for H as universally lower R_A values should lead TSEB to consistently overestimate H. As described above, Fig 3.10 shows modeled H being overestimated at lower magnitude fluxes, and being underestimated at higher magnitudes. Fig 3.15a depicts the R_A values for intermittent periods (orange points), and these show no obvious difference from the other points from all hours. The same is true for u_* values where intermittent hours (green points) in Fig. 3.15b show no different relationship than the other all hour points. Therefore, the calculations of R_A and u_* by TSEB do not conclusively explain the pattern of modeled H errors in Fig 3.10. Given the series of computations performed within TSEB to determine H, further investigation is required to explain how both intermittency and vineyard structure may be affecting model performance.

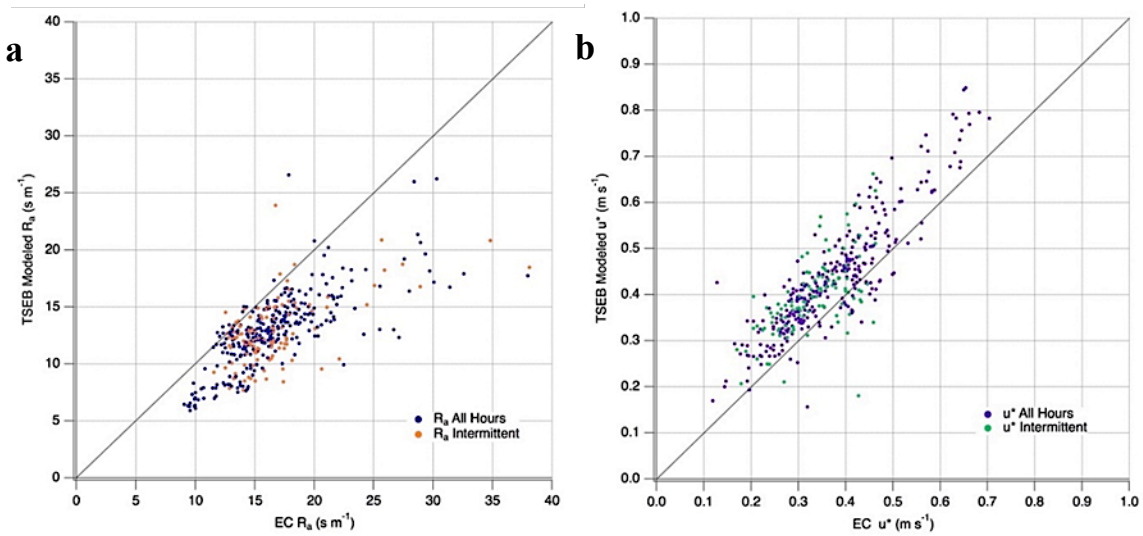

Fig. 3.15 Plots of (**a**) TSEB modeled values of R_A versus the 5 m eddy covariance derived values for all hours (blue) and intermittent hours (orange), and (**b**) TSEB modeled values of u_* versus those measured at 5 m for all hours (purple) and intermittent hours (green).

3.3.4. 1 hz TSEB Model Evaluation

In surveying the measured 1 Hz IRT temperature time series for various days at both sites, considerable variability was noted in the temperatures of both the canopy (T_C) and soil (T_S). Fig 3.16 depicts traces of from the six individual IRTs from the array at site #1 during the late morning of DOY 162 of 2016. Here brown traces are for the two soil-viewing IRTs and the green traces are for the four canopy-viewing IRTs. The two T_S series show a slow change in their relationship to one another across the hour that was associated with changes in shading as the solar angle progressed. Turbulence and humidity time series for this same period were noted for intermittent behavior. Though each of the six traces demonstrate unique behavior, coherent patterns of fluctuation

between them are obvious. These patterns were correlated with changes in turbulent activity where rises in temperature were associated with lower turbulence and drops were associated with more intense exchanges. This is similar to behavior found in other studies of air-surface temperature coupling where during individual turbulent events surface cooling is driven by venting of warm moist air from the canopy airspace and replacement by cooler, drier air from above (Paw U et al., 1992, Kustas et al., 2002). However, not all the variability in T_C and T_S time series could readily be explained by variability in turbulence or humidity time series as even periods of steadier turbulence behavior were often noted to have considerable variability in T_C or T_S or both. This could be attributed to variability in a number of other factors including surface shading of the soil surface, canopy motion effects on IR reflectance/emission from changing leaf angles, or stomatal response behavior (Blonquist et al., 2009).

Given the variability observed in surface temperatures, analysis proceeded to testing the sensitivity of TSEB to these fluctuations. In addition to the individual IRT traces, Fig 3.16 shows a composite IRT radiometric surface temperature (IRT T_{RAD}) time series (light purple) developed by weighting the six individual IRT time series by f_c. In comparing this IRT T_{RAD} to one derived from 15-minute tower net radiometer data (Tower T_{RAD}, dark purple), the IRT T_{RAD} was typically quite similar to, but ~ 1 – 1.5 K higher during the hour. This difference was typical for time series of the two derived T_{RAD} during the midday period of IOP days surveyed. Despite this temperature offset, IRT T_{RAD}, as shown in Fig. 3.16, seems to present a realistic high frequency surface temperature time series that captures the variability noted in T_C and T_S.

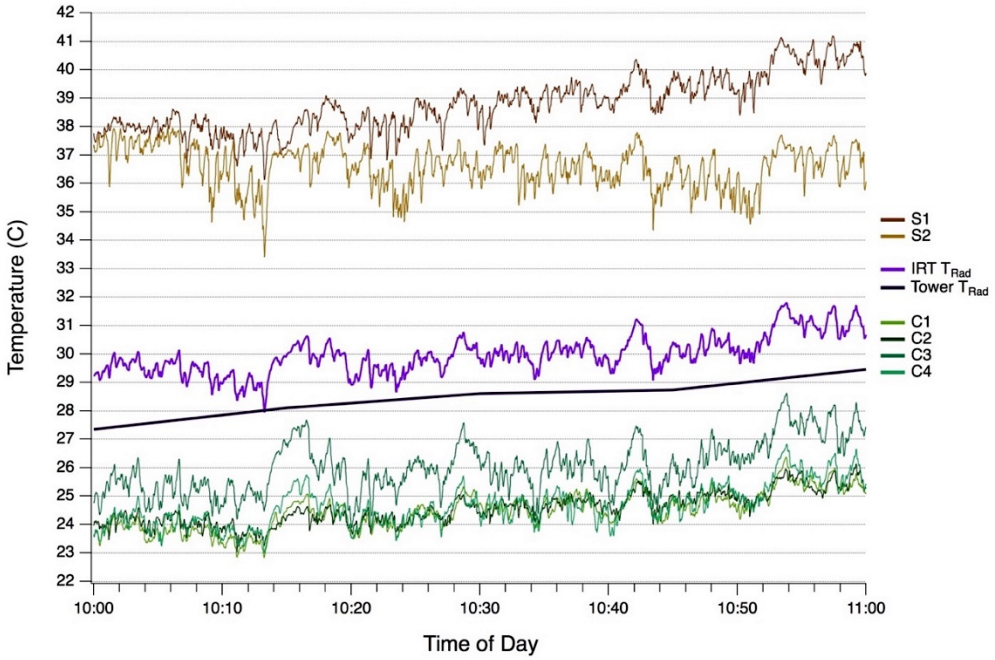

Fig. 3.16. 1-hour time series of 1 Hz IRT measured soil temperatures (S1, S2, browns) and canopy temperatures (C1, C2, C3, C4, greens) during an intermittent period. Also shown are composite radiometric surface temperatures (T_{RAD}) derived from the six IRTs (light purple) and 15-minute mean values from the 6 m tower net radiometer.

Using the IRT T_{RAD} time series as input, TSEB was run for ten different midday (9:00 – 14:00 LST) hours from several IOP days during 2016 corresponding to typical satellite overpass times. All other inputs such as LAI, T_{air}, and mean wind were held constant over the hour. Fig. 3.17a and Fig. 3.17b show results for one such hour from 1300 – 1400 LST on DOY 163 of 2016 at site #2. In Fig. 3.17a are traces for the input IRT T_{RAD} (purple) and T_{air} (yellow), as well as the modeled results for H (red), while Fig. 13.7b depicts modeled values for LE (blue). The dashed lines in 3.17a and 3.17b correspond to the hourly eddy covariance measurement value for each respective flux. TSEB modeled H shows considerable variability in time ranging from a low of 74 W m^{-2}

to a high of 132 W m^{-2}, a nearly two-fold difference. Variability in modeled LE had range of 68 W m^{-2} and inversely mirrors values of H due to TSEB allocating residual energy balance differently for various surface temperatures. These ranges in fluxes result in a Bowen ratio as low as 0.15 or as high as 0.3. This is a considerable difference and a finding of interest given that operationally daily ET is often estimated from a single satellite overpass time by extrapolating the modeled Bowen ratio across the day. This large range of model solutions over the hour was typical of all of the hours tested. It is important to note that the averages for both TSEB modeled flux time series in Fig. 3.17 are actually very close to the hourly eddy covariance values. Given the contrast between this agreement and the large variability of solutions on the one-second time scale, this highlights the inability of averages to capture the dynamic behavior of the canopy temperatures.

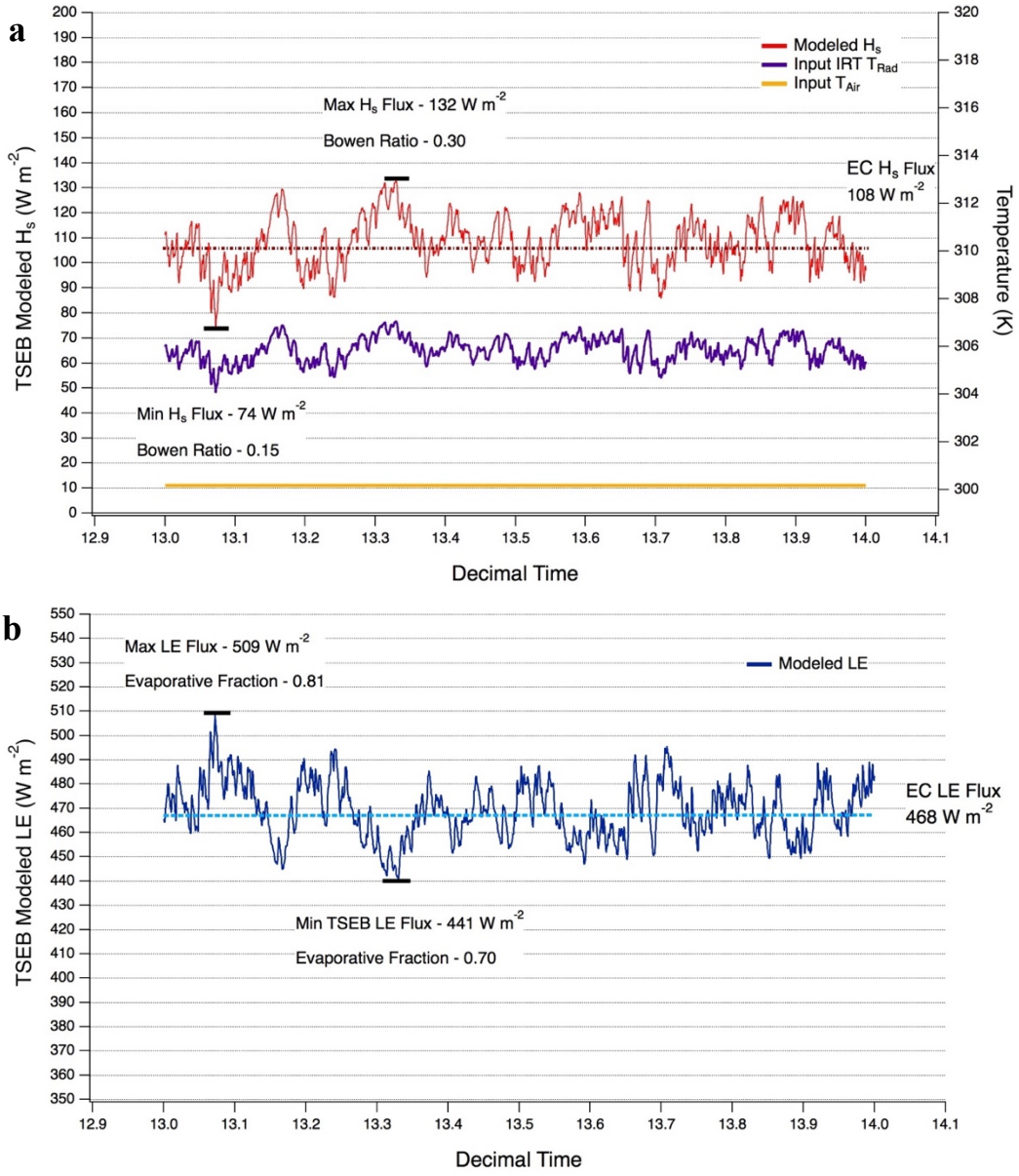

Fig. 3.17. 1-hour time series of modeled sensible heat flux (**a**) (H) (red) and latent heat flux (**b**) (LE) (blue). The red dashed line in (**a**) is the hourly eddy covariance H, while the blue dashed line in (**b**) is the hourly eddy covariance LE. Also shown in (**a**) are time series of the input IRT-derived radiometric temperature ($IRT\ T_{RAD}$) (purple) and the input 5 m air temperature (T_{air})(yellow) which was held constant for the period.

During three of the ten hours tested, a behavior of TSEB fluxes was observed where the modeled solutions became unstable for short periods during a given hour. Fig. 3.18a illustrates this behavior during the second 30 minutes of the hour where modeled H values are seen fluctuating in large, sharp steps of 20 – 40+ W m^{-2}. LE values, not shown, responded by mirroring this behavior. It was found that this was associated with time steps when the difference between the constant T_{air} and IRT T_{RAD} exceeded ~7.5 K. To investigate further the IRT T_{RAD} was manually lowered by 1.5 K during the second 30 minutes of the hour (such that no point was greater than 7.5 K above T_{air}) and the test was run again. Fig. 3.18b shows that the resulting time series of modeled H no longer displays the unstable behavior. This test was then run a third time by creating an IRT T_{RAD} time series that simply rose linearly from 297.5 K (just above T_{air}) to 306.5 K. This third test is depicted in Fig 3.18c where modeled H values increase nearly linearly until there are a series of step-wise increases spaced by periods of continued linear rise. Given that LAI was rather large, ~2.3 m^2 m^{-2}, the behavior in these figures suggests that for a particular combination of input values and a large enough difference in IRT T_{RAD} and T_{air} there are points of instability where the formulations in TSEB struggle to realistically partition energy between soil and canopy, resulting in discontinuous solutions.

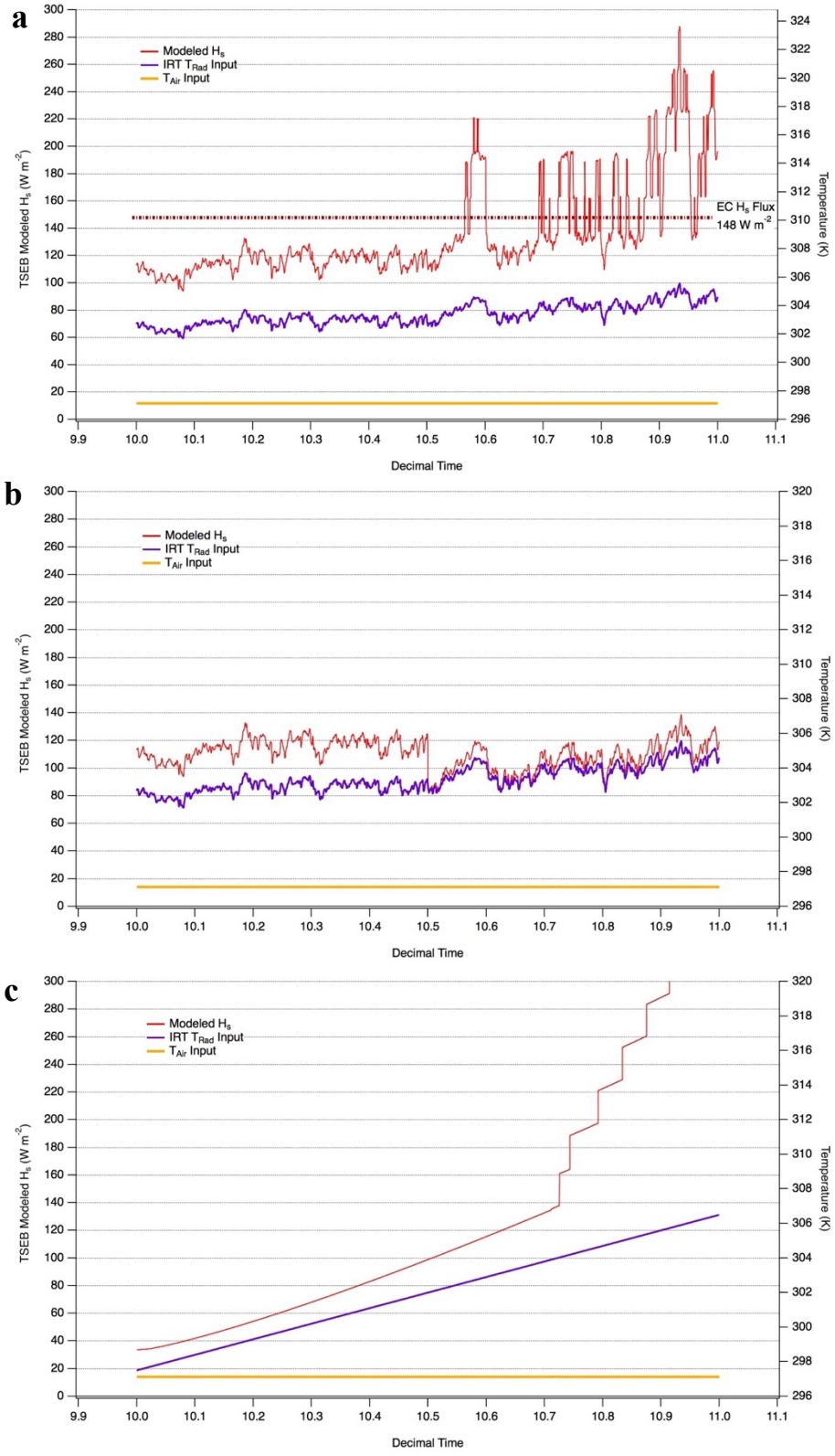
a
Modeled H_s
IRT T_{Rad} Input
T_{Air} Input
EC H_s Flux
148 W m^{-2}
TSEB Modeled H_s (W m^{-2})
Temperature (K)
Decimal Time
b
Modeled H_s
IRT T_{Rad} Input
T_{Air} Input
TSEB Modeled H_s (W m^{-2})
Temperature (K)
Decimal Time
c
Modeled H_s
IRT T_{Rad} Input
T_{Air} Input
TSEB Modeled H_s (W m^{-2})
Temperature (K)
Decimal Time

Fig. 3.18. (**a**) 1-hour time series of TSEB modeled sensible heat flux (H) (red) demonstrating unstable behavior in the solutions during the last half of the hour. Also shown are the hourly eddy covariance H (red dashed line), input IRT radiometric temperature ($IRT\ T_{RAD}$) (purple), and input 5 m air temperature (T_{air}) (yellow). (**b**) Plot of the same period as (**a**) except with a TSEB run using an $IRT\ T_{rad}$ where the values between 10:30 and 11:30 LST were lowered by 1.5 K. (**c**) Plots of the same period except with TSEB run using an $IRT\ T_{RAD}$ that increased linearly through the hour from 297.5 K to 306.5 K.

It must be noted that the observed variability in the time series of IRT T_{RAD} may not represent the variability that would typically be observed by a satellite retrieval. The much larger spatial scale of a 30 – 100+ m satellite pixel compared to that of the IRT array view footprint would likely diminish much of these fluctuations. However, considering the instantaneous nature of remote sensing retrievals and the large range in model solutions produced by the IRT T_{RAD} input, these results should be noted in the implementation of TSEB and other remotely sensed ET models.

3.4. Conclusions

This study investigated the influence of intermittent turbulence on vineyard biophysics and the ability of the Two-Source Energy Balance (TSEB) model to estimate sensible and latent heat fluxes. Comparisons of TKE time series above and within the vineyard canopy show much different behavior when turbulence becomes episodic or intermittent versus more continuous, steady conditions. Periods of intermittent

turbulence often exhibit low coherence and decoupling between activity in the canopy airspace and the flow above the canopy. Conversely more steady turbulence was marked by consonant behavior between the above and within canopy activity suggesting more consistent coupling. Analysis of temperature gradients between soil, canopy foliage, canopy airspace, and above canopy air temperatures on a 1 Hz timescale demonstrate that intermittent transport greatly alters the temporal behavior of these gradients. While the relationships between these temperatures remained rather stable during steady transport periods, during transient exchanges gradients showed considerably more variability and the gradient between canopy surfaces and the air would at times alternate sign over short timescales in conjunction with bursts of turbulent activity.

TSEB modeled fluxes for 417 hours across three growing seasons from two vineyard sites overall displayed favorable agreement with eddy covariance measured fluxes through statistical metrics of r^2, RMSE, MAE, and bias. Modeled fluxes of 115 intermittent hours sub-selected from this group showed considerably less agreement with measurements indicated through increased RMSE and MAE, and evidence of bias. For the 102 sub-selected hours showing steady behavior TSEB demonstrated higher performance than all hours, with consistently lower error statistics. Given a lack of universal agreement in the optimal method for closing energy balance in eddy covariance measurements, whether to allocate residual energy according to the Bowen ratio or by assigning all residual energy to LE remains a matter of debate. Hence, it is useful to make model comparisons considering more than one closure method. In this case, the method of closure noticeably affected the comparison of TSEB fluxes with eddy covariance measurements. Relationships between TSEB modeled sensible heat flux

error, wind speed, and stability demonstrate that model underestimation is correlated with conditions characterized by low winds, large instability, and large sensible heat fluxes. However, analysis of modeled versus measurement derived aerodynamic resistance and friction velocity did not evidence an obvious cause for the lower model performance noted during intermittent periods. TSEB showed substantial sensitivity to temporal variations in "snapshot" radiometric temperature derived from 1 Hz IRT data. Furthermore, unstable model solutions were observed for some combinations of model inputs, particularly temperature gradients between the surface and the above air the canopy of greater than 7.5 K, values not unrealistic in real-world settings. These noted sensitivities of TSEB suggest that effects on variables at time scales shorter than the averaging period are important considerations for the use of quasi-instantaneous satellite retrievals as input into ET models.

The altered, erratic behavior demonstrated in TKE and temperature gradient analysis during intermittency suggests possible limits on flux-gradient models. Typical flux-gradient relationships (such as Eqs. 3.1 – 3.3) implicitly assume that gradients represent a dynamic equilibrium of the transport processes, and the net result of variations is reasonably consistent with the flux from the surface. Although this is valid for many situations, particularly behavior deemed as steady, assumptions that fluxes from these complex surfaces are proportional to average gradients may not always hold when the transport of heat and water vapor (ET) is highly transient. This seems to be confirmed by TSEB model tests where agreement with measured fluxes degraded under intermittent conditions. In contrast, steady periods where average flux-gradient assumptions are most valid, produced the best model agreement. Clearly how the flux

occurs during an averaging interval is important to vineyard ET and further study is required to elucidate the effects of intermittent transport behavior on the ET process in vineyards, and also the ability to effectively monitor water use in vineyards.

3.5. Acknowledgements

Funding provided by NASA Grant #NNX17AF51G and the Utah Agriculture Experiment Station, Project UTAO 1186. Funding provided by E.&J. Gallo Winery and USDA-ARS made possible the collection of much of the data during GRAPEX IOPs. In addition, we would like to thank the staff of the Viticulture, Chemistry and Enology Division of E.&J. Gallo Winery for their logistical support as part of the GRAPEX project. Finally, this project would not have been possible without the cooperation of Mr. Ernie Dosio of Pacific Agri Lands Management, along with the Borden vineyard staff, for logistical support of GRAPEX field and research activities. USDA is an equal opportunity provider and employer.

3.6. Conflicts of Interest

On behalf of all authors, there is no conflict of interest.

3.7. References

Alfieri, J.G., Kustas, W.P., Nieto, H., Prueger, J.H., Hipps, L.E., McKee, L.G., Gao, F., Los, S.A., 2018. Influence of wind direction on the surface roughness of vineyards. Irrigation Sci. https://doi.org/10.1007/s00271-018-0610-z.

Anderson, M.C., Norman, J.M., Li, F., Kustas, W.P., Prueger, J.H., Mecikalski, J.R., 2005. Effects of vegetation clumping on two-source model estimates of surface energy fluxes from an agricultural landscape during SMACEX. J. Hydrometeorol. 6, 892–909.
Ansorge, C., Mellado, J.P., 2014. Global intermittency and collapsing turbulence in the stratified planetary boundary layer. Bound.-Layer Meteorol. 153, 98-116.
.
Ashenfelter, O., Gergaud, O., Storchmann, K., Ziemba, W., 2018. Handbook of the Economics of Wine:Volume 1: Prices, Finance, and Expert, World Scientific Publishing Co. Pte. Ltd.

Blonquist, J.M. Jr., Norman, J.M., Bugbee, B., 2009. Automated measurement of canopy stomatal conductance based on infrared temperature. Agric. For. Meteorol. 149, 1931-1945.

Brutsaert, W., 1975. On a derivable formula for long-wave radiation from clear skies. Water Resour. Res. 11(5), 742-744.

Brutsaert, W., 2005. Evaporation. In hydrology: An introduction. Cambridge: Cambridge University Press.

Brotzge, J., Crawford, K.C., 2003. Examination of the surface energy budget: A comparison of eddy correlation and bowen ratio measurement systems. J. Hydrometeorol. 4, 160-178.

Cammalleri, C., Anderson, M.C., Ciraolo, G., D'Urso, G., Kustas, W.P., La Loggia, G., Minacapilli, M., 2010. The impact of in-canopy wind profile formulations on heat flux estimation in an open orchard using the remote sensing-based two-source model. Hydrol. Earth Syst. Sci. 14, 2643-2659.

Campbell, G.S., Norman, J.M., 1998. Heat flow in the soil. In: An introduction to environmental physics. Springer, New York.

Chahine, A., Dupont, S., Sinfort, C., Brunet, Y., 2014. Wind-flow dynamics over a vineyard. Bound.-Layer Meteorol. 151, 557-577.

Finnigan, J.J., 2000. Turbulence in plant canopies. Annu. Rev. of Fluid Mech. 32, 519-557.

Finnigan, J.J., Clement, R., Malhi, Y., Leuning, R., Cleugh, H.A., 2003. A re-evaluation of long-term flux measurement techniques, part I: averaging and coordinate rotation. Bound.-Layer Meteorol. 107, 1-48.

Foken, T., Leuning, R., Oncley, S.R., Mauder, M., Aubinet, M., 2012. Corrections and data quality control. In: M. Aubinet et al. (eds) Eddy covariance: a practical guide to measurement and data analysis. Springer Atmospheric Sciences. pp 85-131.

Francone, C., Katul, G.G., Cassardo, C., Richiardone, R., 2012. Turbulent transport efficiency and the ejection-sweep motion for momentum and heat on sloping terrain covered with vineyards. Agric. For. Meteorol. 162-163, 98-107.

Gao, W., Shaw, RH., Paw U, K.T., 1989. Observation of organized structure in turbulent flow within and above a forest canopy. Bound.-Layer Meteorol. 47, 349-377.

Gao, F., Anderson, M.C., Kustas, W.P., Wang, Y., 2012. A simple method for retrieving Leaf Area Index from Landsat using MODIS LAI products as reference. J. Appl. Remote Sens. 6(1), 063554.

Katul, G.G., Kuhn, G., Schieldge, J., Hsieh, C.I., 1997. The ejection-sweep character of scalar fluxes in the unstable boundary layer. Bound.-Layer Meteorol. 83.1, 1-26.

Kool, D., Kustas, W.P., Ben-Gal, A., Lazarovitch, N., Heitman, J.L., Sauer, T.J., Agam, N., 2016. Energy and evapotranspiration partitioning in a desert vineyard. Agric. For. Meteorol. 218-219, 277-287.

Kustas, W.P., Prueger, J.H., Hipps, L.E., 2002. Impact of using different time-averaged inputs for estimating sensible heat flux of riparian vegetation using radiometric surface temperature. J. Appl. Meteorol. 41, 319-332.

Kustas, W.P., Alfieri, J.G., Anderson, M.C., Colaizzi, P.D., Prueger, J.H., Evett, S.R., Neale, C.M., French, A.N., Hipps, L.E., Chávez, J.L., Copeland, K.S., Howell, T.A., 2012. Evaluating the two-source energy balance model using local thermal and surface flux observations in a strongly advective irrigated agricultural area. Adv. Water. Res. 50, 120-133.

Kustas, W.P., Anderson, M.C., Alfieri, J.G., Knipper, K., Torres-Rua, A., Parry, C.K., Nieto, H., Agam, N., White, W.A., Gao, F., McKee, L., Prueger, J.H., Hipps, L.E., Los, S., Alsina, M.M., Sanchez, L., Sams, B., Dokoozlian, N., McKee, M., Jones, S., McElrone, A., Heitman, J.L., Howard, A.M., Post, K., Melton, F., Hain, C., 2018. The grape remote sensing atmospheric profile and evapotranspiration experiment. Bull. Amer. Meteor. Soc. 99, 1791-1812.

Lee, Y.-H., 2009. The influence of local stability on heat and momentum transfer within open canopies. Bound.-Layer Meteorol. 132, 383-399.

Lee, Y.-H. 2011. Intermittency of turbulence within open canopies. J. Atmos. Sci. 47.2, 137-149.

Li, D., Bou-Zeid, E., 2011. Coherent structures and the dissimilarity of turbulent transport of momentum and scalars in the unstable atmospheric surface layer. Bound.-Layer Meteorol. 10, 243-262.

Li, S., Tong, L., Li, F., Zhang, L., Zhang, B., Kang, S., 2009. Variability in energy partitioning and resistance parameters for a vineyard in northwest China. Agric. Water. Manage. 96, 955-962. https://doi.org/10.1016/j.agwat.2009.01.006.

Los, S.A., Hipps, L.E., Alfieri, J.G., Kustas, W.P., Prueger, J.H., 2019. Intermittency of water vapor fluxes from vineyards during light wind and convective conditions. Irrigation Sci. https://doi.org/10.1007/s00271018-0617-5.

Mahrt, L., 1998. Stratified boundary layers. Bound.-Layer Meteorol. 90, 375-396.

Massman, W.J., 2000. A simple method for estimating frequency response corrections for eddy covariance systems. Agric. For. Meteorol. 104, 185-198.

Massman, W., Forthofer, J., Finney, M., 2017. An improved canopy wind model for predicting wind adjustment factors and wildland fire behavior. Can. J. For. Res 47(5), 594-603.

Nieto, H., Kustas, W.P., Alfieri, J.G. Gao, F., Hipps, L.E., Los, S.A., Prueger, J.H., McKee, L.G., Anderson, M.C., 2018. Impact of different within-canopy wind attenuation formulations on modelling sensible heat flux using TSEB. Irrigation Sci. https://doi.org/10.1007/s00271-018-0611-y.

Norman, J.M., Kustas, W.P., Humes, K.S., 1995. Source approach for estimating soil and vegetation energy fluxes in observations of directional radiometric surface temperature. Agric. For. Meteorol. 77, 263-293.

Paw U, K.T., Brunet, Y., Collineau, S., Shaw, R.H., Maitani, T., Qiu, J., Hipps, L., 1992. On Coherent structures in turbulence within and above agricultural plant canopies. Agric. For. Meteorol. 61, 55-68.

Peixoto, J.P., Oort, A.H., 1992. Physics of climate. American Institute of Physics.

Poulos, G.S., Blumen, W., Fritts, D.C., Lundquist, J.K., Sun, J., Burns, S.P., Nappo, C., Banta, R., Newsom, R., Cuxart, J., Terradellas, E., Balsley, B., Jensen, M., 2002. CASES-99: A Comprehensive investigation of the stable nocturnal boundary layer. Bull. Amer. Meteor. Soc. 83, 555-581.

Semmens, K.A., Anderson, M.C., Kustas, W.P., Gao, F., Alfieri, J.G., McKee, L.G., Prueger, J.H., Hain , C.R., Cammalleri, C., Yang, Y., Xia, T., Sanchez, L., Alsina, M., Velez, M. 2016. Monitoring daily evapotranspiration over two California vineyards using Landsat 8 in a multi-sensor data fusion approach. Remote Sens. Environ. 185, 155-170.

Shaw, R.H., Tavangar, J., Ward, D.P., 1983. Structure of Reynolds stress in a canopy layer. J. Climate Appl.. Meteorol 22, 1922-1931.

Stull, R., 1988. Introduction to boundary layer meteorology. Kluwer Academic Publishers, Dordrecht, NL.

Sun, L., Gao, F., Anderson, M.C., Kustas, W.P., Alsina, M., Sanchez, L., Sams, B., McKee, L.G., Dulaney, W.P., White, A., Alfieri, J.G., Prueger, J.H., Melton, H., Post, K., 2017. Daily mapping of 30 m LAI, NDVI for grape yield prediction in California vineyard. Remote Sensing. 9(4), 317.

Schymanski, S.J., Or, D., Zwieniecki, M., 2013. Stomatal control and leaf thermal and hydraulic capacitances under rapid environmental fluctuations. PLOS ONE. 8(1), e54231.

van Leeuwen, C., Trégoat, O., Choné, X., Bois, B., Pernet, D., & Gaudillère, J.-P., 2009. Vine water status is a key factor in grape ripening and vintage quality for red Bordeaux wine. How can it be assessed for vineyard management purposes?. *OENO One*. *43*(3), 121-134. https://doi.org/10.20870/oeno-one.2009.43.3.798.

Twine, T.E., Kustas, W.P., Norman, J.M., Cook, D.R., Houser, P.R., Meyers, T.P., Prueger, J.H., Starks, P.J., Wesely, M.L., 2000. Correcting eddy covariance flux measurements over a grassland. Agric. For. Meteorol. 103, 279-300.

Vassilicos, J.C., 2010. Intermittency in turbulent flows. Cambridge: Cambridge University Press.

Webb, E.K., Pearman, G.I., Leuning, R., 1980. Correction of flux measurements for density effects due to heat and water vapour transfer. Q. J. R. Meteorolog. Soc. 106, 85-100.

CHAPTER IV
SUMMARY AND CONCLUSIONS

4.1 Summary of Results

This study investigated the characteristics of intermittent turbulence transport of heat and water vapor and its role in vineyard evapotranspiration. Time series of vertical velocity (u_z) and water vapor density (ρ_v) were surveyed above two vineyard canopies during daytime periods over three growing seasons. Intermittent turbulence resulted in episodic heat and water vapor exchanges and was found to occur often. This behavior was commonly observed when mean winds were low, < 1.5 – 2 m s^{-1}, combined with unstable, convective stratification; conditions common to the warm season climate of arid and semi-arid regions. Sharp transitions in the behavior of turbulence and humidity fluctuations were frequently observed when progressing from a period of light to more moderate winds. Time series of instantaneous water vapor fluxes exhibited transient patches of larger turbulence exchange during very light winds and more consistent behavior during steadier, higher velocity wind conditions.

Power spectra of u_z and ρ_v, and cross-spectra of $u_z * \rho_v$ above the canopy demonstrated that variations were often dominated by lower frequencies during intermittency, light winds, and highly unstable stratification. Comparing spectra and cross-spectra above and within the canopy showed that this effect was enhanced within

the canopy where fluctuations of u_z and ρ_v were more strongly affected by transient, low frequency bursts of turbulence activity. Characteristics of spectra above and within the canopy diverged during intermittent conditions, while exhibiting more commensurate behavior during higher winds and steadier turbulence, indicating that intermittent turbulence is associated with less coherence between the canopy sublayer and surface layer above.

Analysis of appropriate flux-averaging period lengths demonstrated that substantially longer averaging periods than typically used, as long as 90 – 120 minutes, can be necessary during intermittent conditions to maximize energy balance closure. In such cases, a small number of events can drastically affect average fluxes for a given averaging period and this effect must be considered when applying both modeling or measurement methods. These findings suggest that under weak synoptic pressure gradients, light winds, and strong instability, much of the transport of heat and water vapor from the vineyards is associated with infrequent passage of larger eddies.

The transient nature of fluxes was also quantified by calculating proportions of the total flux during active periods, of turbulence. The results highlighted significant differences in the amounts of time over which the majority of exchange occurred for different atmospheric conditions. During intermittent periods short bursts of exchange accounted for 80 – 90% of the water vapor flux while occurring over typically less than 30% of the period. Steady periods on the other hand typically saw the flux much more evenly distributed across the total time period. The values of flux/time ratios were highly effective at delineating intermittent periods from steady periods, proving to be one

method to semi-objectively quantify intermittent transport, though through the use of a subjective threshold technique.

Time series of TKE values were used to quantify the degree on intermittency by using sliding windows of various sizes, and determining the magnitude of the change in standard deviation of TKE with window size. Comparisons of TKE time series above and within the vineyard canopy revealed that within canopy turbulence becomes damped and at times decoupled from activity above suggesting a low coherence during light winds and intermittency. In such cases, the microclimate inside the canopy can differ considerably from that of the air above. Periods of steady turbulence during higher mean winds, showed concurrent behavior and better coupling between the canopy air and surface layer above.

Effects of the episodic nature of the transport on the TSEB remote sensing-based ET model were addressed by using observed temperature gradients between soil, canopy foliage, canopy airspace, and above canopy air temperatures. Examining these at high frequency, 1 Hz, demonstrated that intermittent transport greatly alters their temporal behavior. While the relationships between these temperatures remained consistent during steady periods, transient exchanges resulted in gradients varying greatly with time. In fact, the temperature gradient between the canopy surface and the air above would at times alternate sign over short timescales in conjunction with bursts of turbulent activity.

TSEB modeled fluxes for 417 hours across three growing seasons from two vineyard sites for a range of atmospheric conditions displayed favorable agreement with eddy covariance measured fluxes using traditional statistical metrics of r^2, RMSE, MAE, and bias. But, modeled fluxes of 115 intermittent hours showed considerably less

agreement with increased RMSE and MAE, and evidence of bias. This compared to 102 hours of steady conditions, where TSEB agreed best with eddy covariance fluxes. Relationships of TSEB modeled sensible heat flux error with wind speed and stability demonstrated that model underestimation is correlated with low winds, large instability, and large sensible heat flux values. However, analysis of modeled versus measurement derived aerodynamic resistance and friction velocity did not evidence these as a cause for the lower model performance noted during intermittent periods. Finally, TSEB showed sizeable sensitivity to temporal variations in "snapshot" radiometric temperature derived from 1 Hz IRT data. Furthermore, at times TSEB showed unstable solutions for modeled fluxes when differences between the air and radiometric surface temperatures grew large.

4.2 Conclusions

This thesis demonstrates that the characteristics of heat and water vapor fluxes in vineyards are substantially different between periods displaying intermittency and those displaying steadier conditions in turbulence transport. Both spectral analyses and flux/time ratios confirmed that intermittency significantly alters the timescales over which fluxes take place as compared to steadier periods. Here, intermittent turbulence has been shown to affect both the temporal and spatial properties of mass transport and energy balance that govern vineyard evapotranspiration. Though flux/time ratios did show success in delineating intermittent and steady periods, unambiguously defining and quantifying intermittency remains problematic, and subjective visual selection was relied

on for the classification of turbulence behavior. However, this research was able to utilize several methods to reveal the important role intermittency plays in the processes of vineyard systems.

During periods with light winds and convective conditions, intermittent behavior may not conform to the conceptual model and assumptions inherent in time-averaged gradient approaches. Typical flux-gradient relationships imply that mean gradients represent a dynamic equilibrium of the transport processes, and that the net result of variations is reasonably consistent with the flux from the surface. Clear from this work, however, is that similar mean values from two given averaging periods may conceal very different exchange behavior. The results of TSEB model tests support this by demonstrating degraded performance during periods with intermittency, while performing best during steady periods, when average flux-gradient assumptions are most valid. A key message from this research therefore is: how the flux happens with time over an averaging period does matter for understanding ET from complex plant canopies under these conditions, which are rather common in many winegrowing regions. As remotely sensed ET models become progressively more sophisticated, they will need to resolve ET processes on increasingly fine time and space scales. Crucial to that endeavor will be addressing issues of how to contend with intermittent transport behavior in heterogeneous vegetation.

6/4/19

Sebastian Los
1820 Georgia St NE
Albuquerque, New Mexico 87110

Dear Dr. Joseph Alfieri,

My M.Sc. thesis in the Department of Plants, Soils, and Climate at Utah State University is in final preparation to be placed in USU library digital commons within the next few weeks. The journal article *Intermittency of Water Vapor Fluxes from Vineyards During Light Wind and Convective Conditions*, which appeared in the May 2019 issue of Irrigation Science (DOI 10.1007/s00271-018-0617-5), reports an essential part of my thesis research. Since you are a coauthor, I would like to ask your permission to reprint this article as a chapter in my thesis. Please note that USU sends every thesis and dissertation to ProQuest to be made available for reproduction.

I will include acknowledgment to the published article on the first page of the chapter as shown below. Copyright and permission information will be included in a special appendix. Please contact me via the phone number or email below should you have any questions, or if you would like a different acknowledgment. Please indicate your approval of this request by signing in the space provided and returning this letter. Thank you for your assistance.

Sebastian Los
417-576-4399
sebastian.los@aggiemail.usu.edu

I hereby give permission to Sebastian Los to reprint the requested article in his thesis, with the following acknowledgment:

[Portions of this chapter were published in the journal Irrigation Science of Springer Nature as Los, S.A., Hipps, L.E., Alfieri, J.G., Kustas, W.P., Prueger, J.H. (2019). Intermittency of water vapor fluxes from vineyards during light wind and convective conditions. Irrigation Sci. 37:281-295, DOI 10.1007/s00271-018-0617-5.]

Signed _____

Date: _____ 06/05/19

6/4/19

Sebastian Los
1820 Georgia St NE
Albuquerque, New Mexico 87110

Dear Dr. John Prueger,

My M.Sc. thesis in the Department of Plants, Soils, and Climate at Utah State University is in final preparation to be placed in USU library digital commons within the next few weeks. The journal article *Intermittency of Water Vapor Fluxes from Vineyards During Light Wind and Convective Conditions*, which appeared in the May 2019 issue of Irrigation Science (DOI 10.1007/s00271-018-0617-5), reports an essential part of my thesis research. Since you are a coauthor, I would like to ask your permission to reprint this article as a chapter in my thesis. Please note that USU sends every thesis and dissertation to ProQuest to be made available for reproduction.

I will include acknowledgment to the published article on the first page of the chapter as shown below. Copyright and permission information will be included in a special appendix. Please contact me via the phone number or email below should you have any questions, or if you would like a different acknowledgment. Please indicate your approval of this request by signing in the space provided and returning this letter. Thank you for your assistance.

Sebastian Los
417-576-4399
sebastian.los@aggiemail.usu.edu

I hereby give permission to Sebastian Los to reprint the requested article in his thesis, with the following acknowledgment:

[Portions of this chapter were published in the journal Irrigation Science of Springer Nature as Los, S.A., Hipps, L.E., Alfieri, J.G., Kustas, W.P., Prueger, J.H. (2019). Intermittency of water vapor fluxes from vineyards during light wind and convective conditions. Irrigation Sci. 37:281-295, DOI 10.1007/s00271-018-0617-5.]

Signed: _____
Date: _____